5-2016

Investigation of Advanced Engine Cooling Systems - Optimization and Nonlinear Control

Tianwei (Thomas) Wang
Clemson University, tianwew@g.clemson.edu

INVESTIGATION OF ADVANCED ENGINE COOLING SYSTEMS – OPTIMIZATION AND NONLINEAR CONTROL

A Dissertation
Presented to
the Graduate School of
Clemson University

In Partial Fulfillment
of the Requirements for the Degree
Doctor of Philosophy
Mechanical Engineering

---

by
Tianwei (Thomas) Wang
May 2016

Accepted by:
Dr. John Wagner, Committee Chair
Dr. Georges Fadel
Dr. Xiangchun Xuan
Dr. Todd Schweisinger

ABSTRACT

Advanced automotive engine cooling systems can positively impact the performance, fuel economy, and reliability of internal combustion engines. A smart engine cooling system typically features multiple real time computer controlled actuators: a three way linear smart valve, a variable speed coolant pump, and electric radiator fan(s). In this dissertation, several innovative comprehensive nonlinear control and optimization operation strategies for the next generation smart cooling application will be analyzed.

First, the optimal control has been investigated to minimize the electric energy usage of radiator fan matrix. A detailed mathematical model of the radiator fan(s) matrix operation and the forced convection heat transfer process was developed to establish a mixed integer nonlinear programming problem. An interior points approach was introduced to solve the energy consumption minimization problem. A series of laboratory tests have been conducted with different fan configurations and rotational shaft speed combinations, with the objective to cool a thermal loaded engine. Both the mathematical approach and the laboratory test results demonstrated the effectiveness of similar control strategies. Based on the tests data and mathematical analysis, an optimization control strategy reduced the fan matrix power consumption by up to 67%.

Second, a series of experimental laboratory tests were implemented to investigate the contributions of each electro-mechanical device in automotive thermal management system. The test results established a basis for several key operating conclusions. The smart valve and variable speed pump impacted the engine temperature by adjusting the

heat transfer rate between the engine and the radiator through coolant redirection and/or coolant flow rate. On the other hand, the radiator fan(s) operation affects the engine's temperature by modifying the heat rejection rate of the radiator which can influence the entire cooling system. In addition, the smart valve's operation changes the engine's temperature magnitude the greatest amount followed by the radiator fan(s) and the coolant pump. Furthermore, from a power consumption aspect, the radiator fan(s) consumes the most engine power in comparison to the two other actuators.

Third, a Lyapunov based nonlinear control strategy for the radiator fan matrix was studied to accommodate transient engine temperature tracking at heavy heat load. A reduced order mathematical model established a basis for the closed-loop real time feedback system. Representative numerical and experimental tests demonstrated that the advanced control strategy can regulate the engine temperature tracking error within $0.12°C$ and compensate the unknown heat load. The nonlinear controller provided superior performance in terms of power consumption and temperature tracking as evident by the reduced magnitude when compared to a classical proportional integral with lookup table based controller and a bang bang controller.

Fourth, a nonlinear adaptive multiple-input and multiple-output (NAMIMO) controller to operate the smart valve and radiator fans has been presented. This controller regulates the engine temperature while compensating for unknown wide range heat loads and ram air effects. A nonlinear adaptive backstepping (NAB) control strategy and a state flow (SF) control law were introduced for comparisons. The test results indicated that the NAMIMO successfully regulated the engine temperature to a desired value (tracking er-

ror, $|e| < 0.5°C$, at steady state) subject to various working conditions. In contrast, the NAB control law consumes the least radiator fan power but demonstrated a larger average temperature tracking error (40% greater than the NAMIMO controller), a longer response time (34% greater than the NAMIMO controller), and defected when the heat load was low. Lastly, the SF controller, characterized by greater oscillation and electrical power consumption (18.9% greater than the NAMIMO controller), was easy to realize and maintained the engine temperature to within $|e| < 5°C$.

An important aspect of engineering research is the knowledge gained from learning materials to fully understand the thermal management. As part of the dissertation, advanced three-dimensional (3D) visualization and virtual reality (VR) technology based engineering education methods has been studied. A series of computer aided design (CAD) models with storyboards have been created to provide a step to step guide for developing the learning modules. The topics include automotive, aerospace, and manufacturing. The center for aviation and automotive technological education using virtual e-schools (CA2VES) at Clemson University has developed a comprehensive e-learning system integrated with eBooks, mini video lectures, 3D virtual reality technologies, and online assessments as supplementary materials to engineering education.

DEDICATION

To my wife Shasha,

and to my parents.

ACKNOWLEDGEMENT

First, I would like to thank my advisor Dr. John Wagner for his support, guidance, and motivation throughout my PhD study and research. He has provided me with the research freedom to explore on my own and the guidance to keep me on the right path, which I really appreciate. I would also like to extend my gratitude to Dr. Georges Fadel, Dr. Xiangchun (Schwann) Xuan, and Dr. Todd Schweisinger for serving on my dissertation committee.

I would also like to thank Dr. Kapil Madathil for his constant support and motivation. A special thanks to Mr. Jamie Cole, Mr. Michael Justice, and Mr. Stephen Bass for providing incredible technical support on the construction of the experimental test bench.

Last but not the least, I would like to thank my parents, my wife, and my friends for their continual encouragement and support.

TABLE OF CONTENTS

Table of Contents (Continued)

Page

Table of Contents (Continued)

Page

LIST OF TABLES

List of Tables (Continued)

Table Page

LIST OF FIGURES

List of Figures (Continued)

Figure Page

List of Figures (Continued)

Figure Page

List of Figures (Continued)

Figure Page

List of Figures (Continued)

Figure Page

List of Figures (Continued)

Figure Page

NOMENCLATURE LIST

Symbol	Units	Description
a, b, c, d, e, f, g, h	various	Constants
A, B, C, D	-	Matrix
A_p	m^2	Piston head surface area
A_r	m^2	Radiator surface area
C_e	$kJ/°C$	Specific heat of engine
Cp_a	$kJ/kg°C$	Specific heat of air
Cp_{cool}	$kJ/kg°C$	Specific heat of coolant
C_r	$kJ/°C$	Specific heat of radiator
d	m	Radiator fan diameter
e	$°C$	Engine temperature tracking error
e^*	$°C$	Engine temperature tracking error for bang bang controller
e_{high}	$°C$	Upper error band
e_{low}	$°C$	Lower error band
e_M	$°C$	Mean absolute tracking error
e_{RMS}	$°C$	Error root mean square
e_{ss}	$°C$	Steady state error
$f(.,.)$	-	Optimization objective function

Symbol	Units	Description
$F_f(N_f, n, v_{ram})$	-	Radiator heat rejection mathematical function
$F_f(N_f, n)$	-	Radiator heat rejection mathematical function without ram air effect
$F_{H,p}(H, N_{pump})$	-	Actuators mathematical function of valve and pump combination
$g(e, r, t)$	-	Auxiliary function for Lyapunov stability analysis
$H(.,.,.)$	-	Ram air effect mathematical function
H	-	Smart valve position
$H_{min,nom,max}$	-	Minimum, normal, and maximum valve position
$h(.,.); g(.,.)$	-	Constraint functions for optimization
i	A	Current
k	-	Fan factor
$k_1, k_2, K_1, K_2, K_I, K_P$	-	Controller gains
k_f	-	Fan pressure coefficient
k_I	-	Air inlet pressure coefficient
k_r	-	Radiator pressure coefficient
L_∞	-	Space infinite

Symbol	Units	Description
$\dot{m}_{air}$	kg/s	Radiator air mass flow rate
$\dot{m}^{*}_{air}$	kg/s	Testing radiator air mass flow rate
$\dot{m}_{cmax,min}$	kg/s	Minimum and maximum coolant mass flow rate
$\dot{m}_{cool}$	kg/s	Coolant circulation rate
$\dot{m}_{f}$	kg/s	Fan air mass flow rate
$\dot{m}_{ram}$	kg/s	Ram air mass flow rate
$\dot{M}$	kg/s	Constant coolant circulation rate
M_p	-	Maximum percent overshot
n	-	Fans operating number
n_{max}	-	Maximum number of operating fans
n_s	-	Optimized fan number
N_f	RPM	Radiator fan motor speed
$N_{fmin,nom,max}$	RPM	Minimum, normal, and maximum radiator fan speed
N_{high}	RPM	Motor speed upper limit
N_{low}	RPM	Motor speed lower limit
N_{pump}	RPM	Pump impeller speed
N_s	RPM	Optimized fan motor speed
P_{ave}	kW	Average electrical power

Symbol	Units	Description
P_e	kW	Electrical power
P_{fan}	kW	Fan array power consumption
P_m	kW	Radiator fan mechanical power
P_{pump}	kW	Coolant pump power consumption
P_{sys}	kW	Coolant system power consumption
q_c	kW	Chamber heat transfer rate
q_f	kW	Radiator fan(s) heat transfer rate
q_{in}	kW	Heat input
q_{inu}	kW	Heat input upper bound
q_{in0}	kW	Initial heat input
$\hat{q}_{inh,l}$	kW	Estimated heat load rate thresholds
q_{out}	kW	Radiator heat rejection rate
q_{ram}	kW	Ram air effect heat transfer rate
q_{ramu}	kW	Ram air effect upper bound
Q_{air}	m^3/s	Radiator air volume flow rate
Q_f	m^3/s	Fan air volume flow rate
Q_{ram}	m^3/s	Ram air volume flow rate
r	$°C$	Intermediate tracking error
r_h	m	Fan hub radius
r_m	m	Fan mean radius

Symbol	Units	Description
r_t	m	Fan tip radius
t	s, min	Time
t_d	s	Delay time
t_r	s	Rise time
t_{ss}	s	Settling time
T_{aout}	$°C$	Air outlet temperature
T_c	$°C$	Coolant temperature
T_e	$°C$	Engine temperature
T_{e0}	$°C$	Initial engine temperature
T_{ed}	$°C$	Desired engine temperature
T_g	$°C$	Gas temperature
$T_{H,L,M}$	$°C$	Engine temperature thresholds
T_{HI}	$°C$	Heat exchanger inlet coolant temperature
T_{HO}	$°C$	Heat exchanger outlet coolant temperature
T_j	$°C$	Mixing junction temperature
T_{norm}	$°C$	Normalized temperature
T_r	$°C$	Radiator temperature
T_{rd}	$°C$	Intermediate radiator input temperature
$T_{rdh,m,l}$	$°C$	Desired radiator temperature under various conditions

Symbol	Units	Description
T_{RI}	$°C$	Coolant temperature at radiator inlet
T_{RO}	$°C$	Coolant temperature at radiator outlet
T_{ss}	$°C$	Engine temperature at steady state
T_{∞}	$°C$	Ambient temperature
$u(.,.)$	-	System input
U	$kW/m^2°C$	Overall heat transfer coefficient
v_{air}	m/s	Radiator air velocity
v_{air}^{*}	m/s	Testing radiator air velocity
$\overline{v}_{air}^{*}$	m/s	Average testing radiator air velocity
v_f	m/s	Fan air velocity
v_{ram}	m/s	Ram air velocity
$v_{vehicle}$	m/s	Vehicle velocity
v_{wind}	m/s	Wind velocity
V	-	Lyapunov function
V_s	V	Supply voltage
Z	-	Lyapunov Vector
α_{wind}	deg	Wind attack angle
Φ_m	-	Fan flow rate coefficient
ε_a	-	Air heat transfer efficiency
ε_c	-	Coolant heat transfer efficiency

Symbol	Units	Description
$\varepsilon_e, \varepsilon_r$	-	Positive constant
ρ_{air}	kg/m^3	Air density
ϕ_{1-4}	-	Auxiliary function
ΔT	$°C$	Radiator air temperature drop
∇f	-	Objective function gradient
v	-	Hub ratio
η	-	Efficiency
τ	$N \cdot m$	Torque
$\lambda_{A1,2}$	-	Open loop state matrix eigenvalues
$\lambda_{B1,2,3,4}$	-	Closed loop state matrix eigenvalues
$\sim$	-	Error of estimated parameter
^	-	Estimated parameter
$*$	-	Equilibrium point

CHAPTER I

INTRODUCTION

"Americans rank fuel efficiency as top vehicle purchasing factor"

- PRNewswire, Washington, DC (prnewswire.com, Oct. 16, 2014)

Why is fuel efficiency important for ground vehicles? One obvious reason is that high efficiency vehicles consume less fuel which lowers the expense for petroleum. An ordinary consumer can save on average between $200 and $1,500 per year by choosing a fuel efficient vehicle (Department of Energy, 2014). Second, better fuel mileage helps protect the environment by reducing tailpipe greenhouse gases (GHG), mostly in the form of carbon dioxide (CO_2). Third, improved fuel efficiency promotes energy sustainability as most ground vehicles operate on non-renewable fossil fuels. The global oil producer, British Petroleum, now simply called BP, estimates that the earth's supply of oil will last 53 years at the current extraction rate (BP, 2014). Fourth, fuel efficiency gains can reduce the nation's oil dependence which improves national security. Approximately one-third of the oil utilized in United States is imported, costing the country $192 billion annually. Increasing the fuel performance of internal combustion engines will help the nation diminish the economic impact of oil price changes and the associated political ramifications in the Middle East (Department of Energy, 2014).

1.1 Legislated Global Fuel Economy Standards for Light Duty Vehicles

To encourage the improvement of gasoline and diesel engine efficiency, a number of countries have issued fuel economy standards for light duty vehicles. This section will

briefly describe and discuss the standards enacted in the United States, European Union (EU), China, and Japan which produced around 70% of the total 89,734,228 vehicles manufactured in the year of 2014 (International Organization of Motor Vehicle Manufacturers, 2015).

In the United States, the Corporate Average Fuel Economy (CAFE) standard was initially issued in 1975 by the National Highway Traffic and Safety Administration (NHTSA) to help the country decrease the dependence on imported oil (NHTSA, 1975). Throughout the history of the CAFE standard, several updates have occurred to promote greater fuel economy. The latest two versions of the CAFE standard were issued in May 2010 and August 2012 which declared the fuel economy targets for the Model Years (MYs) 2012-2016 and 2017-2025, respectively. Table 1.1 and Figure 1.1 illustrate the fuel economy historical performances and the enacted CAFE targets from 2012 to 2025 for both passenger cars and light trucks (NHTSA, 2010 and 2012). From Table 1.1, the fuel economy targets are 56.2MPG and 40.3MPG for passenger cars and light trucks, respectively, by the year 2025. As estimated by NHTSA, the nationwide reduction of gasoline consumption itself can reach up to 170.1 billion gallons in 2025. In the meantime, these regulations can reduce GHG emissions by more than 6 billion metric tons over the aggregated vehicles lifetime in the USA. This amount of emission is equivalent to that which the Amazon rainforest absorbs in three years according to White House report. Finally, Table 1.1 and Figure 1.1 show the upward trend in high fuel efficiency to be achieved with technology.

To compare the fuel economy standards in the USA to those in other countries, Table 1.2 is provided which lists the targets for selected years in the USA, EU, China, and Japan. To facilitate the analysis, the fuel economy standards of other countries are normalized to the CAFE (MPG) standard.

Table 1.1: Fuel economy emissions target for Model Year 2012 to 2025 in United States

Model Year	Fuel Economy, MPG		
	Passenger Cars	Light Trucks	Combined Cars and Trucks
2012	33.3	25.4	29.7
2013	34.2	26.0	30.5
2014	34.9	26.6	31.3
2015	36.2	27.5	32.6
2016	37.8	28.8	34.1
2017	40.1	29.4	35.3
2018	41.6	30.0	36.4
2019	43.1	30.6	37.5
2020	44.8	31.2	38.8
2021	46.8	33.3	40.9
2022	49.0	34.9	42.9
2023	51.2	36.6	45.0
2024	53.6	38.5	47.3
2025	56.2	40.3	49.6

In the EU, manufacturers must test and report the CO_2 emissions level for every new vehicle model using the New European Driving Cycle (NEDC) regulation (ICCT, 2014). Note that the CO_2 emission level is an alternative technique to evaluate the vehicle's fuel economy. Unlike other vehicle tailpipe emissions such as nitrogen oxide (NOx) and carbon monoxide (CO), CO_2 emission cannot currently be reduced using pollution control devices. In other words, a vehicle's CO_2 emissions are directly attached to the fuel

economy as a matter of chemistry. As NHTSA defined, "A tailpipe carbon dioxide regulation and a fuel economy regulation are essentially equivalent: they each in effect regulate fuel economy" (NHTSA, 2008). In such a manner, the EU CO_2 emission standard can be normalized into a CAFE Standard (ICCT, 2014). The targets of 56.9MPG for passenger cars and 40.1MPG for light trucks in 2021 were announced by the European Parliament and the Council of the EU in 2013. This standard is also referred to Euro 6 (ICCT, 2014). Table 1.2 shows that the fuel economy targets in EU are much more rigorous than the ones in the USA. This may be attributed to the much higher fuel taxes and greater number of smaller size vehicles (OICA, 2014) than that in the United States. Also, the EU favors technology integration into vehicles which are purchased by the consumers.

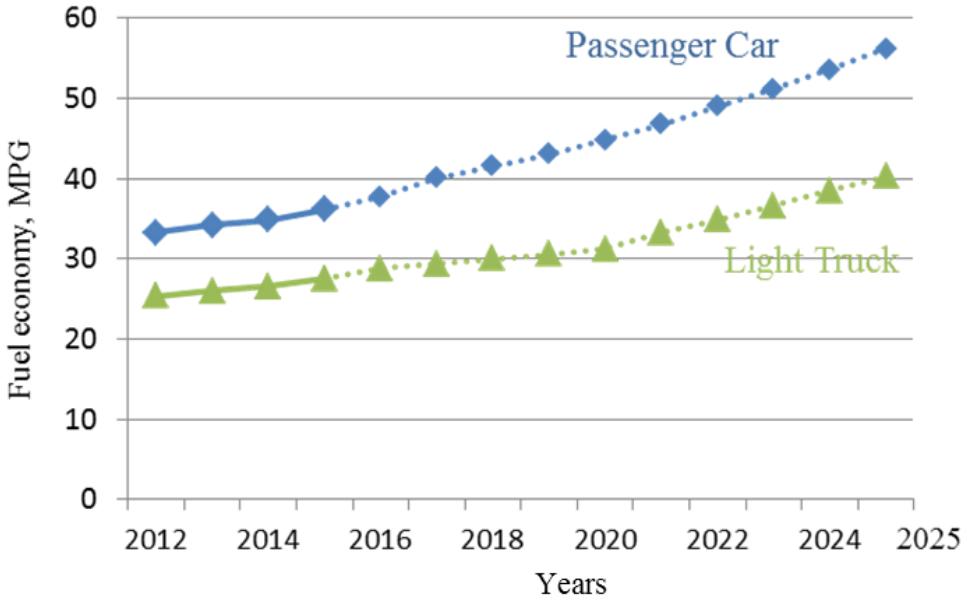

Figure 1.1: Fuel economy emissions target for Model Year 2012 to 2025 in United States Solid line: historical performance; Dash line: enacted targets

China applies a weight-based system and began to test new vehicles using NEDC in 2004. The automotive manufacturers are regulated by the Corporate Average Fuel Consumption (CAFC) metric introduced in 2013. The current enacted regulation is China III which requires a target of 47.7MPG by 2020 for passenger cars. Japan established even more aggressive fuel economy standards, e.g., 44.5MPG in MY 2012 which is 33.6% higher than the standard in the USA. However, the targets for 2020 have less restriction than before. On the other hand, it is worth noting that, Japanese manufacturers use the advanced technology as a selling point and can meet the future targets before the regulations. For example, the new vehicles fuel economy in 2010 has approximately achieved the 2015 regulations in Japan. This phenomenon can be expected in the 2020 year target as well (ICCT, 2014 and TransportPolicy.net, 2014).

Table 1.2: Targets of fuel economy normalized to CAFE* standard (MPG) in USA, EU, China, and Japan for selected years
*CAFE: Corporate Average Fuel Economy

	Fuel Economy, MPG							
Model Year	Passenger Cars				Light Trucks			
	US	EU	China	Japan	US	EU	China	Japan
2012	33.3	43.3	33.5	44.5	25.4	35	29.8	-
2013	34.2	44.9	33.8	-	26.0	-	-	-
2015	36.2	-	35.8	-	27.5	-	-	37.2
2020	44.8	-	47.7	45.9	31.2	-	-	-
2021	46.8	56.9	-	-	33.3	40.1	-	-

1.2 Advanced Technologies to Improve Vehicle Fuel Economy

The enacted fuel economy targets have encouraged the vehicle manufacturers to increase their spending on improving the fuel efficiency. As a result, many advanced

technologies have been rapidly developed. According to the latest released report by the Environmental Protection Agency (EPA), from MY 2009 to MY 2014, the majority of the oil saving from the current vehicles is due to updated gasoline vehicle technologies (EPA, 2014). For example, the gasoline direct injection technology (GDI) which offers a leaner fuel air mixture ratio and a more completely burn of fuel increased from 4.2% to 37.9% of the market share in the past five years. The variable valve timing (VVT) has been applied in almost all the MY 2014 vehicles (97.5%). This technology allows the control of the valve timing, duration and lift precisely to address various operation conditions. For the transmission and driving technologies, the advanced transmission systems, including the six or more gears transmission and continuously variable transmissions (CVT), have been extended around 90% of the market share in MY 2014. Figure 1.2 shows the change of market share for the technologies between MY 2009 and MY 2014. However, the contribution from cooling system innovation which has great potential to promote the fuel economy has not been widely implemented yet.

1.3 Introduction of Advanced Cooling Systems

Typically, the current engine cooling system is designed to keep the engine temperature in a prescribed range even during the worst working conditions (Sermeno *et al.*, 2014). In a traditional structure, the mechanical pump and radiator fan(s) are indirectly connected with the crankshaft. A wax-based thermostat is mounted to determine the coolant flow route pass or not pass the radiator. Although the reliability has been repeatedly demonstrated in past decades, two limitations exist. On the one hand, the mechanical coupling leads the operation of the actuators (pump and radiator fans) to be dependent on

the engine revolution which cannot be controlled accurately and always yields the engine overcooling. It has been investigated that the overcooling degrades the engine performance (Wagner *et al.*, 2002) and increases the lubricate oil friction (Kim *et al.*, 2013), which leads to a lower fuel economy and higher tailpipe emissions. On the other hand, the mechanical connections, such as timing belt or timing chain, generate unnecessary energy loss; according to (Heywood *et al.*, 1988) approximately 25% of the total energy generated from the combustion process is lost to the cooling system (25% is the effective power, 40% to exhaust gas, and 5% lost in friction).

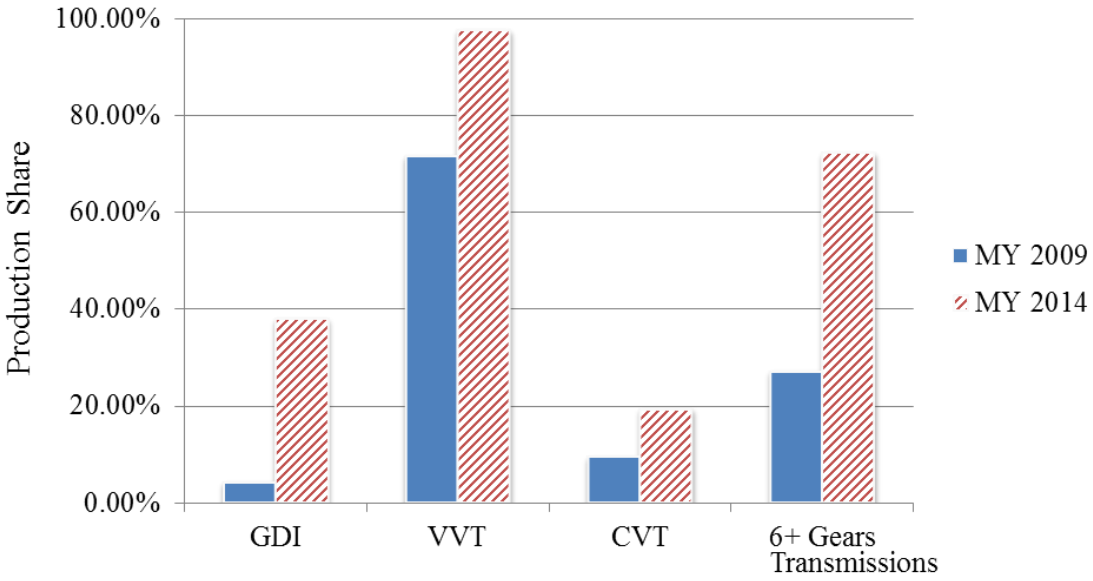

Figure 1.2: Technology production share for MY 2009 and MY 2014; GDI: gasoline direct injection technology, VVT: variable valve timing, CVT: continuously variable transmissions

An advanced engine cooling system introduces the concept of "thermal management" on regulating the engine coolant in a precise desired working temperature with minimum power consumption (Kim *et al.*, 2013 and Setlur *et al.*, *2005*). A smart cooling

system updates the mechanical pump and radiator fan(s) with electrical controlled components and replaces the wax-based valve with a 3-way computer controlled smart valve. Besides the updated configuration of the engine cooling systems, several advanced control strategies have been rapidly developed and applied to the advanced cooling systems. With these features, each actuator can be operated accurately to achieve a certain heat rejection requirement with minimum energy utilization theoretically. Besides, assorted sensors are mounted to monitor the system's dynamics and operation environment. The electronic control unit (ECU) determines the control strategies and sends out command signals to the actuators based on the real time system dynamics and prescribed control algorithm. The block diagram and 3D computer aided model (CAD) of an advanced cooling system are shown in Figure 1.3.

1.4 Dissertation Outline

In this dissertation, the advanced engine cooling system will be investigated from various aspects. As Figure 1.4 displays, the remainder of the article is organized as follows. An optimization control strategy of automotive radiator fan array to reduce power consumption will be introduced in Chapter II. An experimental study of integrated actuator transient behavior will be discussed in Chapter III. Chapter IV proposes a Lyapunov based nonlinear radiator fan matrix control to regulate the engine temperature. Chapter V presents a nonlinear multiple input multiple output controller to regulate the valve, pump and radiator fans. Chapter VI introduces an interactive three dimensional visualization based engineering technology education. Finally, the conclusion will be given in Chapter VII. Appendices A and B provide the supplemental materials to support the mathemati-

cal models in Chapter II. Appendices C and D provide the detailed traditional controllers for compassion for Chapters IV and V, respectively.

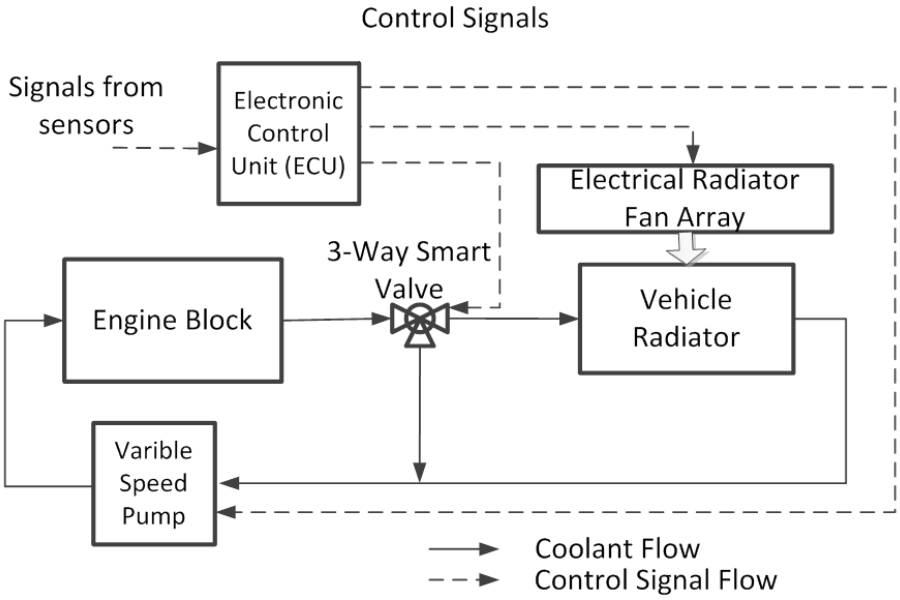

(a)

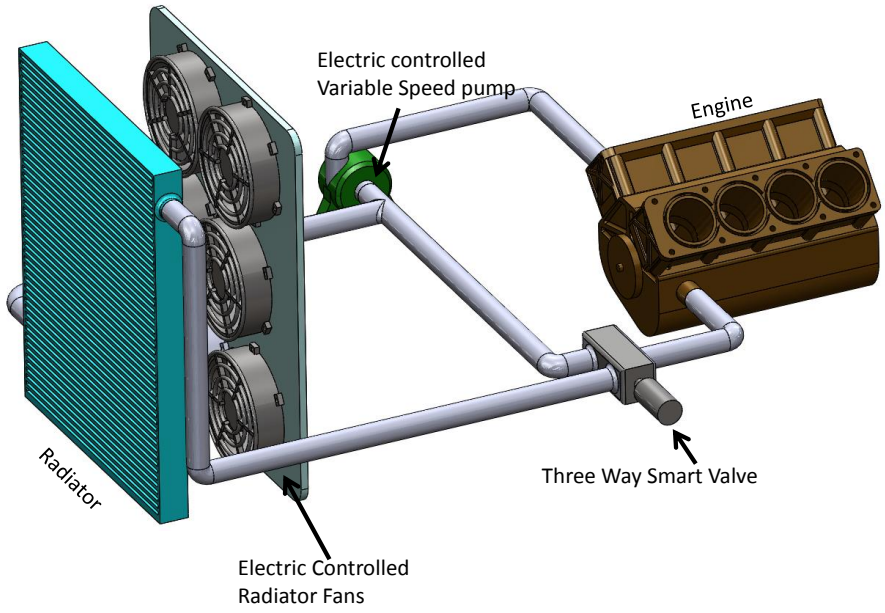

(b)

Figure 1.3: (a) Block diagram, and (b) CAD model of advanced internal combustion engine cooling system

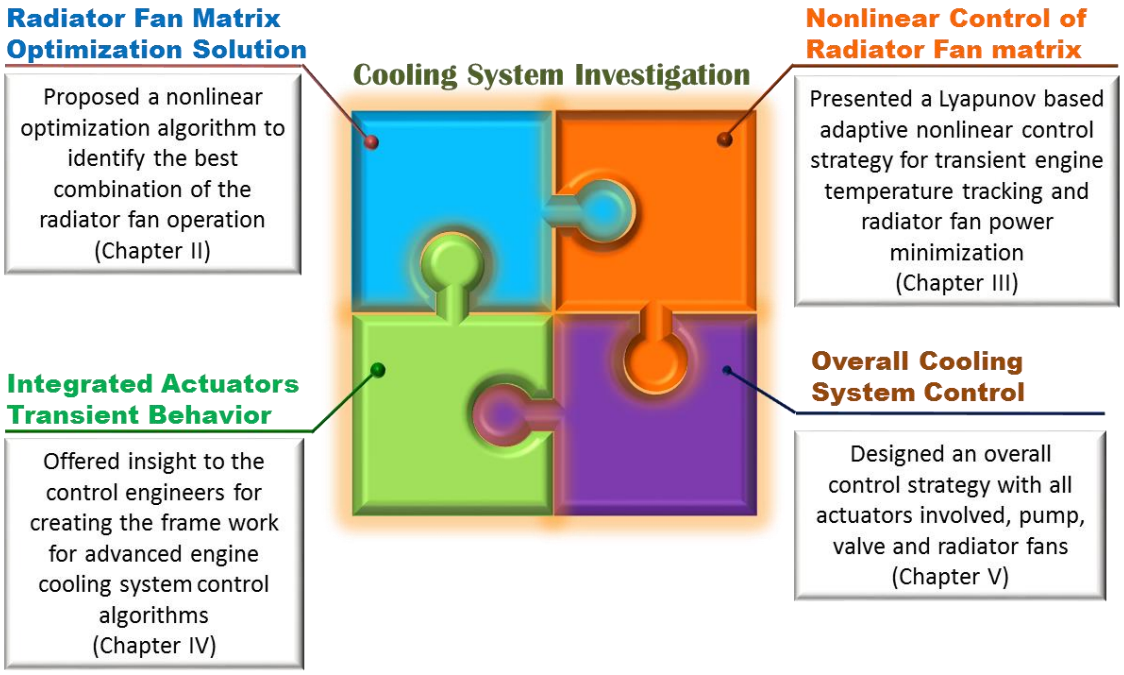

Figure 1.4: Outline of the dissertation

CHAPTER II

OPTIMIZATION OF AN AUTOMOTIVE RADIATOR FAN ARRAY OPERATION TO REDUCE POWER CONSUMPTION

The cooling system for internal combustion engines removes waste heat to ensure a normal in-cylinder combustion process. To accomplish this task, the thermostat valve, radiator, radiator fan(s), and water pump circulate cooling fluid through the engine block and reject heat to the local environment. Since the cooling system consumes a portion of the engine's power, it is important that its operation use minimal input energy. In this chapter, a multiple radiator fan matrix was controlled to minimize energy usage for subsequent efficiency gains. A mathematical model for the radiator fan(s) and the forced convection heat transfer process was developed to establish a mixed integer nonlinear programming problem. An interior points approach was introduced to solve the minimization problem. A series of laboratory tests have been conducted with different fan and speed combinations, with the objective to cool a thermal loaded engine. Both the mathematical approach and test results indicated similar control strategies. Based on the tests data and accompanying mathematical analysis, an optimization control strategy reduced the fan matrix power consumption by up to 67% for the specified thermal load. An improvement in cooling system performance can offer greater vehicle fuel economy to help meet legislated mobility standards.

2.1 Introduction

The cooling system in gasoline and diesel engines serves an important role in maintaining the desired coolant temperature for enhanced performance (Melzer *et al.*,

1999 and Chastain *et al., 2010*). If the engine operates too hot, then abnormal in-cylinder combustion may occur leading to degraded fuel economy and tailpipe emissions. Approximately 25% of the total petroleum energy converted during the spark ignition engine combustion process is lost to the cooling system (Heywood, 1988). As a result, the cooling system must accommodate a significant amount of heat while working under ambient operating conditions. The cooling system also consumes a portion of the crankshaft power, so it is important to develop an optimization control method for minimum power consumption by the thermal system actuators. An interesting cooling system configuration is a radiator fan array with distributed actuators under real time computer control.

A number of research studies have been conducted to investigate the modeling and analysis of advanced vehicle thermal management systems. Mitchell *et al.* (2009) examined the role of thermostatic valves in vehicle cooling systems, comparing the performance of various system designs. Chanfreau *et al.* (2003) developed a method of controlling fan valves and pump actuators to improve cooling system efficiency. Wagner *et al.* (2002) studied the integration of an electrical water pump and an intelligent thermostat valve to achieve faster engine warm-up, reduced temperature fluctuation, and efficient cooling. Page *et al.* (2005) investigated a classical proportional-integral-derivative control system featuring multiple electric radiator fans with heat controlled valves or thermostats. Badekar *et al.* (2006) described a microprocessor-based controller for automotive radiator fans to reduce power consumption and to optimize component size. Salah *et al.* (2005 and 2010) designed a nonlinear control strategy for adjusting the smart valve position and the coolant flow speed to track the desired transient temperature. Although these

articles focused on automotive thermal management, a radiator fan array with speed control was not examined in the context of power reduction.

Forced heat transfer convection, which depends on the size and type of cooling system, may be required in addition to natural (or free) radiator convection. Increased control of the fan motors is possible with electric actuators as they have the potential of making the decoupled fan matrix cooling system energy efficient which may lead to a reduction in engine fuel consumption. In addition, a highly controllable cooling system running on feedback from dynamically acquired sensor data using embedded control algorithms has been shown to help reduce tailpipe emissions (Choi *et al.,* 2007). A number of researchers (Regin 2010, Dube *et al.,* 2007, and Fukano, *et al.,* 2004) have investigated numerical and computational fluid dynamics (CFD) methods to describe the air dynamics within vehicle radiator systems. However, no detailed or validated mathematical model has been published in the open literature which describes the relationship between radiator electric fan matrix operating conditions and the forced convection heat rejected from the radiator.

The optimization of multiple radiator fan(s) speeds to minimize energy usage for certain efficiency gains can impact engine performance. This chapter presents a detailed mathematical model to accurately describe the forced convection heat transfer process in internal combustion engines using multiple variable speed radiator fans. Based on this lumped parameter system model, a nonlinear optimization algorithm has been developed to identify the best combination of the electric motor fan operation. In addition, according to a series of designed experimental tests, a general "Rule of Thumb" is proposed for

the cooling system operation that does not use a mathematical foundation. The control method contained in this chapter establishes a basis for future controller designs.

The remainder of the chapter is organized as follows. In Section 2.2, a mathematical model of the prototype cooling system and fan matrix is offered. The optimization problem is introduced and the interior point method applied to solve this problem in Section 2.3. In Section 2.4, a forced convection cooling system experiment with an electric fan array is created. The test results and engineering analysis of the experiments are presented and discussed in Section 2.5. Finally, the summary is offered in Section 2.6.

2.2 Mathematical Model

The research objective was to cool an internal combustion engine with a matrix of electric radiator fans to minimize power consumption by selecting different fan combinations and motor speeds. To formulate the optimization problem, the governing equations for the thermal system dynamics are derived for the feedback control diagram in Figure 2.1. In this analysis, a series of seven assumptions may be imposed on the thermal system:

A1: No heat losses in the system occur other than forced convection through the radiator.

A2: The heat output from the radiator equals the heat input from the engine at steady-state operation, $q_{in} = q_{out}$.

A3: Ram air effects may need to be considered due to vehicle motion and/or wind.

A4: System temperatures and fluid flows are measured using available sensors.

A5: Coolant flows entirely through the radiator and not the by-pass circuit based

on the thermostat.

A6: Water pump operation is fixed so that system heat rejection is based on fan speeds.

A7: Air temperature drop, ΔT, across the radiator is a known constant.

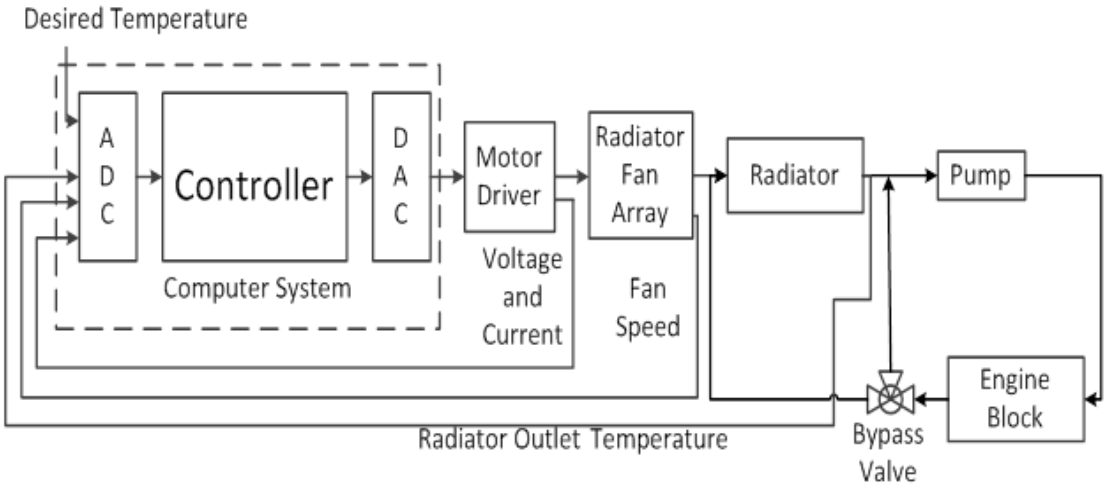

Figure 2.1: Block diagram for radiator fan controller system

2.2.1 Estimation of Heat from Combustion Process

An analytical model for the combustion process generated heat that must be expelled through forced air convection by the radiator fans can be calculated. The heat rejection rate from the engine combustion cylinders to the coolant flowing through the block water jackets, q_c, may be stated (Taylor *et al.*, 1957) as

$$q_c = UA_p(T_g - T_c) \tag{2.1}$$

where U is the overall heat transfer coefficient, A_p is the piston head surface area, T_g is the mean effective gas temperature, and T_c is the coolant temperature. For a given engine application, the variable T_g can either be directly measured by an in-cylinder sensor or

obtained from table look up based on the air/fuel ratio, spark angle, and load per calibration. In this study, the heat rejection from the combustion process is considered to be the input heat supplied to the engine block by an external heat exchanger custom designed for the laboratory test.

The heat supplied to the cooling system, q_{in}, is based on the low pressure steam heat exchanger temperature for the experimental laboratory system, which can be expressed as

$$q_{in} = \dot{m}_{cool} Cp_{cool} (T_{HI} - T_{HO}) \tag{2.2}$$

where $\dot{m}_{cool}$ is the coolant mass flow rate due to the pump, Cp_{cool} is the specific heat of the coolant at constant pressure, and T_{HI} and T_{HO} are the heat exchanger inlet and outlet temperatures, respectively.

2.2.2 Heat Rejected from Radiator and Ram Air Effect

To minimize the power consumed by the radiator fan(s), the heat rejected by forced convection must be adjusted through fan motor speed control. The rate of heat rejection from the radiator, q_{out}, can be expressed as

$$q_{out} = \varepsilon_a \dot{m}_{air} Cp_a (T_{aout} - T_\infty) \tag{2.3}$$

where T_{aout} is the air temperature exiting the radiator, T_∞ is the air temperature at the radiator inlet (ambient temperature), and Cp_a is the specific heat of the air. The radiator heat transfer efficiency, $0 < \varepsilon_a < 1$, depends on the air mass flow rate. In this analysis, a quadratic relationship $\varepsilon_a = a\dot{m}_{air}^2 + b\dot{m}_{air} + c$ was selected where a, b and c are constants (Shome *et al.*, 2006). Please refer to the Appendix A for the selection of the a, b and c values.

The variable $\dot{m}_{air}$ denotes the air mass flow rate through the radiator and may be calculated as

$$\dot{m}_{air} = Q_{air}\rho_{air} = v_{air}A_r\rho_{air} \tag{2.4}$$

where Q_{air} is the volume flow rate, A_r is the radiator area, ρ_{air} is the air density, and v_{air} is the air flow velocity through the radiator. This velocity is a combination of two different sources: the radiator fan(s), and the ram air effect. The total air flow velocity, although complex, can be simplified as

$$k_r v_{air}^2 = k_I v_{ram}^2 + k_f v_f^2 \tag{2.5}$$

where $k_r, k_I,$ and k_f are the pressure coefficients at the radiator, air inlet, and fan respectively as indicated in Figure 2.2.

The expression (2.5) may be rewritten to calculate the air velocity through the radiator as

$$v_{air} = \sqrt{\frac{k_I}{k_r} v_{ram}^2 + \frac{k_f}{k_r} v_f^2} \tag{2.6}$$

The volume flow rate, Q_{air}, and mass flow rate, $\dot{m}_{air}$, in equation (2.4) can now be rewritten as

$$\dot{m}_{air} = \rho_{air}\sqrt{\frac{k_I}{k_r} v_{ram}^2 A_r^2 + \frac{k_f}{k_r} v_f^2 A_r^2} = \rho_{air}\sqrt{\frac{k_I}{k_r} Q_{ram}^2 + \frac{k_f}{k_r} Q_f^2} = \sqrt{\frac{k_I}{k_r} \dot{m}_{ram}^2 + \frac{k_f}{k_r} \dot{m}_f^2} \tag{2.7}$$

where $Q_{ram} = v_{ram}A_r$ and $Q_f = v_f A_r$ are the volume flow rates caused by the ram air effect and fan matrix, respectively. The variables $\dot{m}_{ram} = Q_{ram}\rho_{air}$ and $\dot{m}_f = Q_f\rho_{air}$ denote the ram air and fan air mass flow rates. To obtain the general function for system heat rejection, equation (2.3) may now be rewritten as

$$q_{out} = \varepsilon_a \left(\sqrt{\frac{k_I}{k_r} \dot{m}_{ram}^2 + \frac{k_f}{k_r} \dot{m}_f^2} \right) Cp_a (T_{aout} - T_{ain}) \tag{2.8}$$

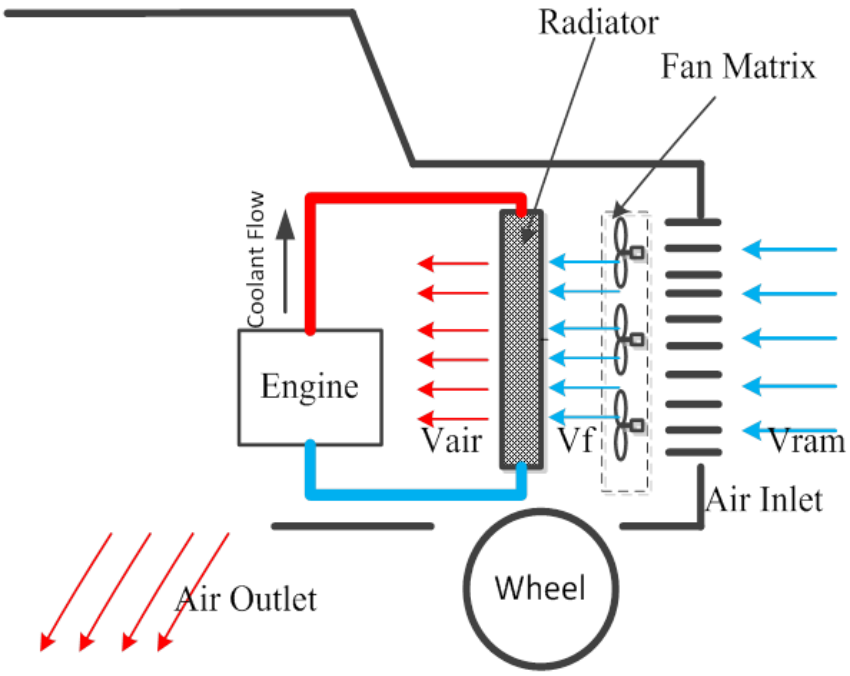

Figure 2.2: Simplified air flow circuit (side view of vehicle)

2.2.3 Fan Laws and Power Consumption

The relationship between the electrical power and fan matrix configuration (fan speed and fan number) must be derived to form the objective equation. The nonlinear function between the fan torque, τ, and the motor speed, N, may be expressed (Lelkes *et al.*, 2004) as

$$\tau = k{N_f}^2 \tag{2.9}$$

where the factor k for fans depends on the blade design and its characteristic curve. However, the factor k tends to be typically independent of the motor. As a result, the electrical power, P_e, of the fan with speed N_f may be determined by introducing the effi-

ciency, η, which is the ratio between the mechanical output power and the electrical input power so that

$$P_e = \frac{P_m}{\eta} = \frac{\tau\omega}{\eta} = \frac{2\pi k}{60\eta} {N_f}^3 \tag{2.10}$$

In this expression, P_m is the mechanical output power. As an alternative, the electrical power can also be determined as $P_e = iV_s$, where i is the current and V_s is the supply voltage.

Further justification for this relationship is based on the fan laws (Jorgensen, 1982) given by

$$\frac{P_1}{P_2} = \left(\frac{N_{f1}}{N_{f2}}\right)^3 \left(\frac{d_1}{d_2}\right)^5 \left(\frac{\rho_{air1}}{\rho_{air2}}\right) \tag{2.11}$$

In other words, the mechanical power can be directly related to the cube of the speed when the diameter and density are constant.

The efficiency, η, of the mechanical output to electrical input power may be represented as a polynomial function of the motor speed, N_f, assuming an uniform load. In this research, a quadratic expression has been considered whose general form may be expressed as

$$\eta = d{N_f}^2 + eN_f + f \tag{2.12}$$

where $d, e,$ and f are constants. The methodology to the select the values of d, e, and f are provided in the Appendix A. Using this relationship, equation (2.10) may now be rewritten as

$$P_e = \frac{2\pi k}{60(d{N_f}^2 + eN_f + f)} {N_f}^3 \tag{2.13}$$

The volume flow rate, Q_f, through a single fan can also determine the required

fan motor speed. The speed for a single axial fan to generate a target volume flow rate may be stated as

$$N = \frac{60Q_f}{4\pi^2 r_m^3 \Phi_m}\left(\frac{1+v^2}{1-v^2}\right) \tag{2.14}$$

where r_m is the mean radius, v is the hub ratio, and Φ_m is the flow rate coefficient.

The fan air mass flow rate, $\dot{m}_f$, can be determined by rewriting this expression as

$$\dot{m}_f = \frac{4\pi^2 \rho_{air} r_m^3 \Phi_m N_f n}{60}\left(\frac{1-v^2}{1+v^2}\right) \tag{2.15}$$

The integer variable n was introduced to denote the number of operating fans in parallel in the radiator configuration. The mean radius, r_m, is dependent on the fan tip and hub radius, r_t and r_h, such that

$$r_m = \sqrt{\frac{1}{2}({r_t}^2 + {r_h}^2)} \tag{2.16}$$

Similarly, the hub ratio, v, may be calculated as

$$v = r_h/r_t \tag{2.17}$$

Finally, the flow rate coefficient, Φ_m, may be obtained for axial flow fans using specific speed and pitch cord ratios (Jorgensen, 1982).

Based on the analysis above, substitute equation (2.15) into equation (2.8), the general function for system heat rejection may be rewritten as

$$q_{out} = \varepsilon_a \sqrt{\frac{k_I}{k_r}\dot{m}_{ram}^2 + \frac{k_f}{k_r}\left(\frac{4\pi^2 \rho_{air} r_m^3 \Phi_m N_f n}{60}\left(\frac{1-v^2}{1+v^2}\right)\right)^2}\, Cp_a(T_{aout} - T_\infty) \tag{2.18}$$

In this chapter, no ram air effects are considered which leads to $\dot{m}_{ram} = 0$, and corresponds to a stationery engine scenario. The application for this case may be a parked vehicle without blowing wind (e.g., silent sentry mode) or an engine-based generator.

Thus, equation (2.18) can be expressed as

$$q_{out} = \varepsilon_a \frac{4\pi^2 \rho_{air} r_m^3 \Phi_m N_f n}{60} \left(\frac{1-v^2}{1+v^2}\right) \sqrt{\frac{k_f}{k_r}} Cp_a (T_{aout} - T_\infty) \tag{2.19}$$

Refer to Appendix B for the details regarding the mathematical model validation efforts.

2.3 Optimization Problem

The theoretical relationship between the fan power consumption and the heat rejected for various fan configurations and fan(s) speeds has been derived. Now an optimization problem is formulated and applied to solve this smart cooling system challenge for power minimization which meets heat transfer demands.

2.3.1 Problem Description

The governing system dynamics stated in equation (2.13) and (2.19) are well suited for a mixed integer nonlinear programming (MINP) which may be expressed as

$$min\ f(N_f, n) \tag{2.20a}$$

$$\text{subject to:} \quad h(N_f, n) = 0 \tag{2.20b}$$

$$g(N_f, n) \leq 0 \tag{2.20c}$$

where N and integer n are programming variables. The objective function, $f(.,.)$, may be stated as

$$f(N, n) = P_e = \frac{2\pi k}{60(d{N_f}^2 + eN_f + f)} {N_f}^3 \tag{2.21}$$

For equations (2.20b) and (2.20c), the equality and inequality constraints $\mathrm{h(N_f, n)}$ and $g(N_f, n)$ can be described as

$$h(N_f, n) = q_{out} - q_{in} = \varepsilon_a \frac{4\pi^2 \rho_{air} r_m^3 \Phi_m N_f n}{60} \left(\frac{1-v^2}{1+v^2}\right) \sqrt{\frac{k_f}{k_r}} Cp_a (T_{aout} - T_\infty) - q_{in} \quad (2.22)$$

$$g(N, n) = \begin{cases} N_{low} \le N_f \le N_{high} \\ 1 \le n \le n_{max} \end{cases} \quad (2.23)$$

where N_{low}, N_{high}, and n_{max} denote the lower and upper fan speeds plus the maximum number of operating fans.

The notation in equations (2.21) and (2.22) may be simplified by defining two constants g and h which $g = \frac{2\pi k}{60}$ and $h = \frac{4\pi^2 \rho_{air} r_m^3 \Phi_m}{60} \sqrt{\frac{k_f}{k_r}} \left(\frac{1-v^2}{1+v^2}\right) Cp_a$. In addition, let $\Delta T = T_{aout} - T_\infty$ correspond to the air temperature drop across the radiator.

The objective function and equality constraint of equation (2.21) and (2.22) may now be expressed as

$$f(N_f, n) = \frac{g}{(dN_f{}^2 + eN_f + f)} n N_f{}^3 \quad (2.24)$$

$$h(N_f, n) = \varepsilon_a h N_f n \Delta T - q_{in} \quad (2.25)$$

The value of ΔT (approximately $10°C \rightarrow 20°C$) does not significantly affect the optimization results if assumed to be a user-specified constant. In this analysis, all the fans were assumed to have uniform rotational speeds.

2.3.2 Optimal Solution to Radiator Fan Consumption

To solve this MINP problem, a related nonlinear constrained programming (NCP) problem is introduced to determine successive solutions, (N_s, n_s). With the Matlab optimization package, the successive solutions may be first calculated. The function "*fmincon*" provides various types of algorithms; the interior-point approach to constrained minimization was selected to solve a sequence of nonlinear programming minimization prob-

lems. Refer to (Byrd *et al.*, 1999 and Biggs *et al.*, 1975) for more details.

The gradient of the objective function, $f(.,.)$, in equation (2.24) may be expressed as

$$\nabla f = \left[\frac{\partial f}{\partial N_f}, \frac{\partial f}{\partial n}\right] = \left[\frac{(dN_f{}^2+2eN_f+3f)gnN_f{}^2}{(dN_f{}^2+eN_f+f)^2}, \frac{gN_f{}^3}{(dN_f{}^2+eN_f+f)}\right] \tag{2.26}$$

which establishes the search direction for the optimization algorithm. To obtain an integer value for the number of fans, n, per given heat load, q_{out}, the system calculates the two nearest points around the successive solution, (N_s, n_s). The point that does not satisfy the stated constraints is dropped. If both of the two points both satisfy the constraints, then the objective function is calculated based on each point. The point which leads to the smallest objective function value is selected as the best solution.

2.4 Experimental System Construction

A test bench was created to provide a safe and repeatable approach for studying automotive engine cooling systems. The experimental station features a wind tunnel and complete set of thermal actuators (variable speed pump, smart valve, and radiator with electric fans) and assorted sensors. A 6.8L International Truck V8 diesel engine with controller area network (CAN) bus controlled the 3×2 fan matrix. Figure 2.3 shows the overall system design which also features a steam drive heat exchanger to mimic the internal combustion engine in-cylinder thermal source while creating a test environment for exact heat situation.

2.4.1 Heat Source (Steam Supply)

In this experimental bench, a low pressure (LP) steam source simulates the heat

generated by the engine. The steam transfers through a multi-pass heat exchanger to the coolant system which then circulates through the conventional automotive cooling system. Safety equipment such as a pressure regulator, pressure gauge, and safety valve were inserted into the steam system. In this project, the flow rate of the LP steam was constant.

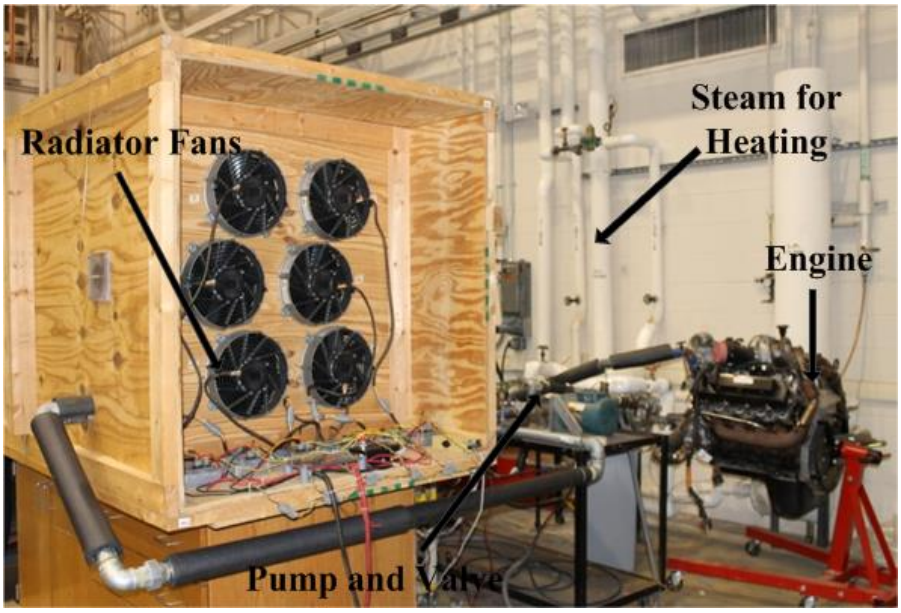

(a)

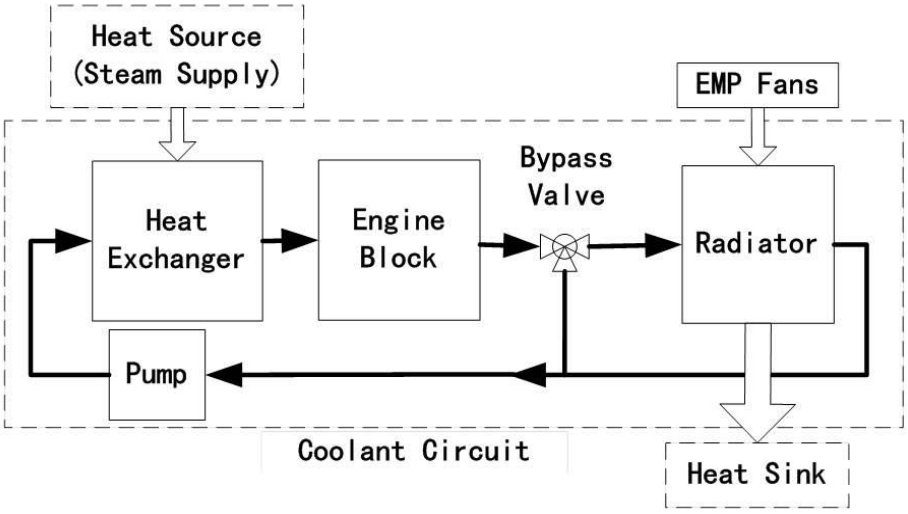

(b)

Figure 2.3: (a) Picture of experimental testing bench, and
(b) system block diagram

2.4.2 Coolant Flow Circuit

The coolant flow circuit consisted of a LP heat exchanger, engine cooling jacket, bypass valve, variable speed coolant pump, and radiator with fan matrix. The coolant received heat from the steam in the multi-pass heat exchanger and then was pumped into the engine block cooling jacket. From the outlet of the engine cooling jacket, the coolant flows into the directional control valve which, according to the computer-based set point temperature, diverts the coolant back into the engine heat exchanger or lets it flow to the radiator. The variable speed coolant pump was driven by an AC motor controlled by the computer algorithm.

For this study, the DC motor thermostat direct all fluid through the radiator. The coolant enters the radiator from the top inlet port and flows through a mesh of tubes with attached fins, expelling its heat energy to the ambient surroundings. The fluid exits through an outlet in the bottom portion of the radiator into the centrifugal pump. The pump circulates it back to the steam heat exchanger, thus completing the cycle. Insulated galvanized pipes and pipe connections were used to transport the coolant between the various system components.

2.4.3 Wind Tunnel

A wind tunnel was constructed to measure the air flow and pressure drop across the radiator on the experimental bench. The wind tunnel has a rectangle matrix arrangement with six fans arranged in three rows and two columns. Each of the fans was connected to a CAN based DC motor controller; the controllers were connected to be CAN card plugged in the computer PCI port. The fan motors are EMP Fil-11 electric with $24V$

brushless DC motors and $0.6kW$ rating power. According to experimental motor results, the relationship between efficiency and speed in equation (2.14) has been concluded.

2.4.4 Sensors, Data Acquisition, and Computer Interface

The experimental bench contained electrical, electronic, and computer subsystems to acquire, process, record, and display data generated during the test runs. Figure 2.4 shows the data flow path. The sensors used in this experiment included an air speed sensor, a turbine type flow meter, a linear variable differential transducer, five thermocouples, and an ammeter.

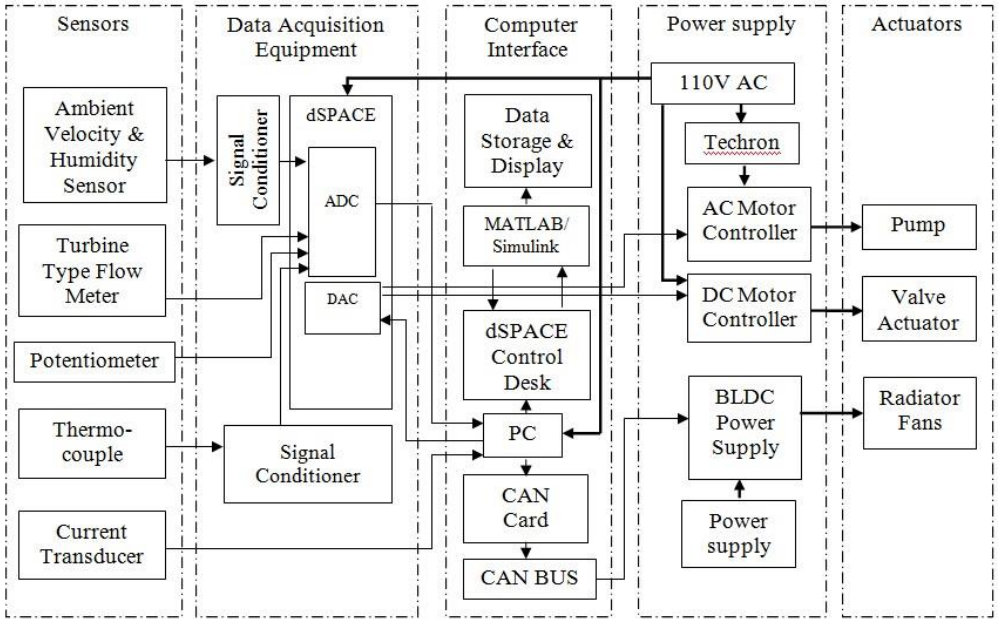

Figure 2.4: Block diagram for data flow among the sensors, data acquisition equipment, computer interface, and actuators

The continuous analog data were then supplied to the dSPACE data acquisition system. The computer interface included the software programs MATLAB/Simulink with the Vehicle Network Tool (VNT) box, and dSPACE. The signal inputs were received

through the dSPACE hardware board, while the output control signals were transmitted via the dSPACE DAC and the CAN bus controller.

2.5 Test Results and Discussion

A series of six tests (varies fan configurations and operating scenarios) were experimentally investigated to study system heat rejection and radiator fan power consumption. The corresponding numerical optimization results were compared with these test results to evaluate the prescribed operating strategy. The system model parameters are listed in Table 2.1 for the optimization problem. In this section, the optimization results are presented and discussed.

Table 2.1: Summary of system model parameters

Symbol	Value	Units	Symbol	Value	Units
A_r	1.1	m^2	$\dot{m}_{cool}$	1.1	kg/s
a	0.0029	$(s/kg)^2$	n_{max}	6	-
b	-0.072	s/kg	N_{high}	5,000	RPM
c	0.86	-	N_{low}	1,000	RPM
Cp_a	1	$kJ/kg \cdot °C$	r_t	0.14	m
Cp_{cool}	4.18	$kJ/kg \cdot °C$	r_h	0.056	m
d	-5.6e-8	$(min/rev)^2$	T_∞	293.5	$°C$
e	5.3e-4	min/rev	ΔT	18	$°C$
f	-0.38	-	ρ_{air}	1.1	kg/m^3
$(k_f/k_r)^{0.5}$	0.78	-	v	0.4	-
k	4.03e-11	-	Φ_m	0.85	-

2.5.1 Fan Matrix and Speed Configuration

The coolant flow direction through radiator is shown in Figure 2.5 for test configuration #1. The indicates that the hottest area of the radiator is right behind fan No. 2 which correspond to the radiator inlet location, similarly, the region behind fans No. 2, 4,

6 are hotter than that behind fans No. 1, 3, 5. Based on this phenomenon, a design of experiment (DOE) can be considered as follows, six various fan combinations were designed to evaluate the fan effect. The fan combinations based on experimental observation and fluid flow inlet condition were selected as shown in Figure 2.5 and the respective operational speeds as listed in Table 2.2. The fan(s) were connected and controlled by the CAN bus based on the control strategy.

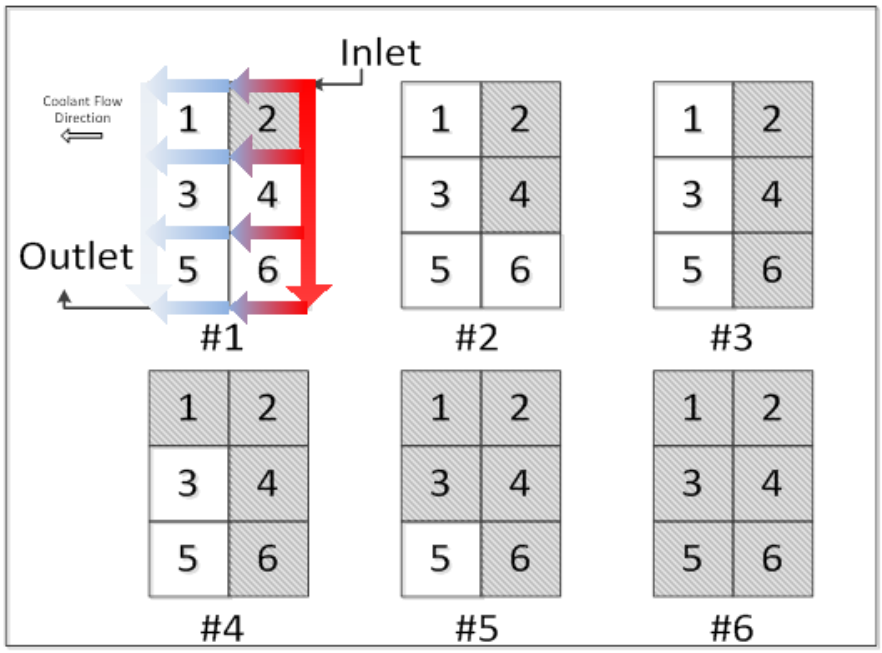

Figure 2.5: Fan selection (shaded) at different speeds for six test configurations (I-VI), the color arrows show the coolant temperature trend through the radiator

2.5.2 Fan Power Consumption

The fan(s) motors voltage, V_s, and the current, i, were used to calculate the power consumption, $P_e = iV_s$. The steady state DC power consumption values were measured and calculated for the given fan number and operating fan(s) speeds. This fan power con-

sumption data was essential in determining the energy usage for the cooling system for a given engine heat load. Figure 2.6 displays the plot of the fan(s) motor electrical power consumption, P_e, for the various fan number, n, with the fan(s) motor speeds, N_f. This graph indicates the general trend that the increased power consumption is dependent on the number of fans and operating speeds. However, there were exceptions observed at $3{,}000RPM$ for the single fan (Test I) and for the five fans (Test V) combinations. In these two cases, the power consumption increased. The power consumption was observed to be almost equal for speeds up to $3{,}000RPM$ when either five (Test V) or six (Test VI) fan motors operated. However, all the fan motor combinations have a comparatively smaller variation in power consumption for motor speeds up to $2{,}000RPM$. According to (Moyle *et al.*, 2006), mechanical fans consume $24kW$ to $50kW$ of engine power to operate. In comparison, radiator electric fans require approximately $0.7kW$ which offer significant energy saving itself.

Table 2.2: Six fan matrix and electric motor speed combinations for the experimental tests

Test No.	Heat Exchanger Outlet Temp, T_{HO} $(°C)$	Ambient Temp, T_∞ $(°C)$	Coolant Flow Rate, $\dot{m}_{cool}$ (kg/s)	Fan Speed Range, N_f, (RPM)	Operating Radiator Fans 1 2 3 4 5 6
I	78-81	22	1.1	1,000 to 5,000 in 1,000 increments	•
II	79-82	24			• •
III	79-81	22			• • •
IV	78-81	23			• • • •
V	79-82	23			• • • • •
VI	78-81	23			• • • • • •

2.5.3 Fan Matrix Performance

The heat rejected versus fan power at various fan speed and fan numbers has been displayed in Figure 2.7 over a $0kW < P_e < 4kW$ operating range. The graphs represent four parameters; heat rejected, q_{out}, fan speed, N_f, fan number, n, and the fan electric power consumption, P_e. The rejected heat is considered as the objective system input, and then both the fan number and the fan(s) speeds were selected to achieve the heat rejection requirement. This graph should offer guidance in selecting the best energy efficient fan number and speed for a given heat load. The odd point in Test I at heat rejected on $20kW$ and fan power at $0.28kW$ may be attributed to diversity of different fans model.

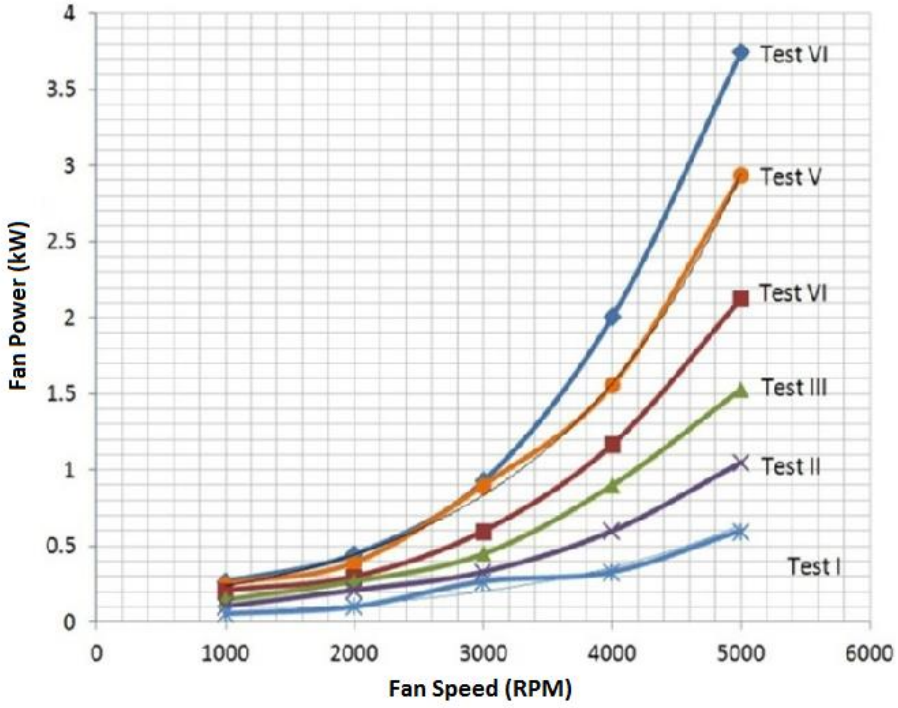

Figure 2.6: Fan motor power consumption, P_e, for various fan configurations and fan speeds, N_f, based on experimental tests to validate the nonlinear relationship between fan speed and power consumption

2.5.4 Discussion of Experimental Results

The data obtained from the experiments indicated that reduced energy consumption can be achieved for heat rejection rates above $q_{out} > 56kW$ using all six fan operating configuration. However, when heat rejection need below $56kW$, other fan configurations were observed to be more energy efficient. For example, a heat rejection rate of $48kW$ shows Test V with a fan matrix power consumption of $P_e = 0.3kW$ while Test VI was $0.33kW$. For heat rejection in the zone $0kW < q_{out} < 16kW$, Test I operated in the range of $1{,}000RPM < N_f < 2{,}000RPM$. Next, the zone of $16kW < q_{out} < 24kW$ and $24kW < q_{out} < 35kW$ corresponds to Test II and III at $N_f = 1{,}000RPM$, respectively. If $35kW < q_{out} < 43kW$, then the Test IV should operate at $1{,}000RPM < N_f < 2{,}000RPM$. Finally, $43kW < q_{out} < 56kW$ and $q_{out} > 56kW$ results in Test V and Test VI at $N_f = 2{,}000RPM$, respectively.

2.5.5 Rule of Thumb and Numerical Optimization Control Strategy

According to the experimental results show on Figure 2.7, a general rule of thumb can be formulated. For heat rejection between $0 - 56kW$, first start with a single fan (Test I) and operate at $N_f = 1{,}000 - 2{,}000RPM$. If more heat rejection is needed, then bring another fan online (Test II – Test V) till all the six fans (Test VI) operate at $N_f = 1{,}000RPM$ (perhaps $2{,}000RPM$ if needed). Above a heat rejection threshold of $56kW$, use all six fans and increase the fan speed as needed to $5{,}000RPM$. Table 2.3 shows the best combination for experimental heat rejection and power configuration with the heat rejection below $56kW$.

Table 2.3: Rule of thumb combination for heat rejection and fan power consumption

Heat Rejected, $q_{out}\ (kW)$	Fan Number, n	Fan Speed, N_f (RPM)	Fan Power, $P_e\ (kW)$
0-16	1	1,000-2,000	0-0.10
16-24	2	1,000	0.10-0.18
24-35	3	1,000	0.18-0.23
35-43	4	1,000-2,000	0.23-0.30
43-56	5	2,000	0.30-0.39
56+	6	2,000+	0.39+

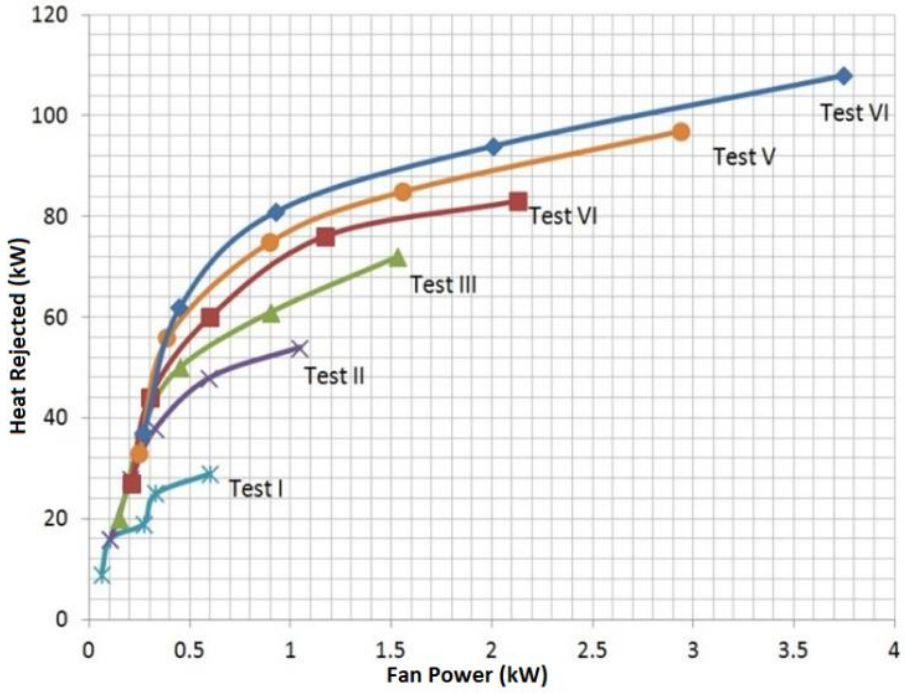

Figure 2.7: Fan power, P_e, verses heat rejection, q_{out}, at various fan and speed configurations based on experimental tests

The numerical optimization strategy offers an alternative approach to the rule of thumb. Figure 2.8 shows the theoretical relationship between the fan power and heat rejection for various configurations and speeds based on Section 2.3. Notice the similarity of the experimental and theoretical curves in Figures 2.7 and 2.8. It suggests the similar

trends which demonstrated that the mathematical model is valid.

Using an interior-point approach to solve the nonlinear optimization problem, the optimization results are calculated and displayed in Figure 2.9 for the ideal selection of fan number, n, and fan(s) speeds, N_f to achieve specific heat rejection. Representative results are listed in Table 2.4. According to Figure 2.9 and Table 2.4, an optimization control strategy can be concluded. First, turn on a single fan with its speed at $N_f = 1{,}000RPM$, and increase the speed to achieve the increasing heat rejection requirement. Second, turn on the other fans one by one and adjust the corresponding fan(s) speeds. It can be easily demonstrated that this method is similar to the rule of thumb based on the experiments results in Table 2.3.

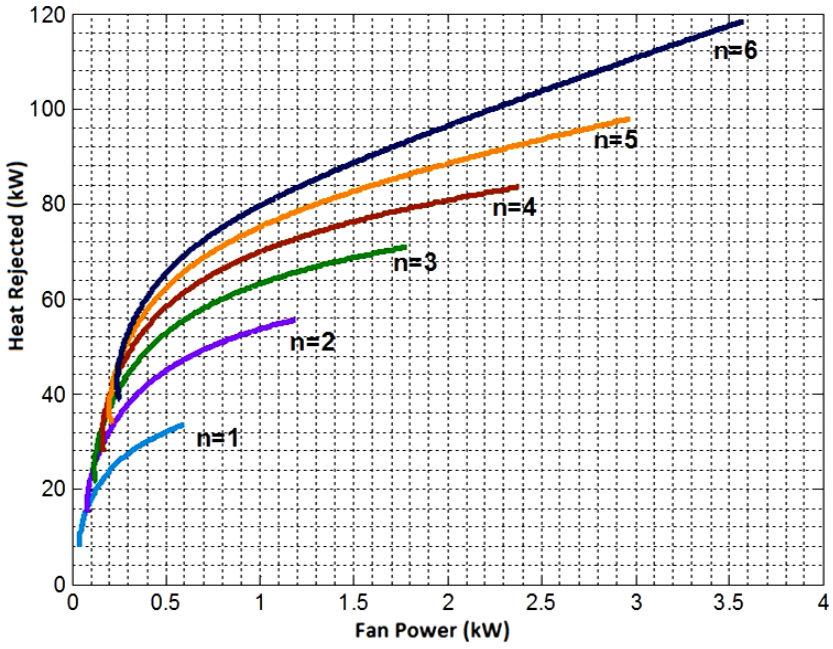

Figure 2.8: Theoretical relationship between the fan power, P_e, and heat rejection, q_{out}, at various fan configurations ($n = 1 - 6$) and speeds

Table 2.4: Optimization solutions for the radiator fan array

Heat Rejected, q_{out} (kW)	Number of Fans, n	Fan Speed, N_f (RPM)	Fan Power, P_e (kW)
0-19	1	1,000-2,994	0-0.09
20-28	2	1,385-2,062	0.09-0.13
29-36	3	1,414-1,824	0.14-0.18
37-42	4	1,447-1,679	0.19-0.22
42-48	5	1,446-1,645	0.23-0.26
49+	6	1,495+	0.27+

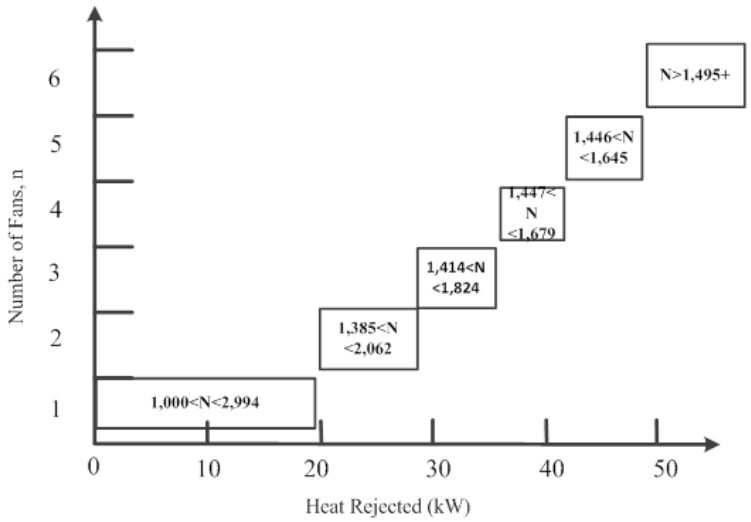

Figure 2.9: Optimization control strategy for the fan number, n, heat rejection, q_{out}, and corresponding fan speed, N_f

To illustrate the concept, two specific case studies are considered. In the first case, $q_{out} = 30kW$ is selected as the heat rejection. The power fan consumption is $P_e = 0.6kW$ for experimental results verses $P_e = 0.51kW$ for the theoretical results when a single fan operates. For the optimization control method, the minimum consumption will reduce to $P_e = 0.2kW$ for experimental result ($P_e = 0.16kW$ for theoretical result) when $n = 3$ fans are operated. In this case, the energy saving is up to 67%. In case 2, the heat rejection selected is $q_{out} = 60kW$. Fan number $n = 3$ is selected as the comparison with

the optimization result. It indicates that the power consumption is $P_e = 0.9kW$ for experimental results ($P_e = 0.81kW$ for theoretical results) when $n = 3$ fans operate. On the other hand, based on the optimization result, the minimum consumption is approximately $P_e = 0.4kW$ for experimental result ($P_e = 0.38kW$ for theoretical result) when $n = 6$ fans are engaged. The total energy saving corresponds to 55%. For these studies, corresponding fan power consumption for both experimental and theoretical result are shown in Table 2.5.

2.6 Summary

An optimization control method for automotive thermal management systems can have a positive impact on the cooling system. This chapter has studied and analyzed a multiple electric fan radiator cooling configuration using an experimental bench and offline mathematic analysis. According to the experiment and simulation results, a rule of thumb and optimization control strategy were introduced which can reduce the fan matrix power consumption for the specified cooling load. In this study, the power consumption was reduced by approximately 67%.

Table 2.5: Case study - Fan power consumption, P_e, for different fan combinations

		$P_e(kW)$ theoretical, experimental		
Case	Heat Rejected, q_{out} (kW)	Fan No. $n = 1$	Fan No. $n = 3$	Fan No. $n = 6$
1	30	0.60, 0.51	0.20, 0.16	NA
2	60	NA	0.90, 0.81	0.40, 0.38

The methodology proposed in this chapter can be used for different radiator fan configurations and heat exchanger sizes to establish operating regime calibrations. The

mathematical model can also be used to develop nonlinear control strategies in future work. For instance, a nonlinear controller is under development based on this chapter's result to regulate the engines working temperature to a precise temperature range.

If the optimization algorithm, or a simplified minimization strategy, is constrained by microprocessor speed, then a real time system can be realized based on table look-ups from either the optimization findings or the "Rule of Thumb" derived from the experimental test results. To further extend the research achievement, the optimization control strategy can also be applied to other transportation applications such as battery pack and electric motor cooling in hybrid powertrain.

CHAPTER III

A SMART ENGINE COOLING SYSTEM – EXPERIMENTAL STUDY OF INTEGRATED ACTUATOR TRANSIENT BEHAVIOR

Smart thermal management systems can positively impact the performance, fuel economy, and reliability of internal combustion engines. Advanced cooling systems typically feature multiple computer controlled actuators: a three way smart valve, a variable speed pump, and a variable speed electric radiator fan(s). To investigate the contributions of these electro-mechanical devices, a scale multifunction test bench was constructed which integrated these actuators, accompanying system sensors, and a controllable engine thermal load with real time data acquisition and control hardware/software. This chapter presents a series of experimental studies that focus on the engine's thermal transient response to various actuators input control combinations. The test results established a basis for several key operating conclusions. First, the smart valve and variable speed pump impact the engine temperature by changing the heat transfer rate between the engine and the radiator through coolant redirection and/or coolant flow rate. On the other hand, the radiator fan(s) operation affects the engine's temperature by changing the heat rejection rate of the radiator which can influence the entire cooling system. Third, the smart valve's operation changes the engine's temperature magnitude the greatest amount (4.0%) followed by the radiator fan(s) (1.6%) and coolant the pump (0.5%). Finally, from a power consumption aspect, the radiator fan(s) consumes the most engine power in comparison to the two other actuators. Overall, the experimental results offer insight to

the control engineers for creating the frame work for advanced engine cooling system control algorithms.

3.1 Introduction

The engine coolant temperature can significantly affect the performance of gasoline and diesel engines. The need for improved automotive efficiency has placed greater demands on the thermal management system (Shutty *et al.* 2013). In general, the engine works more efficiently at high temperatures for increased thermal efficiency (Wagner *et al.,* 2002). Further, high coolant temperature keeps the lubricate oil temperature in an ideal working range (95-100℃) which reduces friction (Kim *et al.,* 2013). However, if the power plant operates too hot, then abnormal in-cylinder combustion may occur which leads to degraded fuel economy and higher tailpipe emissions. Smart cooling systems can improve the engine's overall operating (Wambsganss *et al.,* 2013) by carefully adjusting the coolant temperature and heat removal rate to minimize the phenomenon of over cooling.

The cooling system also consumes a portion of the engine's total produced crankshaft power to operate the three actuators. In a traditional engine design, the cooling components, such as the pump and the radiator fan(s) are driven by the crankshaft. This feature doesn't allow accurate control the cooling actuators and causes unnecessary parasitic losses (Cho *et al.,* 2013). Furthermore, the conventional thermostat does not allow precise engine temperature control.

An advanced engine cooling system replaces the crankshaft driven pump and radiator fan(s) with computer controlled electric motor based variable speed pump and ra-

diator fan(s) (refer to Figure 3.1(a)). It also may use a three way smart valve to regulate fluid flow to the radiator and engine. With this approach, the valve position, coolant flow rate, and radiator fan(s) speed can be precise controlled to avoid unnecessary work and overcooling. Using electric motors can reduce the cooling system power consumption for the electric devices offer greater efficiency without the energy losses caused by the friction of the hydraulic drivers or clutches. The electric actuators can be operated after the engine has shut off to remove heat. Consequently, this cooling approach is applicable to hybrid vehicles for electric motors cooling too.

A number of research studies have been conducted on engine cooling systems. Khaled *et al.* (2012) provided experimental results that focused on the optimization of underhood cooling to reduce the vehicle's fuel consumption. Salah *et al.* (2005 and 2010) developed a nonlinear control method to adjust the engine's temperature based on a user specified temperature trajectory by synchronously adjusting the coolant pump flow rate and the valve position. Wagner *et al.* (2002) created a lumped mathematical real-time thermal model to represent the cooling system's heat transfer process. Brace *et al.* (2008) experimentally investigated the effect of water pump throttling, coolant flow control through the oil cooler, and the adoption of a pressure resistive thermostat. Chastain *et al.* (2010) studied multiple advanced thermal management system designs which demonstrated at least a 54% reduction in actuator power consumption compared to the factory cooling system configuration. Lastly, Wang *et al.* (2014) explored an optimal fan matrix control strategy to minimize the radiator fan power.

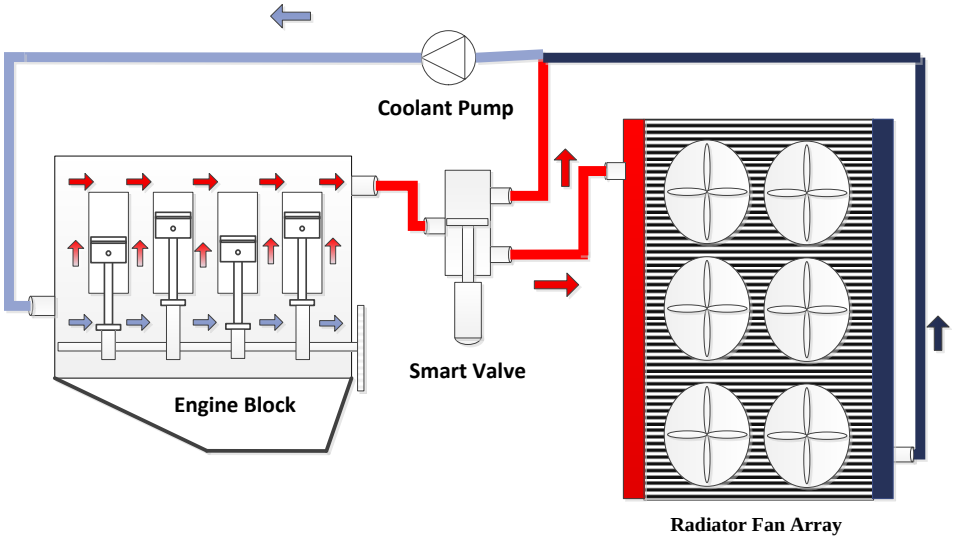

(a)

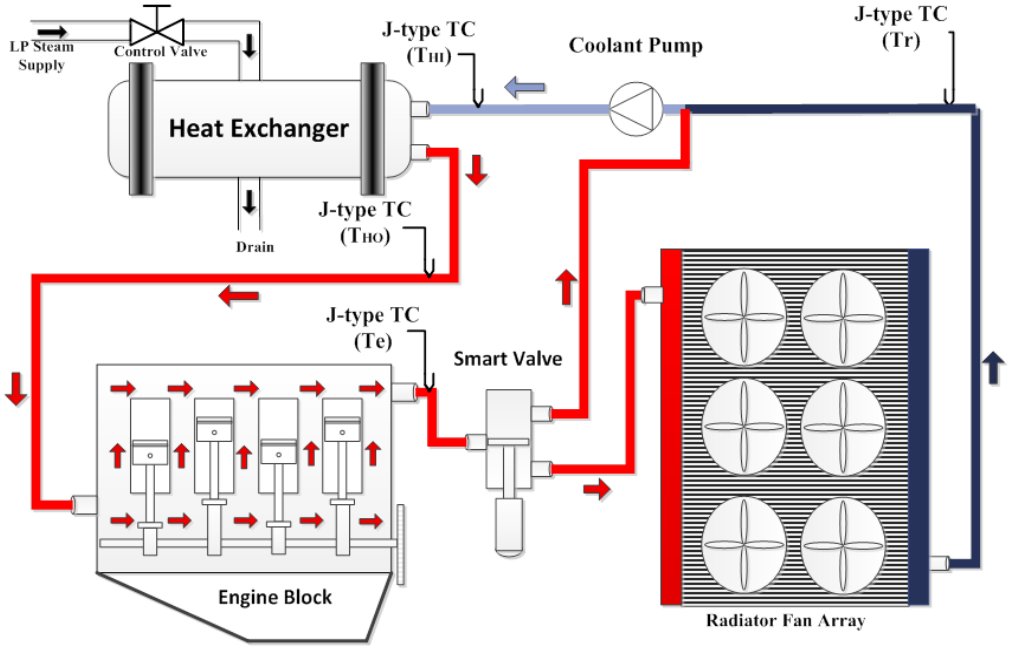

(b)

Figure 3.1: Block diagram of cooling system with coolant flow direction for (a) actual engine configuration, and (b) laboratory experiment with auxiliary heat input and non-operational engine

To develop a thermal management control system which can regulate the engine temperature by adjusting the operation of the actuators, the cooling system actuators properties will be studied. A series of experimental tests were implemented to investigate the engine and radiator temperature transient response for smart valve, variable speed pump, and radiator fan(s) operation. The chapter has been organized as follows. In Section 3.2, a brief description of cooling components and fully function experimental test bench will be introduced with all actuators and corresponding sensors. In Section 3.3, a series of six tests were designed. The test results for the engine temperature transient response to step input will be presented, a summary of the cooling system properties will be given in Section 3.4. Finally, the summary will be offered in Section 3.5.

3.2 Description of Cooling Components and Experimental System

To investigate a prototype of the advanced cooling system configuration, a fully functional experimental bench was built. This test station features a steam driven to coolant heat exchanger, a 6.8L International Truck V8 diesel engine, a three way smart valve, a variable speed coolant pump, a wind tunnel with 3-by-2 radiator fan matrix, and corresponding sensors with data acquisition and control system. This bench provides a safe and repeatable environment for in-depth cooling system studies. The overall structure of the testing system with coolant flow direction is shown in Figure 3.1(b). The color variations indicate the coolant temperature trends as it circulates through the components. In this study, the engine's and radiator's outlets coolant temperatures have been selected as the general engine and radiator temperatures.

3.2.1 Smart Valve

A linear controlled 3-way smart valve is mounted in the system to simulate the bypass valve function (refer to Figure 3.2). The valve is driven by a DC motor through a worm gear assembly. This actuator divides the coolant flow between two paths and mixes the coolant with different temperatures at the union.

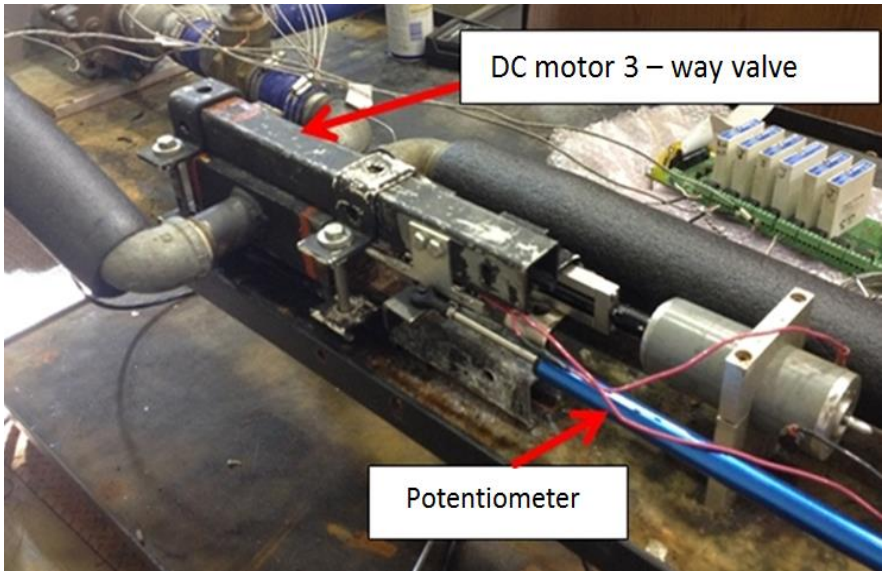

Figure 3.2: Smart valve and potentiometer on test bench

The valve position is defined as $0\% \leq H \leq 100\%$; $H = 100\%$ corresponds to a fully open position which means all the coolant be directed into the radiator, also defined as main route in this study. When $H = 0\%$, the valve is fully closed leads coolant to be routed to the heat exchanger without passing the radiator (i.e., defined as "by pass route"). With this feature, the coolant temperature at the junction, T_j, is a mixing temperature of the coolant flow through main and bypass paths such that

$$T_j = (1 - H)T_e + HT_r \tag{3.1}$$

The variables T_e and T_r denote the engine and radiator coolant temperatures, respectively.

3.2.2 Coolant Pump

In this system, the coolant fills the entire pipeline and works as a thermal carrier. A centrifugal pump, driven by an induction motor, controls the coolant mass flow rate, $\dot{m}_{cool}$, as shown in Figure 3.3. The electric motor is connected with a Genesis KBE2 digital AC adjustable speed driver which converts the 0-12 VDC input signal into a frequency output to realize the commanded motor speed. The rated power of the AC motor is $1.1kW$ The mass flow rate, $\dot{m}_{cool}$, affects the system's thermal response giving in the governing equations

$$C_e\dot{T}_e = -\varepsilon_c\dot{m}_{cool}HCp_{cool}\left(T_e - T_j\right) + q_{in} \tag{3.2}$$

$$C_r\dot{T}_r = \varepsilon_c\dot{m}_{cool}HCp_{cool}(T_e - T_r) - q_{out} \tag{3.3}$$

where Cp_{cool}, C_e, and C_r are the specific heat of the coolant, engine, and radiator at constant pressure. The parameter ε_c is the heat transfer efficacy which depends on the coolant mass flow rate, $\dot{m}_{cool}$. The term q_{in} is the engine input heat due to the combustion (or steam) process while q_{out} is the rejected heat from the radiator. According to the centrifugal pumps affinity law, the coolant mass flow rate, $\dot{m}_{cool}$, is proportion with the pump impeller speed, N_{pump}, so that

$$\dot{m}_{cool} \propto N_{pump} \tag{3.4}$$

Now substitute equation (3.1) into (3.2), so that

$$C_e\dot{T}_e = -\varepsilon_c\dot{m}_{cool}HCp_{cool}(T_e - T_r) + q_{in} \tag{3.5}$$

Add together equations (3.3) and (3.5), the cooling system total heat change rate

can be expressed as

$$C_e\dot{T}_e + C_r\dot{T}_r = q_{in} - q_{out} \tag{3.6}$$

which indicates that the heat input to the engine, q_{in}, and the heat output from the radiator, q_{out}, impact the whole cooling system.

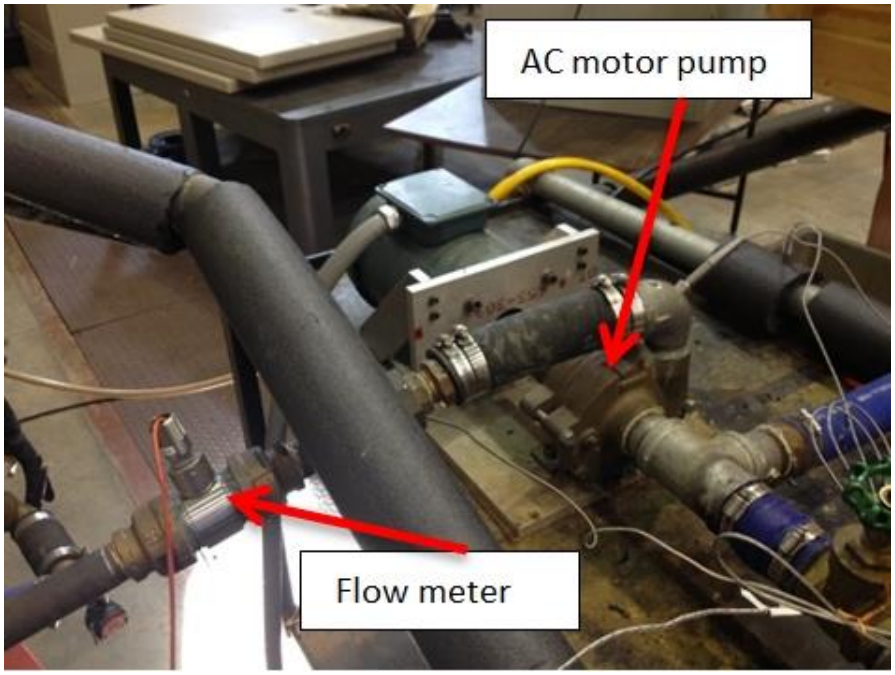

Figure 3.3: Coolant pump and flow meter on test bench

3.2.3 Radiator Fan Array

Six electro-mechanical radiator fans are mounted in a wind tunnel to cool the radiator by increasing the forced convective air flow rate (refer to Figure 3.4). The radiator fans are driven by the 24VDC brushless motors connected to a Controlled Area Network (CAN) bus based DC motor controller. The robust sensor-less DC motor controller accepts commands defined the speed and direction of the motors. The fan status is sent to the control board. Each controller is adjusted with a different value resistor so that it has

an independent CAN bus IP address. The communication signal follows the CAN SAE J1939 protocol.

The fan matrix operation can impact the radiator's heat rejection, q_{out}, which may be calculated as

$$q_{out} = \varepsilon_a \dot{m}_{air} Cp_a (T_{aout} - T_\infty) \tag{3.7}$$

where ε_a is the heat exchanger efficiency and independent to the air flow. The parameter Cp_a is the air specific heat. The variable T_{aout} is the air temperature exiting the radiator, and T_∞ is the air temperature at the radiator inlet (ambient temperature). The variable $\dot{m}_{air}$ denotes the air mass flow rate through the radiator which is a function of the fan speed, N, and can be calculated as

$$\dot{m}_{air} = \sqrt{\frac{k_I}{k_r}\dot{m}_{ram}^2 + \frac{k_f}{k_r}\left(\frac{4\pi^2 \rho_{air} r_m^3 \Phi_m N_f}{60}\left(\frac{1-v^2}{1+v^2}\right)\right)^2} \tag{3.8}$$

where $k_I, k_r,$ and k_f are the pressure coefficients at the radiator, air inlet, and fan, respectively. The term ρ_{air} is the air density, r_m is the mean radius, Φ_m is the flow rate coefficient, and v is the hub ratio. In this study, all six fans will be engaged. The reader is referred to (Wang *et al.*, 2014) for more details. The rated power of each motor is $0.6kW$.

3.2.4 Cooling System Thermal Load

To simulate the heat generated during engine's combustion process, a low pressure steam was introduced using a heat exchanger into the cooling system. The hot steam flows routed through a shell and tube heat exchanger to heat the coolant. A main control valve, installed on the path steam supply, can be adjusted to regulate the heat input, q_{in}, which can be calculated using the coolant temperature change as

$$q_{in} = \dot{m}_{cool} Cp_{cool} (T_{HI} - T_{HO}) \tag{3.9}$$

where T_{HI}, and T_{HO} are the coolant temperature at the heat exchanger inlet and outlet, respectively.

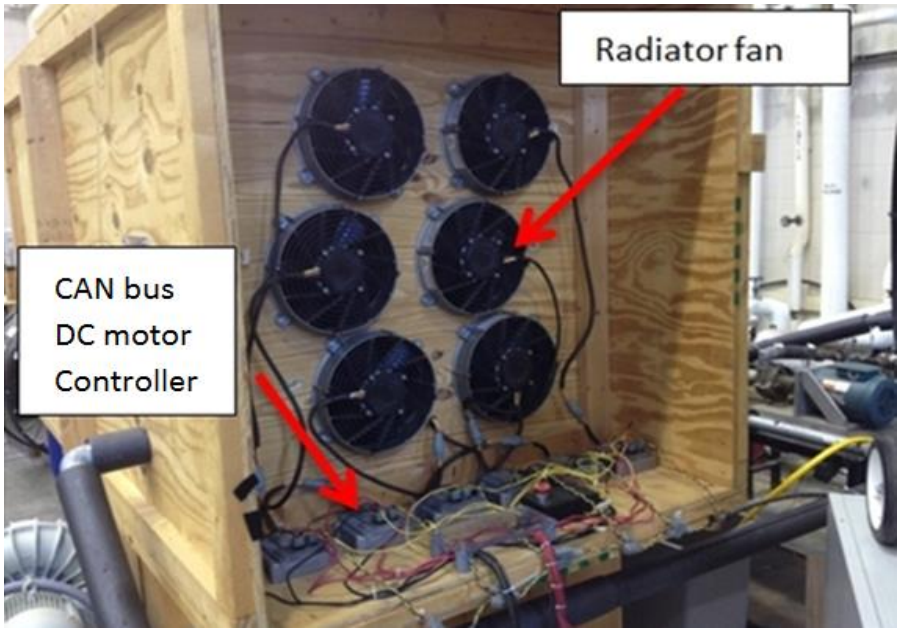

Figure 3.4: Radiator fan array and individual controllers mounted in wind tunnel on test bench

3.2.5 Sensors and Data Acquisition

To track the coolant temperature, four screw head J-type Omega thermocouples are mounted at different locations to measure the coolant temperature: heat exchanger inlet, T_{HI}, and outlet, T_{HO}; the engine and radiator outlets, T_e and T_r (refer to Figure 3.1b). The thermocouples are connected to an OM5-BP-16-C backplane signal conditioner with MO5 amplifier. A potentiometer measures the valve cylinder position. An AW-Lake company turbine type flow sensor TRG-1110 with a MAG-PB magnetic pulse sensor monitors the coolant mass flow rate. The voltage and current of pump and radiator fan

array also can be measured to calculate the electric power consumption.

All the signals generated by the thermocouples, flow sensor, and potentiometer are supplied to a dSPACE data acquisition board (DS1103). Using Matlab/Simulink software, the control algorithm can be compiled into the dSPACE. The signal flow path is shown in Figure 3.5.

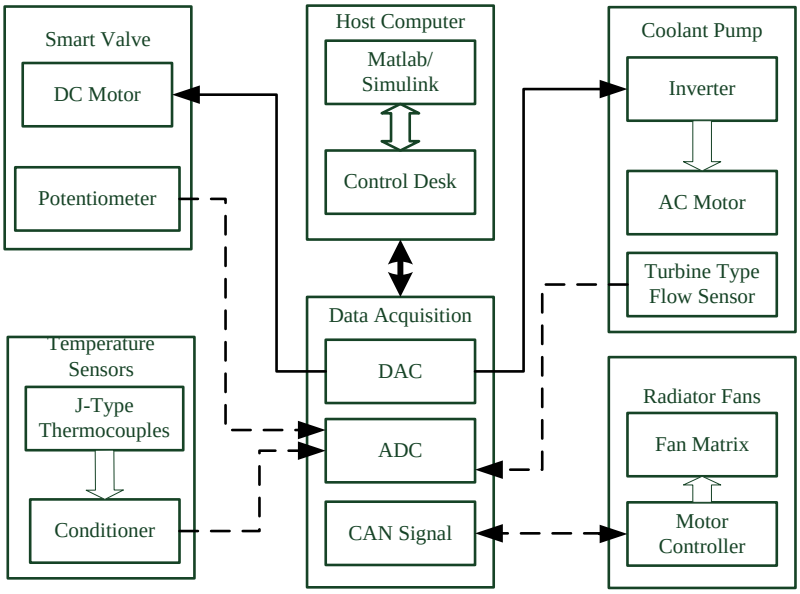

Figure 3.5: Experimental system hardware components and data acquisition on test bench

3.3 Design of Experiments

In this section, six tests are conducted to study the smart cooling system integrated component dynamic response. Specifically, the step input transient response is selected as the effective approach to evaluate the coupled system behavior which has been widely used in broad fields (Han-Sang *et al.*, 2008 and Colwell *et al.*, 2009). In this study, two actuators' operating parameters (i.e. smart valve position, pump speed, and radiator fans speed) are fixed while the other one is controlled to perform a step input with a fixed

amplitude (setting as ±25% to the initial conditions) in each test as shown in Table 3.1. The engine temperature, T_e, and the radiator temperature, T_r, are recorded in experimentally real-time. The heat input, q_{in}, is set as $60kW$ by adjusting and fixing the low pressure steam valve. The actuators' initial operating conditions are set as $H = 80\%$, $\dot{m}_{cool} = 0.8kg/s$, and $N_f = 2{,}000RPM$. Based on this setting, the initial steady state engine temperature is $T_e = 77.0°C$. The total testing time is $500s$, and the ambient temperature was $20°C$.

Tests 1 to 3 are designed for the engine cool down so the three actuator operations lead the engine temperature to decrease; smart valve opening, pump speed high, and increased radiator fans speed. In contrast, Tests 4 to 6 are designed for engine to heat up so the engine temperature will increase; smart valve closing, pump speed becoming lower, and reduced radiator fans speed.

To characterize the engine temperature step input transient response, six specifications (*S1*-*S6*) are defined as follow:

S1. Temperature Change, ΔT_i: Engine temperature difference between the initial engine temperature, $T_{e_{0i}}$, and the engine temperature at steady state, T_{ss_i}, for the ith test.

$$\Delta T_i = T_{ss_i} - T_{e_{0i}} \tag{3.10}$$

S2. Delay Time, t_{d_i}: Time required for the system response to reach 50% of the final value for the ith test.

S3. Rise Time, t_{r_i}: Time required for the system response to rise from 10% to 90% of its final value for the ith test.

S4. Settling Time, t_{ss_i}: Time required for the response curve to reach and stay within an error band of usually 5% or 2% (5% was selected for this study), about the final value for the ith test.

S5. Maximum Percent Overshoot, M_{p_i}: Maximum peak value of the system response curve over the final value.

$$M_{p_i} = \frac{MAX(T_{e_i}) - T_{ss_i}}{T_{ss_i}} \tag{3.11}$$

Let $MAX(T_{e_i})$ denote the peak engine temperature, T_{e_i}, for the ith test and T_{ss_i} represent the engine temperature, T_{e_i}, at steady state.

S6. System Power Consumption, P_{sys}: System power consumption during the tests include the coolant pump power, P_{pump}, and the radiator fan array power, P_{fan}. The power consumed by the smart valve is considered to be quite small and has been neglected.

To facility the laboratory study, the experimental test engine temperature transient response was normalized into a unit step input. Specifically, the temperature response begins at $T_{norm_i} = 0$ and the steady state value corresponds to unity. The normalized temperature T_{norm_i} is defined as

$$T_{norm_i} = \frac{T_{ei} - T_{e_{0i}}}{T_{ss_i} - T_{e_{0i}}} \tag{3.12}$$

where $T_{e_{0i}}$ is the initial engine temperature for the ith test. According to this definition, the original response will be transformed as shown in Figure 3.6. Also, due to the thermocouple sensor properties, the raw data has been processed to reduce noise. In this

chapter, moving average filter was applied (Smith, 1999) to each test. Figure 3.6 illustrates the normalized data and filtered data. With this approach, the tests results can be summarized using the same scale. Notice that the initial engine temperature, $T_{e_{oi}}$, for each test is uniform.

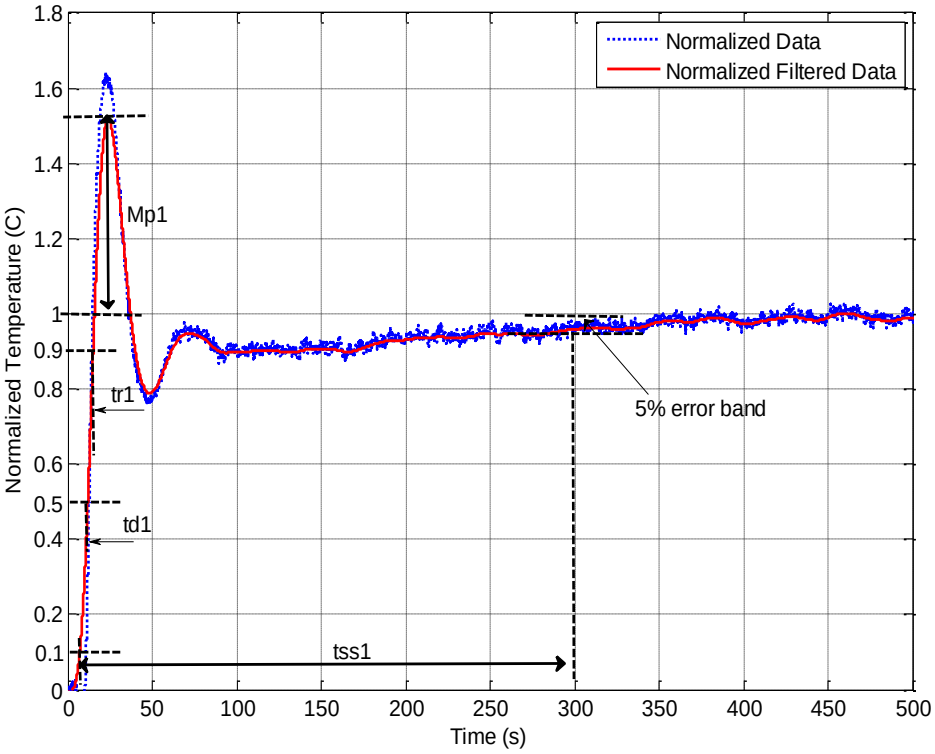

Figure 3.6: Normalized and filtered engine temperature response to a step input smart valve for Test 1

Table 3.1: Experimental test profiles investigated in the laboratory

Test No.	Engine Profile	Cooling Configuration	Input Heat, q_{in}, (kW)	Smart Valve Position, H (%)		Coolant Pump Mass Flow Rate, $\dot{m}_{cool}$, (kg/s)		Radiator Fan Array Speed, N_f (RPM); Air Mass Flow Rate, $\dot{m}_{air}$, (kg/s)	
				t=0(s)	0<t<500(s)	t=0(s)	0<t<500(s)	t=0(s)	0<t<500(s)
1	Cool Down	Valve Open-ing	60	80.0	100.0	0.8	0.8	2,000; 0.52	2,000; 5.52
2		Pump Speed Increase			80.0		1.0		2,000; 5.52
3		Fan Speed Increase			80.0		0.8		2,500; 6.90
4	Heat Up	Valve Closing			60.0		0.8		2,000; 5.52
5		Pump Speed Decrease			80.0		0.6		2,000; 5.52
6		Fan Speed Decrease			80.0		0.8		1,500; 4.14

3.4 Test Results and Discussion

The experimental test results will now be presented and analyzed to offer insight into automotive cooling system behavior. The temperature transient responses for the same sequence of actuator operations will be discussed for engine cool down and heat up. The test results in Figures 3.7-3.9 display the engine and radiator temperature transient responses for the valve, pump, and radiator fan operation per Tests 1-6. A combined plot of all six tests is shown in Figure 3.10 and the summarized results are listed in Table 3.2. The six specifications S1-S6 are compared and ranked separately for the different actuators. The rules to rank the transient response metrics are defined as follows:

S1: A larger absolute temperature change, $|\Delta T_i|$, leads to a higher rank.

S2-S6: A smaller delay time, T_{di}, rise time, T_{ri}, settling time, T_{ssi}, percent overshoot, M_{pi}, and system power consumption, P_{sys}, yields a higher rank.

The relative rank of each test for the given metric is listed in Table 3.2, and the corresponding radar plots are shown in Figure 3.11. According to these test results, the following smart engine cooling system characteristics can be stated.

Smart Valve: The engine and radiator temperatures, T_e and T_r change in different directions as the valve's position changes per Figure 3.7. The valve directs the coolant along different paths within the thermal network. For instance, as the valve position increases, more coolant is directed into the radiator node in which the heat transfer between the ambient air and the hot coolant increases through the heat exchanger surface. This process allows the engine temperature to decrease while the radiator temperature increas-

es based on fluid mixing from the two thermal reservoirs. The opposite is true for a valve position decrease since the coolant remains in the radiator longer and experiences a lower temperature due to greater heat transfer and vice versa for the engine. As expected, the mixing temperature, T_j, in equation (3.1) moves toward the engine temperature, ($T_j \rightarrow T_e$), as the valve opens ($H \rightarrow 100\%$). Similarly, the mixing temperature approaches the radiator temperature, ($T_j \rightarrow T_r$), when the valve closes ($H \rightarrow 0\%$). As a result, the heat input term, q_{in}, indicated in equation (3.2) becomes the dominate factor when the mixing temperature, T_j, approaches to the engine temperature, ($T_j \rightarrow T_e$), under the same coolant flow rate, $\dot{m}_{cool}$, which leads the engine temperature, T_e, to increase from the last steady state.

Coolant Pump: A coolant mass flow rate, $\dot{m}_{cool}$, increase will result in a small engine temperature decrease and a larger radiator temperature increase in the transient response. In contrast, a reduced fluid flow rate, $\dot{m}_{cool}$, will decrease the heat transfer rate so a higher engine temperature and a lower radiator temperature will be realized per Figure 3.8. Equations (3.2) and (3.3) demonstrate this phenomenon. An interesting phenomenon is the temporary change in the engine temperature signal as it eventually reverts back toward the initial value during the transient response. This can be attributed to the large thermal capacitance of the engine. When the coolant flow rate increases, the cooler fluid in the radiator enters the engine quickly but the heat transfer between the engine and coolant is insufficient to keep the engine temperature after the initial transient response.

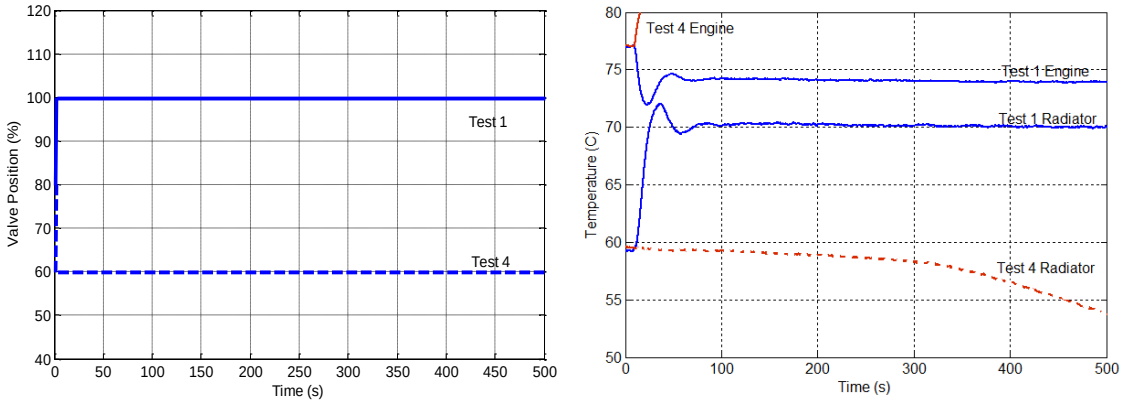

(a) (b)

Figure 3.7: Tests 1 and 4 experimental results - (a) commanded valve position, and (b) engine and radiator temperatures

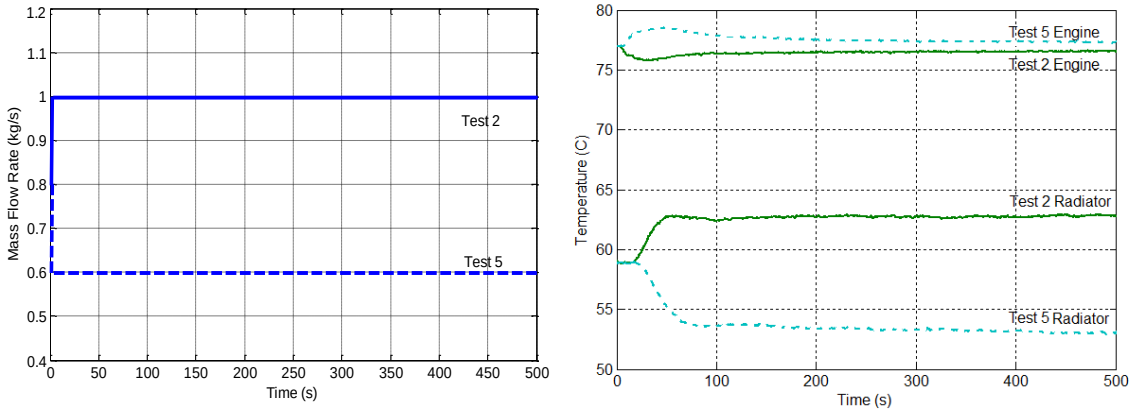

(a) (b)

Figure 3.8: Tests 2 and 5 experimental results - (a) commanded pump speed, and (b) engine and radiator temperatures

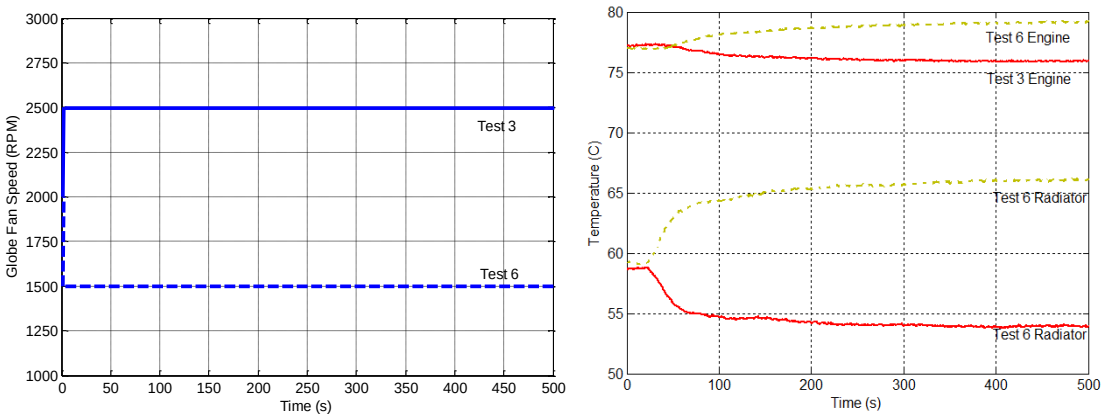

(a) (b)

Figure 3.9: Tests 3 and 6 experimental results - (a) commanded global fan speed, and (b) engine and radiator temperatures

Table 3.2: Test results of the engine temperature, T_e, transient response specifications with relative rank listed in footnotes for Tests 1-6

Test No.	Engine	Cooling Mode	T_{ss} $(°C)$	$S1: \Delta T$ $(°C)$	$S2: t_d$ (s)	$S3: t_r$ (s)	$S4: t_{ss}$ (s)	$S5: M_p$	P_{pump} (kW)	P_{fan} (kW)	$S6: P_{sys}$ (kW)
1	Cool Down	Valve Opening	73.9	-3.1 (1)	11.9 (2)	15.0 (2)	287.5 (1)	52% (2)	0.06	0.46	0.52 (1)
2		Pump Speed Increase	76.6	-0.4 (3)	6.3 (1)	8.9 (1)	458.3 (3)	188% (3)	0.07	0.46	0.53 (2)
3		Fan Speed Increase	75.7	-1.3 (2)	90.3 (3)	243.4 (3)	321.0 (2)	0% (1)	0.06	0.66	0.72 (3)
4	Heat Up	Valve Closing	Temperature exceeded upper safety limit; test halted								
5		Pump Speed Decrease	77.3	0.3 (2)	7.0 (1)	9.2 (1)	437.8 (2)	347% (2)	0.05	0.46	0.51 (2)
6		Fan Speed Decrease	79.2	2.2 (1)	94.4 (2)	289.7 (2)	369.5 (1)	0% (1)	0.06	0.35	0.41 (1)

Radiator Fan Array: The impact of the radiator fan(s) is clearly different than the valve and pump as the engine and radiator temperatures change in the same direction per Figure 3.9. A global fan speed increase lowers both the engine and radiator temperatures and vice versa. From a transient signal perspective, the system response is the slowest among the three components due to heat transfer changes at the radiator (e.g. coolant, air, and metal) interface. Further, there is no overshoot in the temperatures due to the slower system time constant. These features demonstrate that the operation of the fan array influences the entire cooling system by changing the heat rejection rate from the radiator. As shown in equation (3.6), when the heat output, q_{out}, greater than the heat input, q_{in}, then the total system heat will decrease.

Comparison of Thermal System Actuators: The smart valve and coolant pump operation promote engine and radiator temperature changes in opposite directions. These two actuators impact the heat transfer rate between the engine and the radiator through coolant redirection and/or coolant flow rate. In contrast, the radiator fan array operation cools down the entire system by impacting the forced convection air flow and changes the air-metal-coolant heat transfer rate.

From Table 3.2, Figures 3.10 and 3.11, for both cool down and heat up modes, the smart valve operation causes the greatest engine temperature change (4.0%) followed by the radiator fan(s) (1.6%). The pump speed does not significantly the engine temperature (less than 0.5%). From a transient response view, the pump operation shows a quicker response time (e.g. delay time, t_d, and rise time, t_r) but a larger fluctuation (e.g. settling time, t_{ss} and max percent overshoot, M_p) than the valve operation. The radiator fans op-

eration illustrates a much longer response time when compared to the valve and the pump operations.

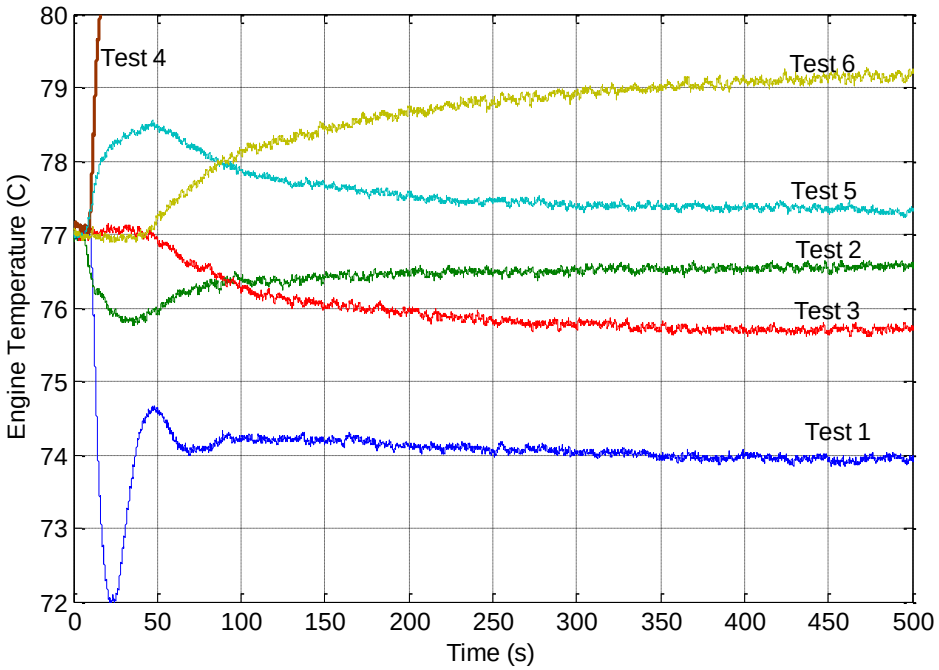

Figure 3.10: Summary of engine transient response, T_{ei}, for Tests 1-6

3.5 Summary

This study investigates an advanced cooling system for ground vehicles which features three computer controlled actuators: a three way smart valve, a variable speed pump, and a variable speed electric radiator fan matrix. Six experimental tests were performed to study the engine temperature transient response to a sequence of actuator step input profiles. From the experimental results, the valve operation causes the most engine temperature change (4.0%) followed by the radiator fan(s) (1.6%). Only controlling the pump speed hardly changes the engine temperature. From a transient response view point, the radiator fan(s) operation illustrates a much longer response time when com-

pared to the valve and the pump operations. Furthermore, the radiator fan(s) consume significantly more power energy the pump and valve. In conclusion, the experimental results provide insight to fabricate a frame work for advanced engine cooling system control strategy.

This smart cooling system can be applied to the automotive industries by replacing the existed mechanical actuator(s) with the computer controlled electrical ones and updating the electronic control unit (ECU) with corresponding control strategy. The fuel economy is expected to be improved $3\% - 5\%$ after applying this advanced technology.

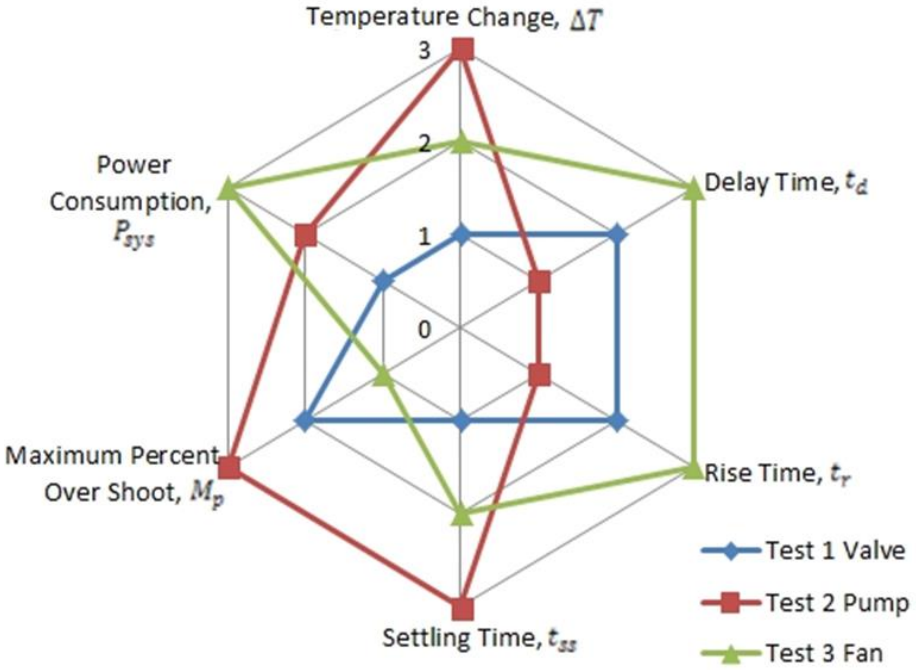

(a)

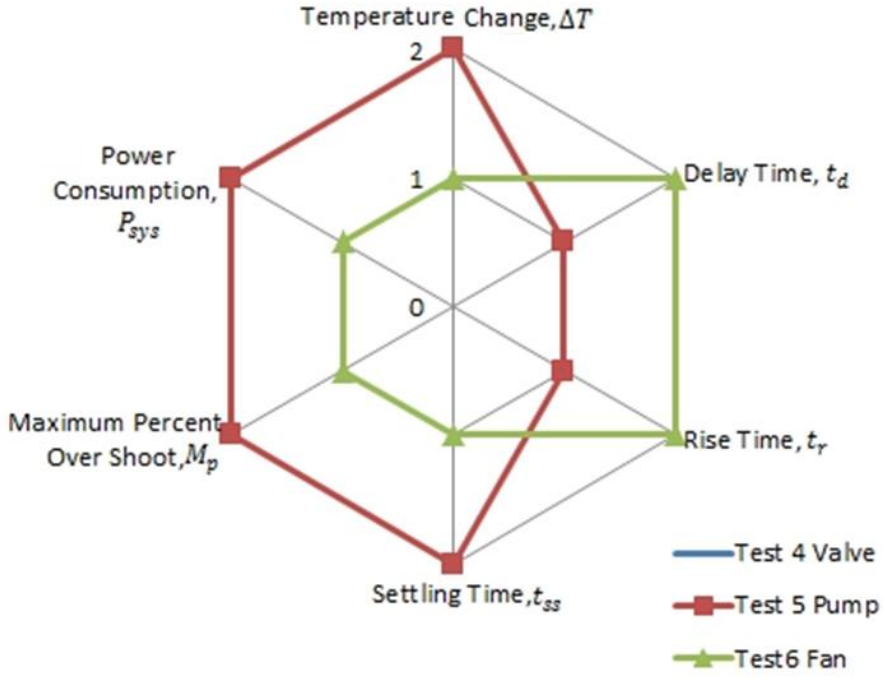

(b)

Figure 3.11: Radar plot of the engine temperature transient response specifications for (a) Tests 1-3, and (b) Tests 4-6

CHAPTER IV

ADVANCED AUTOMOTIVE THERMAL MANAGEMENT – NONLINEAR RADIATOR FAN MATRIX CONTROL

Advanced automotive cooling systems for gasoline and diesel engines can improve the powertrain performance. The replacement of the mechanical driven coolant pump and radiator fans with computer controlled servo-motor actuators, and update of the wax-based thermostat valve with a 3-way variable position smart valve, allow the coolant flow rate and proportion directed through the radiator to be carefully adjusted. A smart thermal management system approach can regulate the forced convection heat transfer process to match the engine's cooling needs. This chapter presents a Lyapunov based nonlinear control strategy for transient engine temperature tracking. A reduced order mathematical model serves as the basis for the closed-loop feedback system. An experimental test bench with multiple radiator fans, heat exchanger, wind tunnel, coolant pump, three way valve, and engine thermal load has been fabricated. Representative numerical and experimental tests demonstrate that the advanced control strategy can regulate the engine temperature tracking error within $0.12°C$ and compensate the unknown heat load. The nonlinear controller provided superior performance in terms of power consumption and temperature tracking as evident by the reduced magnitude when compared to a classical PI with lookup table based controller and a bang bang controller.

4.1 Introduction

According to the corporate average fuel economy (CAFE) standards, the average miles per gallon will increase to 49 (20.8 km per liter) and 39 (16.6 km per liter) for pas-

senger cars and light trucks, respectively, in the United States by 2020 (National Highway Traffic Safety Administration, 2014). Advanced automotive cooling systems for internal combustion (IC) engines can improve the engines' performance and fuel economy (Melzer *et al.*, 1999). Kanefsky *et al.* (1999) and Wagner *et al.* (2002) reported that the precise control of the engine coolant temperature can enhance a vehicle's fuel economy by increasing thermal efficiency and reducing the friction losses.

For the traditional ground transportation cooling system, the mechanical pump and radiator fan(s) are indirectly connected with the engine's crankshaft. This mechanical approach does not allow accurate control of the pump and fan(s). Specifically, the coolant maybe overcooled with less fluids routed through the engine by the thermostat so that the powertrain net effect tends to be higher emissions, reduced fuel economy, and decreased overall system efficiency (Wambsganss, 1999). An alternative thermal management system replaces the mechanical components with computer controlled servo-motor actuators; the wax-based thermostat valve is updated with a 3-way variable position smart valve. Geels *et al.* (2003) proposed that 5% of the engine power consumption and 10% of the carbon monoxide, CO, tailpipe emissions can be reduced using electric cooling components instead of mechanical ones. Page *et al.* (2005) discussed several benefits of mechanically decoupling the cooling system including reduced fuel consumption, increased engine reliability, and improved temperature control.

Several intelligent real time control techniques have been studied and implemented for advanced thermal management systems. Wagner *et al.* (2002) investigated the integration of an electrical water pump and an intelligent thermostat valve to achieve faster

engine warm-up, and reduced temperature fluctuations by creating a lumped mathematical thermal model to represent the real time heat flow. Chanfreau *et al.* (2003) developed a new approach to control the radiator fans and pump actuators for improving cooling system efficiency. Salah *et al.* (2005 and 2010) designed different nonlinear control strategies to adjust the smart valve position and the coolant flow rate to track the desired engine temperature. Aschemann *et al.* (2011) presented a differential flatness nonlinear controller using the engine outlet temperature as the output and demonstrated improved trajectory tracking. Finally, Butt *et al.* (2014) investigated different nonlinear control strategies and linearization method on a small prototyping test configuration.

The vehicle thermal management system also consumes a portion of the engine's power to drive the cooling actuators. In comparison to passenger vehicles, the power requirement for these components increases significantly in larger displacement engines (e.g., heavy trucks, buses) (Salah *et al.*, 2009). As a result, the power consumption should be considered when developing the cooling control strategy. Among the different thermal management system actuators (e.g., variable speed pump, smart valve, radiator fans), the radiator fan(s) use the greatest amount of power following by the coolant pump and smart valve (Moyle *et al.*, 2006). Consequently, the operation of the radiator fan(s) should be reduced unless the desired heat rejection cannot be achieved by controlling the pump and valve alone.

According to previous studies (Wang *et al.*, 2014), to realize the minimum cooling system power consumption, an optimization control strategy can be formulated as shown in Figure 4.1 which offers three levels of actuator control as the heat rejection

needs increase overtime.

In Level I, the coolant pump speed will be designed to operate at its lower limit working condition. Based on possible ram air effects (note: no ram air exits for a stationary engine), the fan array will be controlled to work as its lower limit or not operate. The only actuator to control is the smart valve; it will be set to increase from a fully closed to a fully open position. At the end of Level I, the valve position approaches its maximum open position.

To remove more engine heat, the pump speed will be increased until its higher limit is researched in Level II. However, the fan array will remain in the same working condition as Level I. After the pump speed reaches its upper limit at the end of Level II, the radiator fan array will be controlled to realize more heat rejection in Level III. This chapter will focus on the Level III radiator fan array control problem.

This study investigates a nonlinear controller for a distribution radiator fan matrix to achieve the prescribed heat rejection. A nonlinear adaptive backstepping controller will be introduced to regulate the engine (coolant) temperature in tracking a designed thermal trajectory. The remained of the article is organized as follows. In Section 4.2, the cooling system property will be studied and corresponding mathematical model will be presented. The backstepping adaptive control law will be applied in Section 4.3. A fully function experimental test bench will be introduced in Section 4.4, followed by the discussion of test results in Section 4.5. Finally, the summary will be offered in Section 4.6. The appendices contain the details for two classical controller designs.

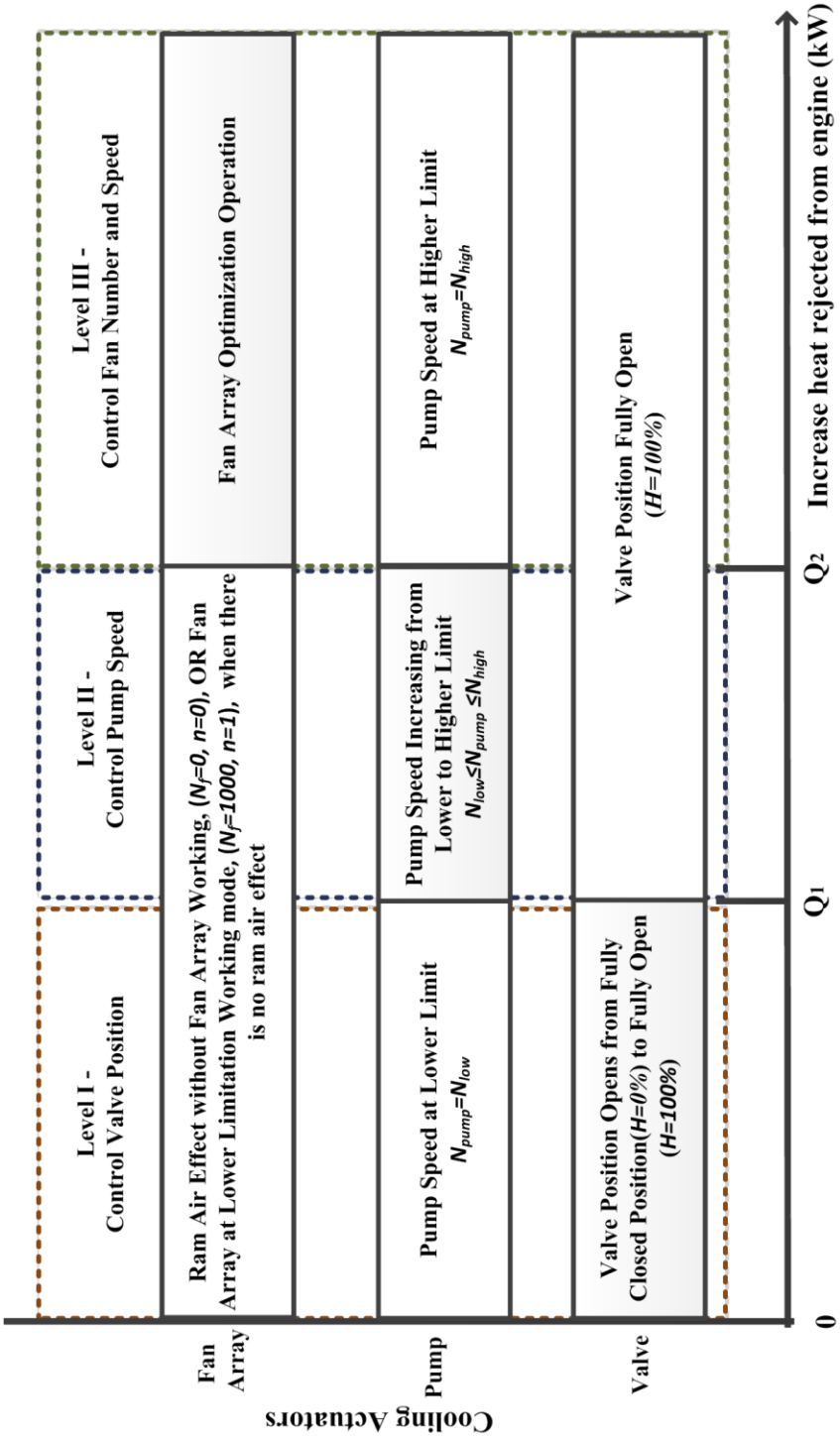

Figure 4.1: Three levels of a cooling system control strategy

4.2 Cooling System Mathematical Description

A mathematical model was created to describe the cooling system transient thermal behavior. The thermal management components include a smart valve, variable speed coolant pump, radiator fan matrix, and assorted sensors. Figure 4.2 displays the simplified system block diagram with the coolant flow directions.

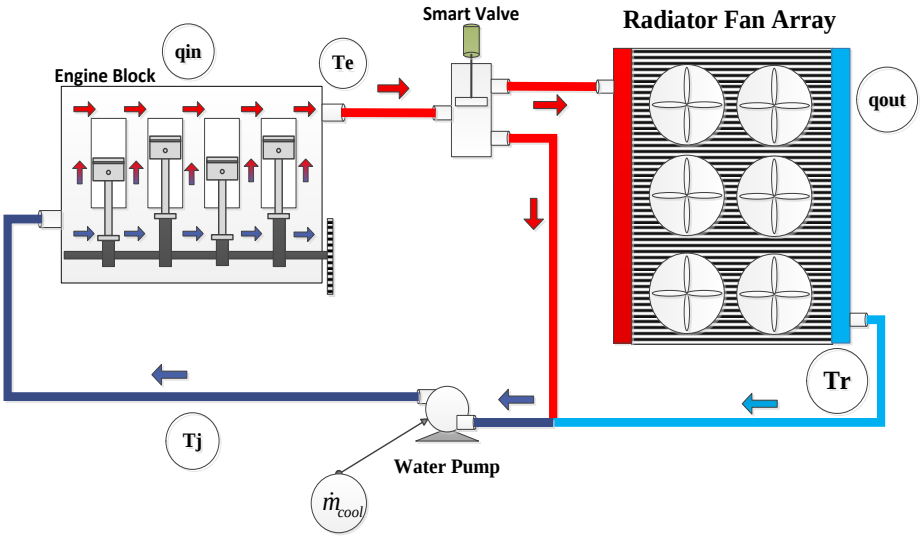

Figure 4.2: Block diagram of internal combustion engine cooling system with sensor, measurement and analytic variable locations

4.2.1 Cooling System General Description

To model the system using a lumped parameter approach, the cooling network has been divided into two thermal nodes–the engine, and the radiator. The governing equations for these two entities can be described as

$$C_e\dot{T}_e = -\dot{m}_{cool}HCp_{cool}(T_e - T_j) + q_{in} \tag{4.1}$$

$$C_r\dot{T}_r = \dot{m}_{cool}HCp_{cool}(T_e - T_r) - q_{out} \tag{4.2}$$

where the variables T_e and T_r denote the coolant temperature at the engine and radiator

nodes. Similarly, $\dot{m}_{cool}$ is the coolant pump mass flow rate. The parameters C_e, Cp_{cool}, and C_r are the specific heat of the coolant, engine and radiator at constant pressure. The term q_{in} is the engine heat flux due to the combustion process, while q_{out} is the radiator rejected heat.

The variable H represents the smart valve position which satisfies $H = 1(0)$ and corresponds to a fully open (closed) position. The coolant temperature at the junction, T_j, is the mixing temperature of the coolant flow through the bypass and radiator, and may be calculated as

$$T_j = (1 - H)T_e + HT_r \tag{4.3}$$

4.2.2 Heat Rejected in Radiator

The heat rejected from the radiator node to the ambient air, q_{out}, in equation (4.2) may be expressed as

$$q_{out} = \varepsilon_a Cp_a \dot{m}_{air} \Delta T \tag{4.4}$$

where ε_a is the heat exchanger efficiency which is independent of the air flow. The term $\dot{m}_{\mathrm{air}}$ denotes the mass air flow rate through the radiator. The parameter Cp_a *i*s the air specific heat, and $\Delta T(t) = T_{aout} - T_\infty$ is the air temperature change across the radiator.

$$q_{out} = \varepsilon_a Cp_a \dot{m}_{air} \Delta T = F_f(N_f, n, v_{ram}) \tag{4.5}$$

where $N_f, n,$ and v_{ram} are the radiator fan speeds, number of fans, and ram air speed, respectively. No ram air effects will be considered in this chapter which leads to $v_{ram} = 0$, and corresponds to a stationary engine scenario and/or no blowing winds. If the vehicle is moving at a given speed and/or wind blowing, the ram air speed can be expressed as $v_{ram} = v_{vehicle} + v_{wind}$ where $v_{vehicle}$ and v_{wind} are the vehicle and wind speed, re-

spectively. Interested readers are referred to (Wang *et al.* 2014) for an explicit expression for $F_f(N_f, n, v_{ram})$.

4.2.3 Simplified Model

A simplified mathematical model may be realized by substituting equations (4.3) and (4.4) into equations (4.1) and (4.2), so that

$$C_e\dot{T}_e = -\dot{m}_{cool}HCp_{cool}(T_e - T_r) + q_{in} \tag{4.6}$$

$$C_r\dot{T}_r = \dot{m}_{cool}HCp_{cool}(T_e - T_r) - \varepsilon_a Cp_a\dot{m}_{air}\Delta T \tag{4.7}$$

Next, these expressions show an inseparable system input defined as $u(\dot{m}_{cool}, H) \triangleq \dot{m}_{cool}H$ which denotes the variable speed coolant pump and three way smart valve effects. An independent system input may be defined as $u(N_f, n, v_{ram}) \triangleq q_{out} = F_f(N_f, n, vram)$ for the air flow effect due to the forced convection (driven by fan matrix) and ram air flow. Based on these definitions, equations (4.6) and (4.7) can be rewritten as

$$C_e\dot{T}_e = -u(\dot{m}_{cool}, H)Cp_{cool}(T_e - T_r) + q_{in} \tag{4.8}$$

$$C_r\dot{T}_r = u(\dot{m}_{cool}, H)Cp_{cool}(T_e - T_r) - u(N_f, n, v_{ram}) \tag{4.9}$$

A series of four assumptions will be imposed on the thermal management system:

A1: No heat losses occur in the system other than forced convection through the radiator.

A2: System temperatures and fluid flows rates may be measured using available hardware.

A3: Coolant flow rate in the system is fixed and bounded at its prescribed higher limit; $\dot{m}_{cool} = \dot{M}\epsilon L_\infty$ (constant).

A4: Bypass valve position is fixed as fully open so that all of the coolant will flow through the radiator; $H(t) = 1, T_j = T_r$.

Based on Assumptions (*A3*) – (*A4*), equations (4.8) and (4.9) may now be rewritten as

$$C_e\dot{T}_e = -\dot{M}Cp_{cool}(T_e - T_r) + q_{in} \tag{4.10}$$

$$C_r\dot{T}_r = \dot{M}Cp_{cool}(T_e - T_r) - u(N, n, v_{ram}) \tag{4.11}$$

4.3 Control Strategy Development

A Lyapunov-based adaptive nonlinear control algorithm will be derived and applied to the system for engine temperature tracking under different heat flux conditions. In real life, the heat generated in the combustion process is hard to physically measure in real time, so the system heat flux, q_{in}, will be considered as an unknown parameter and an estimate value of $\hat{q}_{in}$ has been introduced to compensate this uncertain parameter. Other system parameters can be either measured by sensors or are fully known.

4.3.1 Closed-Loop Feedback System Description

To evaluate the temperature tracking control objective, the tracking error signal, e, is defined as

$$e = T_{ed} - T_e \tag{4.12}$$

where T_{ed} represents the desired engine temperature trajectory. The control objective is to ensure that the actual engine temperature tracks the desired temperatures so that

$$e \leq \varepsilon_e \quad \text{as} \quad t \to \infty \tag{4.13}$$

where ε_e is a small positive constant. To formulate the state equations, substitute equation (4.12) into the reduced order system (4.10) where by equations (4.10) and (4.11) become

$$\dot{e} = \dot{T}_{ed} + \frac{\dot{M}Cp_{cool}}{C_e}(T_{ed} - e - T_r) - \frac{q_{in}}{C_e} \tag{4.14}$$

$$\dot{T}_r = \frac{\dot{M}Cp_{cool}}{C_r}(T_{ed} - e - T_r) - \frac{u(N_f,n,v_{ram})}{C_r} \tag{4.15}$$

The developed control law also needs the capability to compensate for the uncertain heat flux, q_{in}, in equation (4.14).

4.3.2 Lyapunov Based Backstepping Adaptive Controller

According to the derivation above, a Lyapunov-based adaptive nonlinear control algorithm will be designed. Equations (4.14) and (4.15) show that the error tracking system has two state variables, $\dot{e}$ and $\dot{T}_r$, and one input, $u(N_f, n, vram)$. To develop the control law $u(N, n, vram)$, define the intermediate tracking error, r, as

$$r = T_{rd} - T_r \tag{4.16}$$

where T_{rd} represents the intermediate system input. The intermediate control objective can be stated as

$$r \leq \varepsilon_r \quad \text{as} \quad t \to \infty \tag{4.17}$$

where ε_r is a positive constant.

In the meantime, define $\tilde{q}_{in1}$ and $\tilde{q}_{in2}$ as the estimate errors of the heat flux, q_{in}, which can be expressed as

$$\tilde{q}_{in1} \triangleq q_{in} - \hat{q}_{in1};\ \ \tilde{q}_{in2} \triangleq q_{in} - \hat{q}_{in2} \tag{4.18}$$

where $\hat{q}_{in1}$ and $\hat{q}_{in2}$ are the designed feed forward estimate terms.

According to the physic dynamics, Assumption (*A5*) will be introduced to formulate the adaptive controller.

A5: Heat flux q_{in} always remains positive and bounded; $q_{in} \epsilon L_\infty$. The value of q_{in}

was considered to change gradually which lead $\dot{q}_{in} = 0$. *The bounds of the heat flux is* $0kW \leq q_{in} \leq 120kW$ *which is not greater than the maximum heat rejection from the radiator,* $q_{in} \leq MAX(q_{out})$.

Assumption *A5* states $\dot{q}_{in} = 0$; take the time derivative of equation (4.18), which results in

$$\dot{\tilde{q}}_{in1} = -\dot{\hat{q}}_{in1};\ \dot{\tilde{q}}_{in2} = -\dot{\hat{q}}_{in2} \tag{4.19}$$

Based on above the definitions and equations (4.14) and (4.15), a backstepping adaptive control law can be developed as

$$u(N_f, n, vram) = \left[\phi_1 + \phi_2 + \phi_3 + \phi_4 + K_2 r + \frac{\dot{M}Cp_{cool}}{C_e} e\right] \tag{4.20a}$$

where

$$\phi_1 = \frac{C_e \ddot{T}_{ed} + \dot{M}Cp_{cool}\dot{T}_{ed} - \dot{\hat{q}}_{in1}}{\dot{M}Cp_{cool}} \tag{4.20b}$$

$$\phi_2 = \frac{C_e K_1 - \dot{M}Cp_{cool}}{\dot{M}Cp_{cool}} [\dot{T}_{ed} + \frac{\dot{M}Cp_{cool}(T_{ed} - e - T_r)}{C_e}] \tag{4.20c}$$

$$\phi_3 = -\frac{\dot{M}Cp_{cool}(T_{ed} - e - T_r)}{C_r} \tag{4.20d}$$

$$\phi_4 = -\frac{C_e K_1 - \dot{M}Cp_{cool}}{\dot{M}Cp_{cool}} \hat{q}_{in2} \tag{4.20e}$$

$$T_{rd} = \frac{C_e \dot{T}_{ed} + \dot{M}Cp_{cool}T_{ed} + (C_e K_1 - \dot{M}Cp_{cool})e - \hat{q}_{in1}}{\dot{M}Cp_{cool}} \tag{4.20f}$$

$$\hat{q}_{in1} = -\frac{1}{C_e}\int_{t_0}^{t} e\, d\tau \tag{4.20g}$$

$$\hat{q}_{in2} = -\frac{C_e K_1 - \dot{M}Cp_{cool}}{\dot{M}Cp_{cool}C_e}\int_{t_0}^{t} r\, d\tau \tag{4.20h}$$

The terms K_1 and K_2 are the controller gains bounded at all time; $K_1, K_2 \in L_\infty$.

4.3.3 Stability Analysis

A detailed Lyapunov based stability analysis will be presented to guarantee that (i) all the closed-loop system states, input, and output remain bounded all the time, and that (ii) the tracking errors, e and r, will go to zero as time goes to infinity.

According to the vehicle's thermal dynamics, another Assumption, *A6*, may be imposed.

A6: The desired engine temperature, T_{ed} , always remain positive and bounded, that is $T_{ed}\ (t) \epsilon L_\infty$. Also, its first and second time derivatives exist and remain bounded all the time, such that $\dot{T}_{ed}, \ddot{T}_{ed}\ \epsilon L_\infty$.

Now substitute the intermediate tracking error, r, and intermediate system input, T_{rd}, into equations (4.14) and (4.15), so that these two expressions can be rewritten as

$$\dot{e} = \dot{T}_{ed} + \frac{\dot{M}Cp_{cool}}{C_e}(T_{ed} - e - T_{rd} + r) - \frac{q_{in}}{C_e} \tag{4.21}$$

$$\dot{r} = \dot{T}_{rd} - \frac{\dot{M}Cp_{cool}}{C_r}(T_{ed} - e - T_{rd} + r) + \frac{u(N_f, n, vram)}{C_r} \tag{4.22}$$

The control law introduced in equations (4.20a)-(4.20f) can be substituted into (4.21) and (4.22). The tracking errors, e and r, can be rewritten as

$$\dot{e} = -K_1 e + \frac{\dot{M}Cp_{cool}}{C_e} r - \frac{1}{C_e}\tilde{q}_{in1} \tag{4.23}$$

$$\dot{r} = -K_2 r - \frac{\dot{M}Cp_{cool}}{C_e} e - \frac{C_e K_1 - \dot{M}Cp_{cool}}{\dot{M}Cp_{cool} C_e}\tilde{q}_{in2} \tag{4.24}$$

Define the Lyapunov candidate function, V, as

$$V = \frac{1}{2} Z^T Z\ , \quad Z = [e\ r\ \tilde{q}_{in1}\ \tilde{q}_{in2}]^T \tag{4.25}$$

The time derivative of equation (4.24) yields the expressions

$$\dot{V} = \nabla V \cdot [e\ r\ \tilde{q}_{in1}\ \tilde{q}_{in2}]^T = e\dot{e} + r\dot{r} + \tilde{q}_{in1}\dot{\tilde{q}}_{in1} + \tilde{q}_{in2}\dot{\tilde{q}}_{in2} \tag{4.26}$$

Substitute equations (4.19), (4.20a) - (4.20f), (4.23) and (4.24) into (4.26) and simplify. The time derivative of candidate Lyapunov function will be calculated as

$$\dot{V} = -K_1 e^2 - K_2 r^2 \tag{4.27}$$

Equations (4.25) and (4.27) conclude that V is positive definite and radially unbounded while $\dot{V}$ is negative semi-definite. The tracking errors e and r, and parameter estimate errors $\tilde{q}_{in1}$ and $\tilde{q}_{in2}$ are all bounded along with time increasing, such that $e, r, \tilde{q}_{in1}, \tilde{q}_{in2} \epsilon L_\infty$. Take the time derivative of equation (4.20g) and (4.20h); it clearly shows that $\dot{\hat{q}}_{in1} = -\frac{e}{C_e}$, and $\dot{\hat{q}}_{in2} = -\frac{C_e K_1 - \dot{M} C p_{cool}}{\dot{M} C p_{cool} C_e} r$. Both of the $\dot{\hat{q}}_{in1}$ and $\dot{\hat{q}}_{in2}$ terms are bounded. Then according to Assumption *A5*, $q_{in} \epsilon L_\infty$ and equation (4.18), it can be derived that $\hat{q}_{in1}, \hat{q}_{in1} \epsilon L_\infty$. As a result, from the expression of T_{rd} in equation (4.20f) and Assumption *A6*, $\dot{T}_{ed}, \ddot{T}_{ed} \epsilon L_\infty$, yield that $T_{rd} \epsilon L_\infty$.

In equations (4.25) and (4.27) and the analysis above, it implies that $\dot{e}, \dot{r} \epsilon L_\infty$. From the expression of equation (4.20a), it can be concluded that the system input is bounded such that $u(N_f, n, vram) \epsilon L_\infty$. Hence all the system signals are bounded.

The Lyapunov-like Lemma (Barbalat's Lemma) (Dequeiroz *et al.*, 2000) may be introduced as

If 1) $V \geq 0$; (4.28)

2) $\dot{V} \geq -g(t),\ where\ g(t) \geq 0$; (4.29)

3) $g(t)$ *is uniformly continuous (* $\dot{g}(t) \epsilon L_\infty$*)*

then

$$\lim_{t\to\infty} g(t) = 0 \tag{4.30}$$

Define the positive definite auxiliary function as

$$g(e,r,t) \triangleq K_1 e^2 + K_2 r^2 \geq 0 \tag{4.31}$$

Equation (4.27) shows that $\dot{V} = -K_1 e^2 - K_2 r^2 \geq -g(e,r,t)$. Now take the time derivative of $g(e,r,t)$ which leads to

$$\dot{g} = 2K_1 e\dot{e} + 2K_2 r\dot{r} \tag{4.32}$$

In this study, the terms on the right hand side are all bounded as demonstrated in the previous paragraphs. Hence, $e, r, \dot{e}, \dot{r}\ \epsilon L_\infty$, so that $\dot{g}\ \epsilon L_\infty$ which implies that $\dot{g}$ is uniformly continuous. According to the Lyapunov-like Lemma, it can be derived that $\lim_{t\to\infty} g(e,r,t) = 0$ which leads to $e, r \to 0\ as\ t \to \infty$.

From the analysis, the engine temperature tracking error tends to zero as time goes to infinity. When applying the proposed control law, the system is stable.

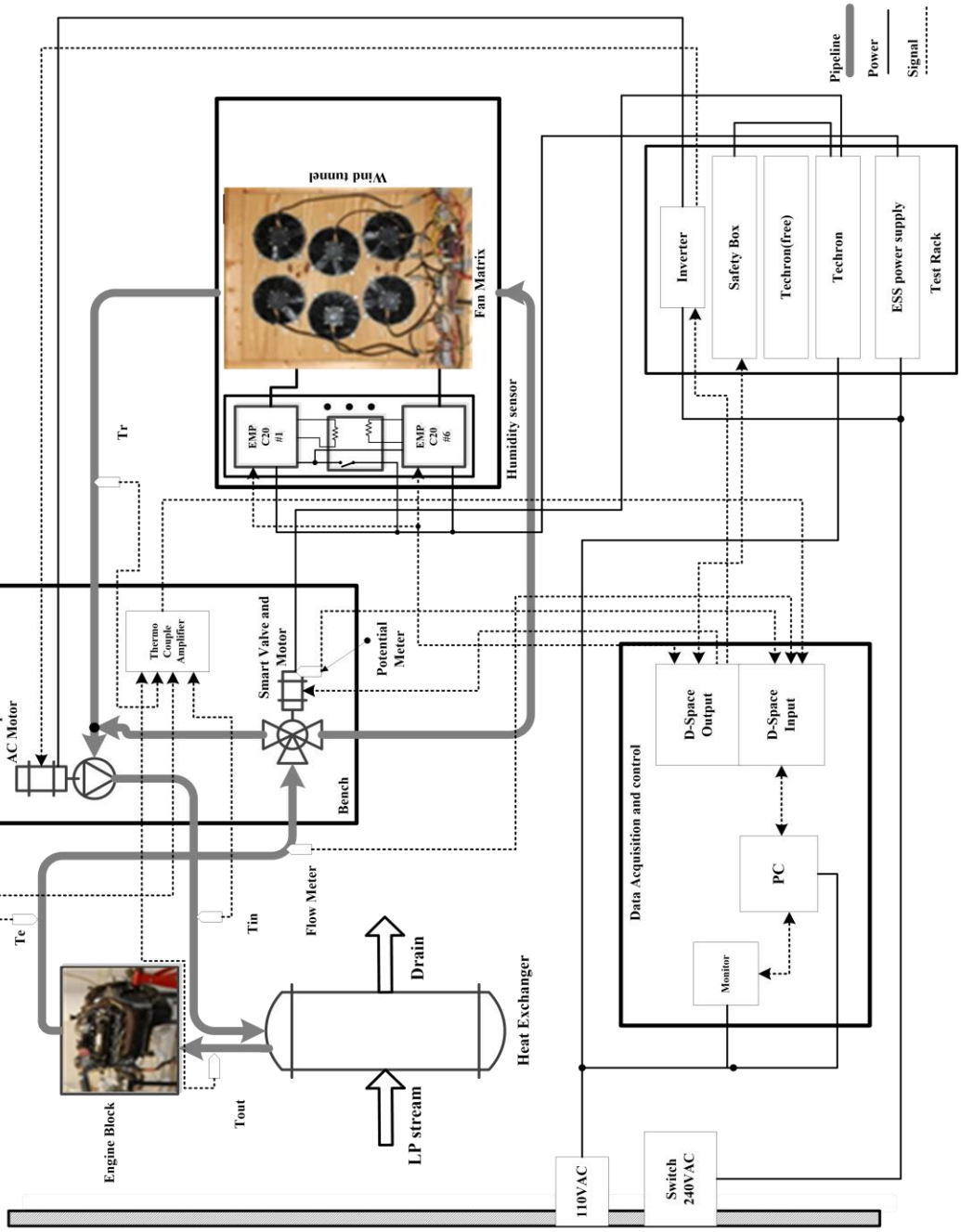

Figure 4.3: Experimental test bench block diagram

4.4 Introduction of Experimental System

An experimental bench was fabricated at Clemson University to provide a steady and repeatable test environment. The bench features a wind tunnel with radiator fan array and heat exchanger plus the corresponding cooling system actuators and sensors. A 6.8L International Truck V8 diesel engine supplies the thermal inertia. Figure 4.3 displays the overall test configuration and will be discussed in this section.

For the actuators, a three way smart coolant valve is driven by a worm gear assembly with a DC motor that may be controlled by the supply voltage. To circulate the coolant in the system, an AC motor variable speed pump is installed. At the radiator node, six EMP FiL-11, 11 inch electric radiator fans with 24V brushless DC motors are mounted in a wind tunnel. Each fan was electrically connected using a CAN (Controlled Area Network) Bus based DC motor controller (EMP C20). Different values of resistance were used to establish the specific IP address for each motor controller.

The system sensors include four Omega TC series J-types thermocouples located at the heat exchanger's inlet, T_{HI}, and outlet, T_{HO}, and the engine's and radiator's outlets, T_e and T_r. Each thermocouple is connected to a corresponding amplifier. A turbine type flow meter is located between the engine and smart valve to measure the coolant flow rate. A potentiometer is attached to the smart valve to monitor the valve's position. A multimeter measures the radiator fan matrix current, i, and supplied voltage, V_s, to calculate the radiator fan matrix power consumption, $P = iV_s$

Matlab/Simulink is selected as the programming software; the control algorithm can be compiled and downloaded to a dSPACE DS1003 board. Figure 4.3 also indicates

the signal transmission directions (as represented by the dotted lines).

A low pressure steam line is routed to a double-pass heat exchanger to heat the system to simulate the lumped heat generated by the engine's combustion process. The amount of heat supplied can be controlled by adjusting the steam supply and can be calculated for steady state condition as

$$q_{in} = \dot{m}_{cool} Cp_{cool} (T_{HI} - T_{HO}) \tag{4.33}$$

where T_{HI} and T_{HO} are the heat exchanger inlet and outlet temperatures, respectively. Prior tests were conducted to determine the estimated heat supplied to the coolant for various steam valve positions.

4.5 Test Results and Discussion

A representative set of numerical and experimental results will be presented in this section to investigate the performance of the nonlinear backstepping adaptive control law. In addition to the proposed nonlinear controller, two traditional control methods were considered, including a bang bang (also known as ON/OFF) controller and a proportional integral (PI) with lookup table based controller, for comparison. The reader is referred to Appendix C for more details. Three variables have been selected to compare the overall performance: the absolute steady state error, $|e_{ss}|$, the root mean square error, e_{RMS}, and the average radiator fan matrix power consumption, P_{ave}, can be calculated as

$$P_{ave} = \frac{1}{t} \int_0^t P_{fan} d\tau \tag{4.34}$$

where t is the total testing time ($t = 1800s$ in this instance), and P_{fan} is the power consumption of radiator fans at time τ. The reader should refer to (Wang *et al.*, 2014) for a completed radiator fan power consumption analysis. Table 4.1 lists the parameters values

used in the numerical and experimental tests. The experiment profiles are summarized in Table 4.2 and test results contained in Table 4.3.

Table 4.1: Summary of system model parameters

Symbol	Value	Units
C_e	17.14	$kJ/°C$
Cp_a	1	$kJ/kg°C$
Cp_{cool}	4.18	$kJ/kg°C$
C_r	8.36	$kJ/°C$
e_{high}	1	$°C$
e_{low}	-1	$°C$
H	1	-
K_1	0.5	-
K_2	0.5	-
K_I	-0.2	-
K_p	-2	-
$\dot{M}$	1	kg/s
n	6	-
ΔT	20	$°C$

Tests 1-4 of Case I were implemented to evaluate the controllers' performance in maintaining the engine's working temperature at a desired value, $T_{ed} = 72°C$, when subjected to various heat loads. Both the numerical Matlab/Simulink simulation and the experimental test bench were engaged. The input heat, q_{in} supplied to the cooling system in these tests was selected as an increasing step pattern with $75kW$, $80kW$, and $85kW$ at $t = 0s,\ 600s,$ and $1200s$. To get a more realistic test environment for Test 1, white noise with a 1% amplitude was added to the simulation. The initial engine temperature was set at $T_{e0} = 72.5°C$ for $t = 0s$.

Table 4.2: Design of experiment for Case I and II

*Initial engine temperature, T_{e0}, was set to 72.5°C for all tests

Case	Test No.	Controller Selection	Heat Flux, q_{in} (kW)			Reference Engine Temperature, $T_{ed}(°C)$		
			Time Period (s)					
			0≤t<600	601≤t<1200	1201≤t<1800	0≤t<600	601≤t<1200	1201≤t<1800
I	1	Backstepping Adaptive (Simulation Only)	75	80	85	72		
	2	Backstepping Adaptive						
	3	Bang bang						
	4	PI with Lookup Table						
II	5	Backstepping Adaptive (Simulation Only)	75			70	72	70
	6	Backstepping Adaptive						
	7	Bang bang						
	8	PI with Lookup Table						

Table 4.3: Test results to establish overall controller performance

Case	Test No.	Controller Selection	$\lvert e_{ss} \rvert$, $(°C)$	e_{RMS}, $(°C)$	P_{ave}, (kW)	Rank
I	2	Backstepping Adaptive	0.12	0.24	1.05	1
	3	Bang bang	N/A	2.18	1.96	3
	4	PI with Lookup Table	0.23	0.44	1.08	2
II	6	Backstepping Adaptive	0.11	0.62	0.73	1
	7	Bang bang	N/A	1.66	1.20	3
	8	PI with Lookup Table	0.36	0.83	0.74	2

The results of Tests 1 and 2 are given in Figures 4.4 and 4.5. The engine and radiator temperature responses in Figures 4.4(a) and 4.5(a), compare favorably with the desired engine temperature trajectory. As the heat load increases, the radiator temperature was controlled to a lower value to maintain the engine temperature at the given set point. Figures 4.4(b) and 4.5(b) show the engine temperature tracking errors verses time. The corresponding global radiator fan speeds in Figures 4.4(c) and 4.5(c) illustrate that the radiator fan speeds increase as the heat load increases. As expected, the radiator fan matrix operation directly impacts the radiator temperature, T_r, by air/coolant heat transfer, then affects the engine temperature, T_e, through the coolant flow. In these two tests, the nonlinear adaptive controller was successful in maintaining the tracking error within $\lvert e_{ss} \rvert = 0.05°C$ for the numerical simulation and $\lvert e_{ss} \rvert = 0.12°C$ for the experimental test at steady state. The nonlinear backstepping adaptive controller demonstrated robust performance when subjected to input heat changes at $t = 600s \; and \; 1200s$. The root mean square error deviation is $e_{RMS} = 0.24°C$ and the average radiator fan power consumption is $P_{ave} = 1.05kW$ per Test 2.

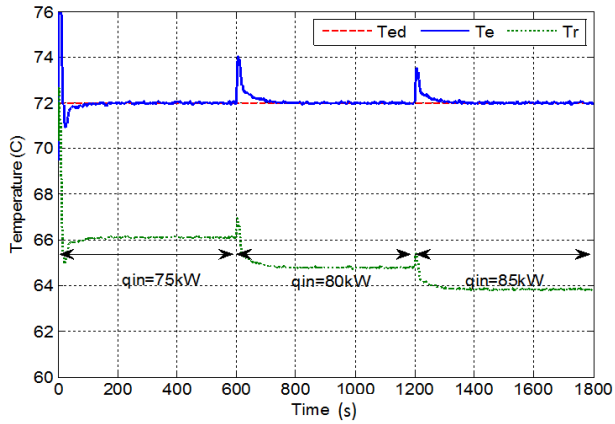

(a)

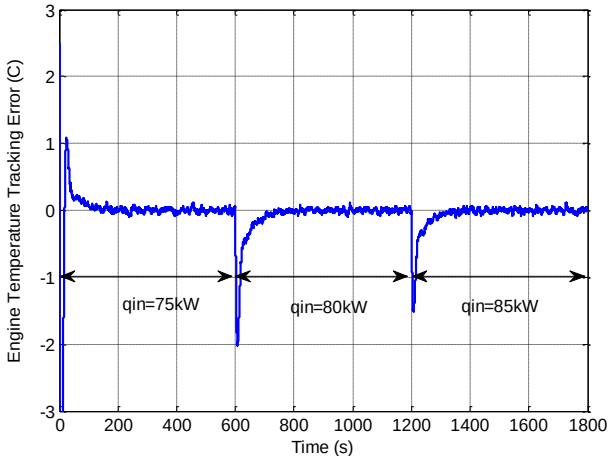

(b)

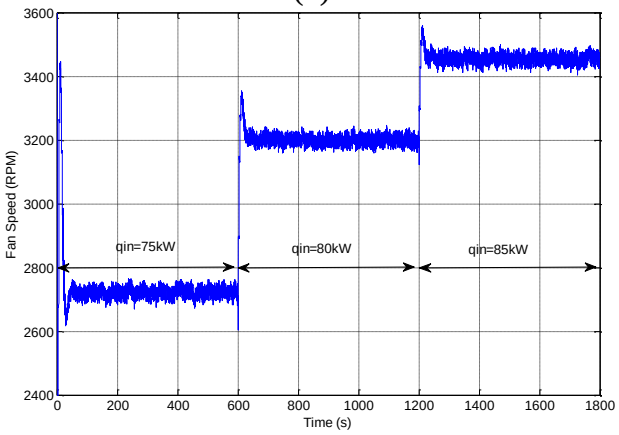

(c)

Figure 4.4: Test 1 numerical results - (a) engine and radiator temperatures, (b) engine temperature tracking error, and (c) global fan speeds verses time

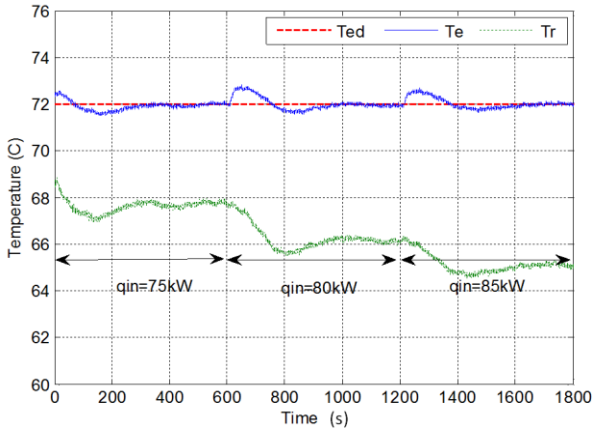

(a)

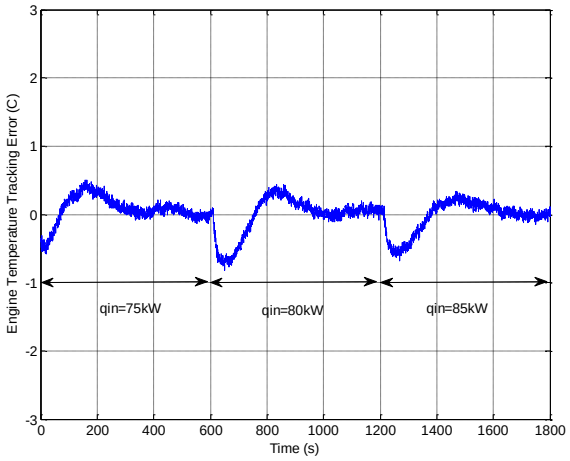

(b)

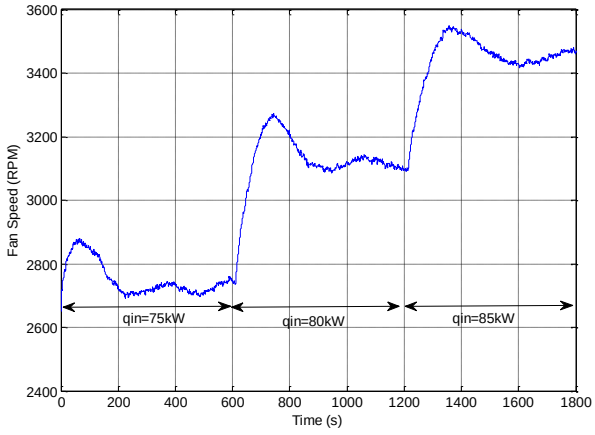

(c)

Figure 4.5: Test 2 experimental results - (a) engine and radiator temperatures, (b) engine temperature tracking error, and (c) global fan speeds verses time

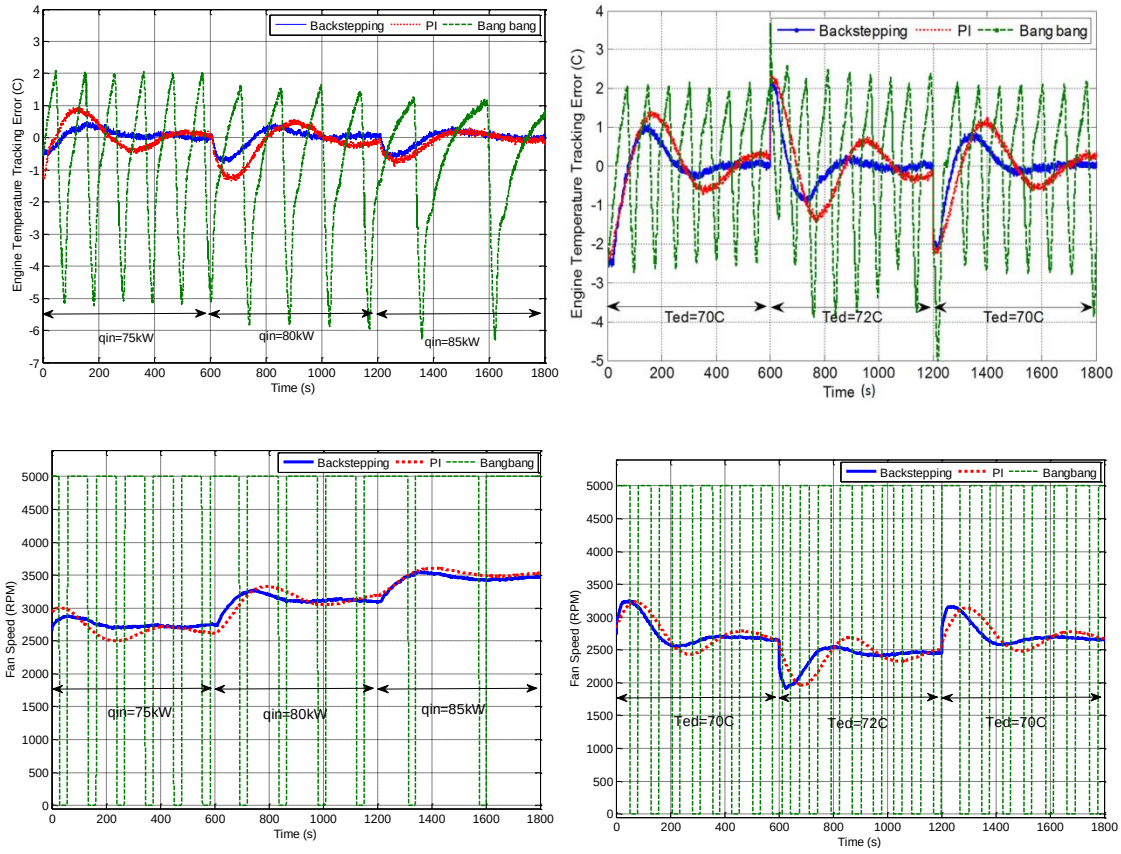

(a) (b)

Figure 4.6: Compared experimental results with engine temperature tracking errors and corresponding fan speed - (a) Tests 2-4 in Case I, and (b) Tests 6-8 in Case II

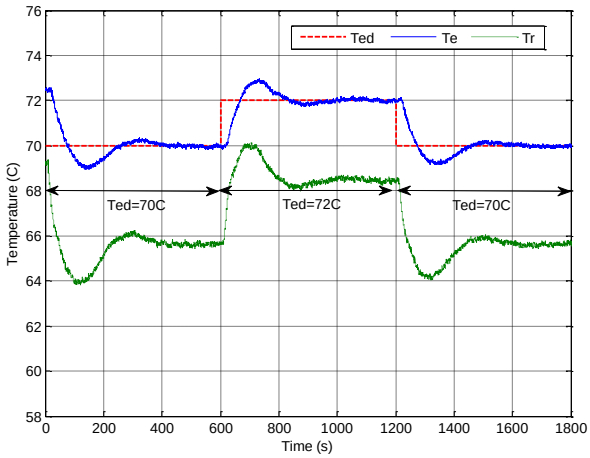

(a)

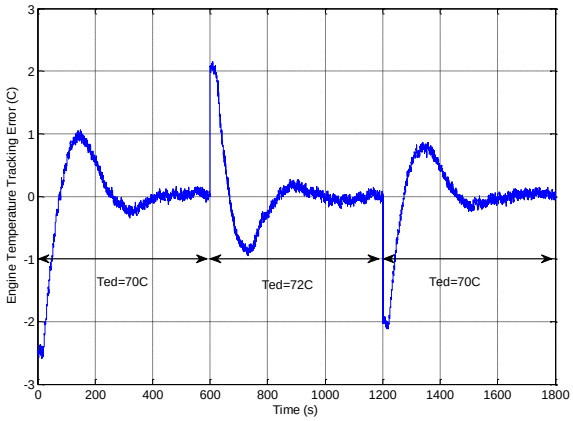

(b)

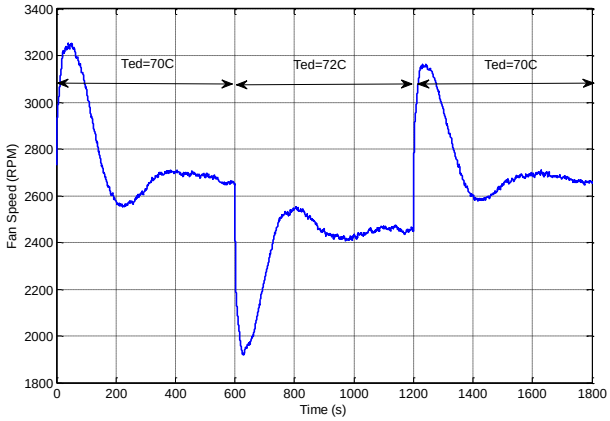

(c)

Figure 4.7: Test 6 Experimental results - (a) engine and radiator temperatures, (b) engine temperature tracking error, and (c) global fan speed verses time

The bang bang and proportional integral (PI) with lookup table based controllers were evaluated in Tests 3 and 4 in the same environment. A performance comparison of the different controllers has been displayed in Figure 4.6 (a). The test results indicate that the PI with lookup table based controller provided $|e_{ss}| = 0.23°C$. The root mean square error deviations of these two traditional controllers are $2.18°C$ and $0.44°C$. The power consumption is $P_{ave} = 1.96kW$ and $1.08kW$ for the bang bang and PI with lookup table based controllers. From this aspect, the nonlinear adaptive controller consumes 3% to 46% less total radiator fan power than the traditional controllers.

Two observations can be made for the cooling system bang bang controller (green dotted line in Figure 4.6(a)). First, as the heat load, q_{in}, increased, the fan matrix operation switching period approximately doubled. This phenomenon illustrates that when the engine heat load increased, it required a longer time to cool down the system using full fan matrix operation. Second, the bang bang control method struggled to cool the engine as the heat load increased for the engine temperature quickly exceeded the upper error limit, e_{high}, when the radiator fans were shut off. For instance, at $t = 257s$, the engine temperature move from $T_e = 70°C$ $(e = +2.0°C)$ to $T_e = 77.1°C$ $(e = -5.1°C)$ over a $32s$ time period with fans were off and then required 76s to recover using full fan matrix operation. Consequently, internal combustion engine tends to heat quickly but cool slowly based on heat transfer constraints so the fan matrix should operate continually under many scenarios. The phenomenon also demonstrated the limitation of the symmetric switching threshold. A switching model predictive control may be applied to increase the

control accuracy.

A fixed value of heat flux, $q_{in}(t) = 75kW$, was applied to the experimental system by maintaining the low pressure valve at a specific flow position in Case II (Tests 5-8). This test is designed to evaluate the controller's ability to regulate the engine's temperature to a set point from last steady-state operation. The prescribed desired temperature, T_{ed}, was selected as a step profile with a $2°C$ amplitude for transient analysis. The first and second time derivative of desired temperature are considered to be zero, (i.e., $\dot{T}_{ed} = \ddot{T}_{ed} = 0$). The initial engine temperature was $T_{e0} = 72.5°C$ for $t = 0s$. Figure 4.7 illustrates the real time temperature responses for both the engine and the radiator in Test 6. Figure 4.7(b) shows the engine temperature tracking error which was regulated within $|e_{ss}| = 0.11°C$ at steady state with $2°C$ peak errors at $t = 600s$ and $1200s$ moments. Figure 4.7(c) displays the corresponding global fans speeds. The root mean square error deviation is $e_{RMS} = 0.62°C$ and the average radiator fan power consumption is $P_{ave} = 0.73kW$. Similarly, the bang bang and proportional integral (PI) with lookup table based controllers were implemented under the same testing environment (Tests 7 and 8). A performance comparison of the different controllers has been displayed in Figure 4.6(b) for Tests 6-8 in Case II. The root mean square error is $e_{RMS} = 1.66°C$ and the power consumptions is $P_{ave} = 1.20kW$ for bang bang controller. On the other hand, the steady state error is $|e_{ss}| = 0.36°C$ when the PI with lookup table based controller is applied and the corresponding root mean square error is $e_{RMS} = 0.83°C$ with power consumption of $P_{ave} = 0.74kW$.

From the above discussions, it clearly shows that the nonlinear adaptive controller

offers smaller errors and fewer fluctuations than the two traditional control laws for both Cases I and II. Also, the nonlinear controller provides a faster response per Figure 4.6. From the power consumption aspect, the nonlinear controller is also the best operation strategy followed by the PI with lookup table based controller and the bang bang controller. Overall, the backstepping adaptive controller successfully regulated the engine temperature and compensated for unknown heat flux with minimum power consumption.

4.6 Summary

Advanced engine cooling systems can positively impact the performances of gasoline and diesel engine. In this study, a nonlinear adaptive control strategy for transient engine temperature tracking has been presented based on Lyapunov technique. An experimental test bench features with completed actuators and sensors have been fabricated. The control algorithm has been studied using both numerical and experimental tests. Two independent cases were investigated to demonstrate the control strategy can regulate the engine temperature tracking error within $0.12°C$ and compensate the unknown heat load generated in the combustion. Besides, the backstepping adaptive controller offered smaller error, less fluctuation, and faster response when compared with a traditional bang bang controller and a classical proportional-integral with lookup table based controller as well as less radiator fan power consumption.

CHAPTER V

ADVANCED ENGINE COOLING SYSTEM SUBJECTED TO RAM AIR EFFECT - NONLINEAR ADAPTIVE MULTIPLE INPUT AND MULTIPLE OUTPUT (NAMIMO) CONTROL

Advanced engine cooling systems typically replace the traditional mechanical cooling actuators with electrical controlled ones to reduce unnecessary power losses. The real time adjustment of the pump, valve, and radiator fans allow the engine temperature to be more accurately regulated. This chapter investigates a nonlinear adaptive multi-input and multi-output (NAMIMO) controller to operate the valve and radiator fans to control the engine temperature under different operating conditions. A nonlinear adaptive backstepping (NAB) control strategy and a state flow (SF) control law are introduced for comparisons. An experimental laboratory station has been fabricated to evaluate the proposed controllers. The test results show that the NAMIMO controller can regulate the engine temperature to a desired value ($|e| < 0.5°C$ at steady state) and compensate for unknown heat loads and ram air effects. In contrast, the NAB control law consumes the least radiator fan power but realized a larger average temperature tracking error (40% greater than NAMIMO controller), longer response time (34% greater than NAMIMO controller), and shows weakness when the heat load is low. Lastly, the SF controller, characterized by greater oscillation and electrical power consumption (18.9% greater than the NAMIMO controller), was easy to realize and maintained the engine temperature within $|e| < 5°C$.

5.1 Introduction

Typically, the current engine cooling system is designed to keep the engine temperature in an acceptable range even during the worst working conditions (Sermeno *et al.,* 2014). In a traditional setup, the mechanical pump and radiator fan(s) are indirectly connected with the crankshaft. A wax-based thermostat is mounted to regulate the coolant flow route through the radiator. Although the system reliability has been repeatedly demonstrated in past decades, two limitations exist. On the one hand, the mechanical coupling leads the operation of the actuators (pump and radiator fans) to be dependent on the engine speed which cannot be controlled accurately for cooling purposes and typically yields engine overcooling. It has been suggested that overcooling can degrade the engine performance (Wagner *et al.,* 2002), increase the lubricate oil friction (Kim *et al.,* 2013) and necessitate more work than needed by this subsystem which lead a lower fuel economy. On the other hand, the mechanical connections, such as accessory belts and clutches, generate unnecessary energy losses but provide proven interface.

An advanced engine cooling system introduces the concept of "thermal management" by regulating the engine coolant to a precise working temperature with minimum power consumption (Setlur *et al.,* 2014). A smart engine cooling system updates the mechanical pump and radiator fan(s) with electrical controlled components and replaces the wax-based valve with a 3-way computer controlled smart valve. With these features, each actuator can be operated accurately to achieve a certain heat rejection requirement with minimum energy utilization theoretically. Besides, assorted sensors are mounted to monitor the system's dynamics and operating environment. The electronic control unit (ECU)

hosts the control strategy and sends out commanded signals to the actuators based on the real time system dynamics and prescribed control algorithm. The diagram of an advanced cooling system is shown in Figure 5.1.

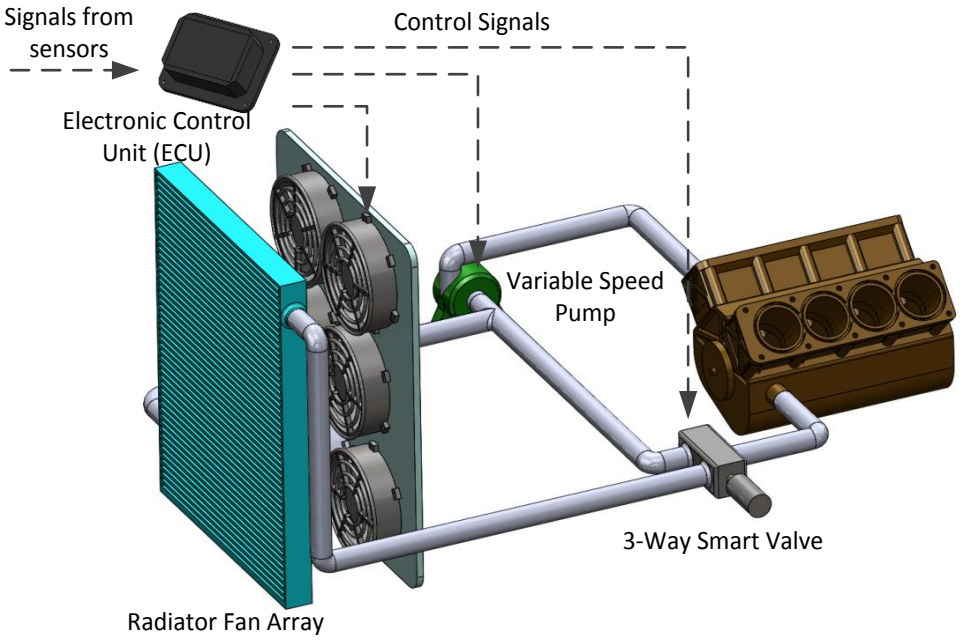

Figure 5.1: Advanced internal combustion engine cooling system

To complement the updated configuration of the cooling system, assorted control strategies have been proposed for these actuators. Wang *et al*. (2015) explored an optimal fan matrix control strategy to minimize the radiator fan power while achieving the requested heat rejection. Wang *et al.* (2015) proposed a Lyapunov based backstepping nonlinear control strategy to adjust the radiator fan matrix operation to track a desired engine temperature while compensating the unknown heat input with minimum power consumption. Salah *et al.* (2009 and 2010) designed nonlinear control strategies to control the smart valve position or the coolant pump speed to realize the desired engine temperature.

Wagner *et al.* (2002) investigated the electrical water pump and a thermostat valve control approach to achieve faster engine warm-up. Butt *et al.* (2014) investigated input-output linearization and model-predictive control strategies by implementing the experimental test on a small prototype configuration. Khodabakhshian *et al.* (2014) proposed a model predictive control method and a global optimal solution to improve the fuel efficiency of conventional trucks.

This chapter investigates a nonlinear adaptive MIMO (NAMIMO) controller for the operation of the cooling system actuators. The remained of the article is organized as follows. A detailed mathematical model and system analysis will be presented in Section 5.2. The NAMIMO controller with stability analysis will be introduced in Section 5.3. Section 5.4 contains the fully experimental test bench description, followed by the discussion of test results in Section 5.5. Finally, the summary will be offered in Section 5.6.

5.2 Mathematical Models

To investigate the smart automotive engine cooling system, a lumped parameter mathematical model has been formulated to describe the thermal dynamics. The cooling system configuration with fluid flow direction has been displayed in Figure 5.2. The color variation indicates the coolant temperature changes. In this research, three assumptions have been imposed on the thermal system:

A1: No heat losses occur in the system other than forced convection through the radiator.

A2: Engine heat load due to the combustion process can be removed by the cooling system once warm up has been accomplished.

A3: The desired engine and radiator working temperatures are assumed to be quasi constants.

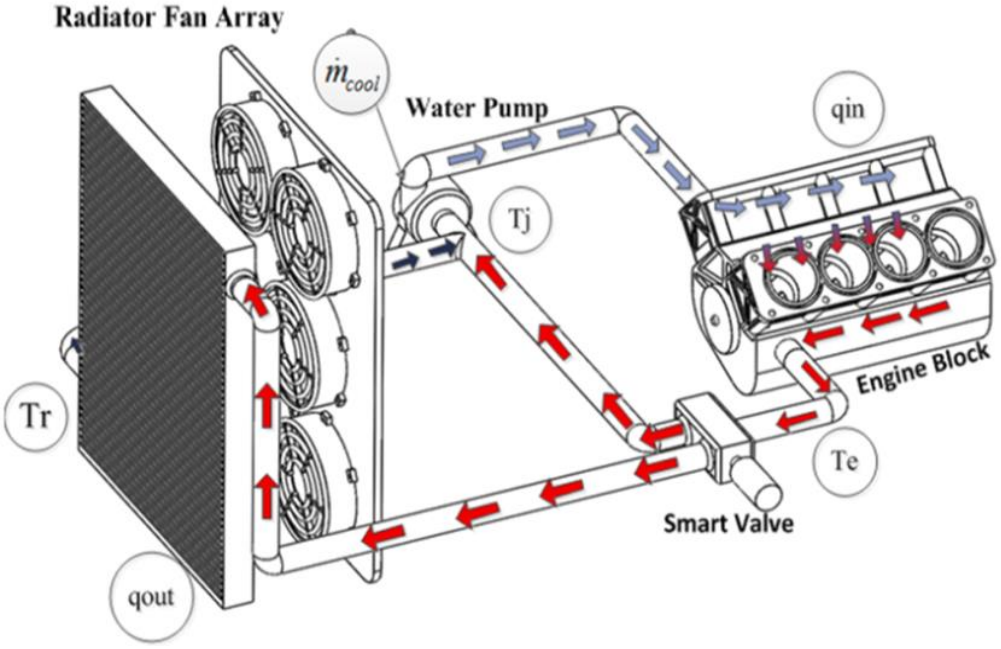

Figure 5.2: Engine cooling system and coolant flow directions

5.2.1 Cooling System Thermal Dynamics

Two heat exchangers, engine and radiator, can be considered in a standard automotive cooling system. The governing equations for these two thermal components can be described as

$$C_e\dot{T}_e = -\dot{m}_{cool}Cp_{cool}(T_e - T_j) + q_{in} \tag{5.1}$$

$$C_r\dot{T}_r = \dot{m}_{cool}HCp_{cool}(T_e - T_r) - q_f - q_{ram} \tag{5.2}$$

where the variables T_e and T_r denote the engine and radiator temperatures. The variable $\dot{m}_{cool}$ represents the coolant mass flow rate. The parameters Cp_{cool}, C_e, and C_r are the heat capacity of the coolant, engine, and radiator at constant pressure. The term q_{in} is the

heat load generated by the combustion process. The variable H represents the smart valve position with $H = 0$ and $H = 1$ corresponding to fully closed and open positions, respectively.

The coolant temperature at the junction, T_j, depends on the mixing temperature of the fluids flowing through the bypass and radiator, or

$$T_j = (1 - H)T_e + HT_r \tag{5.3}$$

The variables q_f and q_{ram} in equation (5.2) describe the heat rejected due to the radiator fan(s) and the ram air effect. The explicit expression for q_f can be written as

$$q_f = \dot{m}_f Cp_a(T_r - T_\infty) \tag{5.4}$$

where Cp_a is the heat capacity of the air, and the variable T_∞ is the ambient temperature. According to a previous study, the air mass flow rate due to the radiator fans, $\dot{m}_f$, is a nonlinear function of the number of fans, n, and the radiator fan speed, N, so that $\dot{m}_f = F_f(N_f, n)$. The ram air effect, q_{ram}, can be expressed as

$$q_{ram} = H(v_{vehicle}, v_{wind}, \alpha_{wind}) \tag{5.5}$$

where $v_{vehicle}$ and v_{wind} are the vehicle and wind speeds. The term α_{wind} denotes the attack angle of the wind with respect to the vehicle's radiator position.

5.2.2 Dynamic Analysis of Open Loop System

The open loop behavior of the cooling system's thermal dynamics can be analyzed to determine the operating space. This effort offer insight into the control system design to accommodate the desired engine heat rejection. First, substitute equation (5.3) into (5.1) so that the engine temperature becomes

$$C_e\dot{T}_e = -\dot{m}_{cool}HCp_{cool}(T_e - T_r) + q_{in} \tag{5.6}$$

Now, add equations (5.2) and (5.6) together such that the rate of the entire cooling system heat change may be expressed as

$$C_e\dot{T}_e + C_r\dot{T}_r = q_{in} - q_f - q_{ram} \tag{5.7}$$

Equation (5.7) indicates that the system heat, $C_eT_e + C_rT_r$, depends on the difference between the engine heat load, q_{in}, and the active, q_f, and ram air, q_{ram}, heat rejected through the radiator. Equation (5.4) may be substituted into equation (5.2), and then rewrite equations (5.2) and (5.6) rewritten in a compact state space form as

$$\dot{x} = Ax + C \tag{5.8}$$

where

$$x = [T_e \;\; T_r]^T \tag{5.9a}$$

$$A = \begin{bmatrix} \frac{-\dot{m}_{cool}HCp_{cool}}{C_e} & \frac{\dot{m}_{cool}HCp_{cool}}{C_e} \\ \frac{\dot{m}_{cool}HCp_{cool}}{C_r} & \frac{-\dot{m}_{cool}HCp_{cool} - \dot{m}_fCp_a}{C_r} \end{bmatrix} \tag{5.9b}$$

$$C = \begin{bmatrix} \frac{q_{in}}{C_e} \\ \frac{\dot{m}_fCp_aT_\infty - q_{ram}}{C_r} \end{bmatrix} \tag{5.9c}$$

The equilibrium point of this system (constant solution to equation (5.8)), T_e^* and T_r^*, can be calculated as

$$\dot{x} = 0; \quad \begin{bmatrix} T_e^* \\ T_r^* \end{bmatrix} = \begin{bmatrix} \frac{q_{in}}{\dot{m}_{cool}HCp_{cool}} + \frac{q_{in} - q_{ram}}{\dot{m}_fCp_a} + T_\infty \\ \frac{q_{in} - q_{ram}}{\dot{m}_fCp_a} + T_\infty \end{bmatrix} \tag{5.10}$$

Equation (5.10) implies that the fixed point exists only when $\dot{m}_{cool}HCp_{cool}$ and $\dot{m}_fCp_a$ are non-zero (i.e., the pump and radiator fans are not idle and the valve is not in a

fully closed position). The sign of eigenvalues of the open-loop system state matrix *A*, $\lambda_{A1,2}$, can be determined by the matrix invariant

$$\lambda_{A1} + \lambda_{A2} = tr(A) = \frac{-\dot{m}_{cool} HCp_{cool}}{C_e} + \frac{-\dot{m}_{cool} HCp_{cool} - \dot{m}_f Cp_a}{C_r} < 0 \qquad (5.11a)$$

$$\lambda_{A1}\lambda_{A2} = det(A) = \frac{\dot{m}_c HCp_{cool}\dot{m}_f Cp_a}{C_e C_r} > 0 \qquad (5.11b)$$

Equation (5.11) reveals that the eigenvalues for the matrix A are always negative. As a result, the engine and radiator temperatures (T_e, T_r) can approach the equilibrium point (T_e^*, T_r^*) as time goes to infinity. On the other hand, the equilibrium point may not exist for two special situations.

Case 1: Coolant pump is shut off or the smart valve is at a fully closed position, (i.e., $\dot{m}_c H = 0$). In this situation, equation (5.8) becomes

$$\begin{bmatrix} \dot{T}_e \\ \dot{T}_r \end{bmatrix} = \begin{bmatrix} 0 & 0 \\ 0 & \frac{-\dot{m}_f Cp_a}{C_r} \end{bmatrix} \begin{bmatrix} T_e \\ T_r \end{bmatrix} + \begin{bmatrix} \frac{q_{in}}{C_e} \\ \frac{\dot{m}_f Cp_a T_\infty - q_{ram}}{C_r} \end{bmatrix} \qquad (5.12)$$

which demonstrates that the engine temperature, T_e, keeps increasing since $\dot{T}_e$ is always positive when $q_{in} > 0$. This situation may happen during an engine warm up (i.e., cold start) scenario.

Case 2: Radiator fans are shut off, $q_f = 0$, such that equation (5.8) becomes

$$\begin{bmatrix} \dot{T}_e \\ \dot{T}_r \end{bmatrix} = \begin{bmatrix} \frac{-\dot{m}_{cool} HCp_{cool}}{C_e} & \frac{\dot{m}_{cool} HCp_{cool}}{C_e} \\ \frac{\dot{m}_{cool} HCp_{cool}}{C_r} & \frac{-\dot{m}_{cool} HCp_{cool}}{C_r} \end{bmatrix} \begin{bmatrix} T_e \\ T_r \end{bmatrix} + \begin{bmatrix} \frac{q_{in}}{C_e} \\ \frac{-q_{ram}}{C_r} \end{bmatrix} \qquad (5.13)$$

Consider equation (5.7) first. If $q_f = 0$ and the ram air effect, q_{ram}, is greater than the heat load, q_{in}, then the entire system heat will decrease. Predictably, a pump-valve combination control strategy exists to maintain the engine temperature, T_e, at the

desired point. This phenomenon may be considered as highway operation with abundant ram air. On the other hand, if $q_f = 0$, and the ram air effect, q_{ram}, is less than the heat load, q_{in}, then the system heat will increase. According to the cooling system configuration, it is not possible to maintain the engine temperature, T_e, for the heat input directly supplied to the engine. This corresponds to a vehicle under high load and low speed (not enough ram air) which requires the radiator fans to be operated to prevent overheating.

5.3 Control Strategies

A nonlinear adaptive multi-input and multi-output (NAMIMO) controller has been developed to regulate the engine and radiator temperatures, T_e and T_r. The challenge of this controller design is from two uncertain system variables. Namely, the heat load generated by the combustion process, q_{in}, and the heat rejection due to the ram air effect, q_{ram}. As these two entities cannot be easily measured, the controller must compensate for them. For compassion purposes, two other control methods have been considered, a nonlinear adaptive backstepping (NAB) and a state flow (SF). The reader is referred to Chapter IV and Appendix D for more details of the NAB and SF controllers.

5.3.1 Closed-Loop Feedback System Description

To evaluate the temperature tracking control objective, the tracking error signals e and r are defined as

$$e = T_{ed} - T_e \tag{5.14}$$

$$r = T_{rd} - T_r \tag{5.15}$$

where T_{ed} and T_{rd} represent the desired engine and radiator temperatures, respectively. Note that the set point temperatures are assumed constant (*A3*), so that $\dot{T}_{ed} = \dot{T}_{rd} = 0$.

The control objective is to ensure that the engine and radiator temperatures track the desired values, such that

$$e, r \to 0 \text{ as } \quad t \to \infty \tag{5.16}$$

Furthermore, the controller must compensate for the unknown system parameters q_{in} and q_{ram} or

$$\hat{q}_{in} \to q_{in}, \hat{q}_{ram} \to q_{ram} \qquad \text{as} \quad t \to \infty \tag{5.17}$$

where $\hat{q}_{in}$ and $\hat{q}_{ram}$ are the estimated variables of the heat load and ram air effect, respectively.

Now, substitute equations (5.4), (5.14), and (5.15) into equations (5.2) and (5.6), so that the closed-loop feedback system can be formulated as

$$\dot{e} = \frac{u_1 Cp_{cool}}{C_e}(T_{ed} - e - T_{rd} + r) - \frac{q_{in}}{C_e} \tag{5.18}$$

$$\dot{r} = -\frac{u_1 Cp_{cool}}{C_r}(T_{ed} - e - T_{rd} + r) + \frac{u_2 Cp_a(T_{rd} - r - T_\infty) + q_{ram}}{C_r} \tag{5.19}$$

where $u_1 = \dot{m}_{cool} H = F_{H,p}(H, N_{pump})$ denotes the system input '1' which is an inseparable system input of the 'pump-valve combination'. The second system input, '2', or $u_2 = \dot{m}_f = F_f(N_f, n)$ corresponds to the operation of the radiator fans.

5.3.2 NAMIMO Controller Design and Stability Analysis

The feedback system inputs, u_1 and u_2, and the estimated parameters $\hat{q}_{in}$ and $\hat{q}_{ram}$ can be designed based on the definitions above as

$$u_1 = \dot{m}_{cool} H = \frac{\hat{q}_{in} - C_e k_1 e}{Cp_c(T_e - T_r)} \tag{5.20}$$

$$u_2 = \dot{m}_f = \frac{u_1 HCp_{cool}(T_e - T_r) - \hat{q}_{ram} - C_r k_2 r}{Cp_a(T_r - T_\infty)} \tag{5.21}$$

$$\hat{q}_{in} = -\frac{1}{C_e}\int_{t_0}^{t} e\, d\tau \tag{5.22}$$

$$\hat{q}_{ram} = \frac{1}{C_r}\int_{t_0}^{t} r\, d\tau \tag{5.23}$$

where k_1 and k_2 are the positive controller gains.

To demonstrate the stability of the feedback system, first substitute equations (5.20) and (5.21) into equations (5.18) and (5.19), which leads to

$$\dot{e} = -k_1 e + \frac{\hat{q}_{in}}{C_e} - \frac{q_{in}}{C_e} \tag{5.24}$$

$$\dot{r} = -k_2 r - \frac{\hat{q}_{ram}}{C_r} + \frac{q_{ram}}{C_r} \tag{5.25}$$

Next, rewrite equations (5.22)-(5.25) in compact form as

$$\dot{y} = By + D \tag{5.26}$$

where

$$y = [e \quad r \quad \hat{q}_{in} \quad \hat{q}_{ram}]^T \tag{5.27a}$$

$$B = \begin{bmatrix} -k_1 & 0 & 1/C_e & 0 \\ 0 & -k_2 & 0 & -1/C_r \\ -1/C_e & 0 & 0 & 0 \\ 0 & 1/C_r & 0 & 0 \end{bmatrix} \tag{5.27b}$$

$$D = \begin{bmatrix} -\frac{q_{in}}{C_e} & \frac{q_{ram}}{C_r} & 0 & 0 \end{bmatrix}^T \tag{5.27c}$$

The equilibrium point for equation (5.26) becomes

$$\dot{y} = 0; \qquad \begin{bmatrix} e^* \\ r^* \\ \hat{q}_{in}^* \\ \hat{q}_{ram}^* \end{bmatrix} = \begin{bmatrix} 0 \\ 0 \\ q_{in} \\ q_{ram} \end{bmatrix} \tag{5.28}$$

The eigenvalues of the closed loop state matrix B may be written as

$$\begin{bmatrix}\lambda_{B1,2}\\ \lambda_{B3,4}\end{bmatrix}=\begin{bmatrix}-\frac{k_1}{2}\pm\sqrt{\frac{k_1}{4}-\frac{1}{{C_e}^2}}\\ -\frac{k_2}{2}\pm\sqrt{\frac{k_2}{4}-\frac{1}{{C_r}^2}}\end{bmatrix} \tag{5.29}$$

Equation (5.29) indicates that the eigenvalues always have negative real parts with the designed controller, equations (5.20)-(5.23) applied. It demonstrates an attractor at the point $(0,0,q_{in},q_{ram})$. Note that, the eigenvalues may or may not have an imaginary part dependent on the selected controller gains, k_1 and k_2, which indicates that the system may or may not oscillate.

Remark 1: Internal combustion engines generate a certain amount of heat based on the size and configuration. As a result, the estimated parameter $\hat{q}_{in}$ has the upper bound $\hat{q}_{in} \leq q_{inu}$.

Remark 2: Vehicle movement and wind speed can remove a finite amount of heat so that the estimated parameter $\hat{q}_{ram}$ has the upper bound $\hat{q}_{ram} \leq q_{ramu}$.

5.3.3 Selection of Desired Reference Values

The desired engine temperature, T_{ed}, may be selected according to the vehicle's operation to realize the imposed working condition. On the other hand, the selection of the desired radiator temperature, T_{rd}, should be based on the power consumption. It is important to carefully determine the system reference values since they impact the controller's performance and the actuator power usage.

Remark 3: Radiator fans consume the most electric power (about 85%) followed by the coolant pump (about 15%) and the smart valve (less than 1%) for a standard electro-mechanical thermal management system. One of the best control strategies is to decrease the radiator fan "on time" to reduce the power demand.

Consider the steady state scenario for the feedback system in equation (5.18), when $e = \dot{e} = r = 0$. This operating condition allows the closed-loop feedback system to be rewritten at the equilibrium point as

$$0 = \frac{u_1 Cp_{cool}}{C_e}(T_{ed} - T_{rd}) - \frac{q_{in}}{C_e} \tag{5.30}$$

which leads to

$$T_{ed} - T_{rd} = \frac{q_{in}}{u_1 Cp_{cool}} \tag{5.31}$$

Equation (5.31) implies that the temperature difference between the two system references, $T_{ed} - T_{rd}$, is a function of the heat load, q_{in}, and the pump-valve combination, u_1. Consider the working spectrum of the pump-valve combination, $u_{1min} \leq u_1 < u_{1max}$. The range of possible temperature differences in equation (5.31) can be expressed as

$$\frac{q_{in}}{u_{1max} Cp_{cool}} < T_{ed} - T_{rd} \leq \frac{q_{in}}{u_{1min} Cp_{cool}} \tag{5.32}$$

where $u_{1min} = \dot{m}_{cmin} H_{min}$ and $u_{1max} = \dot{m}_{cmax} H_{max.}$ In addition, the radiator temperature cannot generally be controlled lower than the ambient temperature, T_∞. As a result, T_{rd} may be bounded between

$$T_{ed} - \frac{q_{in}}{u_{1max} Cp_{cool}} > T_{rd} \geq MAX(T_{\infty}, T_{ed} - \frac{q_{in}}{u_{1min} Cp_{cool}}) \tag{5.33}$$

From a power consumption perspective (*Remark 3*), the coolant pump and smart valve should be operated at maximum capacity ($u_1 = u_{1max}$) to allow a possible decrease in the radiator fan speed. Specifically, the target radiator temperature expression becomes $T_{rd} = T_{ed} - \frac{q_{in}}{u_{1max} Cp_{cool}}$.

In practice, the heat load, q_{in}, cannot generally be measured in real time. For the NAMIMO controller, T_{rd} can be considered to be a function of the estimated heat load, $\hat{q}_{in}$. However, the estimated heat load, $\hat{q}_{in}$, is an integral term of the time-variant engine temperature tracking error, e, as shown in equation (5.22). Further, the operation of the radiator fan is characterized by a large time constant to regulate the radiator temperature. A time-varying desired radiator temperature, T_{rd}, will cause a large fluctuation of the radiator fan speed which is not applicable. To compensate for the fluctuation, a "slow change" reference should be prescribed. In this project, based on the baseline calibrations, the selection of T_{rd} shall be defined as a step function with

$$T_{rd} = \begin{cases} T_{rdl}; & \hat{q}_{in} \geq \hat{q}_{inh} \\ T_{rdm}; & \hat{q}_{inh} > \hat{q}_{in} > \hat{q}_{inl} \\ T_{rdh}; & \hat{q}_{in} \leq \hat{q}_{inl} \end{cases} \tag{5.34}$$

where T_{rdh}, T_{rdl}, and T_{rdm} are the selected radiator temperatures. Similarly, $\hat{q}_{inh}$ and $\hat{q}_{inl}$ are the heat input thresholds according to the baseline calibration.

5.3.4 Calibration Approach for System Input u_1 and u_2

From a power consumption viewpoint (*Remark 3*), the coolant pump consumes much more power than the valve. Equation (5.20) offers the system input '1', pump-valve

combination, u_1. An engineering calibration approach can be formulated. For example, in 3, as the value of the pump-valve combination u_1 increases, first calibrate the valve position from H_{min} to H_{max} while keeping the coolant mass flow rate at its lower limitation, $\dot{m}_c = \dot{m}_{cmin}$. As u_1 increases, the pump speed can then be raised once the valve position has reached its maximum value (green solid line). On the other hand, when the system input '1', u_1, decreases, the coolant mass flow rate is first adjusted followed by the valve closing (dotted yellow line).

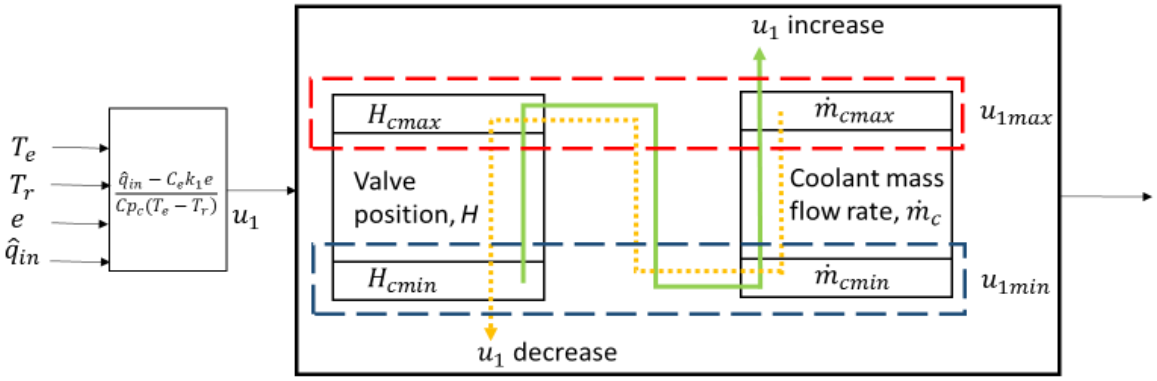

Figure 5.3: Calibration turning method for the system input '1', u_1, increasing (solid green line) and deceasing (dotted yellow line) with thermal loading

A previous study proposed an optimal radiator fan operating strategy (i.e., system controller u_2), for various heat loads. In this research, the number of fans is selected as $n = 6$ to simplify the testing and analysis. In other words, the same operating path is traced for all thermal load variations.

5.4 Experimental Test Bench

An experimental laboratory bench was created to evaluate the performance of the proposed control strategies. A static 6.8L International Truck V8 diesel engine was se-

lected as the test subject. Low pressure (LP) steam was supplied to emulate the heat generated by the engine's combustion process using a shell-tube heat exchanger with the engine coolant and the steam. The heat supplied to the system can be estimated using the coolant dynamics given as

$$q_{in} = \dot{m}_{cool} Cp_{cool} (T_{HI} - T_{HO}) \tag{5.35}$$

where T_{HI} and T_{HO} are the heat exchanger inlet and outlet temperatures, respectively.

To redirect the coolant flow path, a worm gear assembly driven three way smart coolant valve was installed. An AC motor driven pump was mounted to circulate the coolant. Six CAN (Controlled Area Network) bus controlled 24V brushless DC fans were installed in a wind tunnel along with a radiator. Four Omega J-type thermocouples measured the temperature at the heat exchanger's inlet, T_{HI}, and outlet, T_{HO}, and the engine's and radiator's outlets, T_e and T_r. The coolant flow rate was measured using a turbine type flow meter. The valve's position was monitored by a potentiometer. The working state of the radiator fans was obtained through the CAN bus signals. An auxiliary axial fan, Triangle SPL4223, was located in front of the fan matrix to simulate the ram air effect, q_{ram}. The test bench is shown in Figure 5.4 and a complete experimental bench description can be found in Chapter IV.

Figure 5.4: Picture of experimental test bench - smart valve, coolant pump, and radiator fans with ram air axial fan

5.5 Presentation and Discussion of Test Results

A series of experimental tests were conducted to evaluate the performance of the three proposed control laws. The design of experiment and the parameters values used in the tests are listed in Table 5.1 and 5.2. For each test, a step heat input was applied at time $t = [1min, 11min, 21min]$. The ram air axial fan was turned 'ON' in Tests 2, 4, and 6 for time $t \geq 1min(60s)$. In Tests 1-6, the pump speed was not adjusted automatically but rather the coolant flow rate was fixed at $\dot{m}_{cool} = \dot{m}_{cmax}$. The valve was operated in real time, so the system input '1' corresponded to $u_1 = \dot{m}_{cmax}H$. The radiator fans were operated between $0RPM$ to $5{,}000RPM$. For Test 7, the pump speed was manually adjusted to illustrate the pump-valve combination concept. The desired engine temperature was selected as $T_{ed} = 80°C$ for safety considerations.

In all tests, four metrics have been chosen to evaluate the overall performance with the test results summarized in Table 5.3.

S1: Settling time, t_{ss}: Time required for the engine temperature to reach the 2% ($\pm 1.6°C$) error band after a step heat input change.

S2: Average radiator electric power consumption, P_{fan}: Average total radiator fan power consumption during the test time.

S3: Average pump electric power consumption, P_{pump}: Average pump power consumption during the test time.

S4: Mean absolute error, e_M: Average difference between the measured engine temperature, T_e, and the desired engine temperature, T_{ed}, during the tests.

5.5.1 NAMIMO Controller

In the laboratory tests, an engine undergoes two moderate thermal loadings which are subsequently removed to evaluate the general cooling system's temperature tracking performance. The results of Test 1 are shown in Figure 5.5. The engine and radiator temperature responses in Figure 5.5(a) favorably compare with the desired engine and radiator temperature trajectories. Figure 5.5(b) displays the engine tracking error, e, verses time which shows that the NAMIMO controller successfully regulated the engine temperature about $80°C$ when subjected to three different heat loads with less than a $2\text{min}(120s)$ recovery time. Figures 5.5(c) and 5.5(d) present the cooling actuator (e.g., valve, radiator fans) operations. As expected, when the heat load increased at times $t = 1min$ and $t = 11min$, the valve opened more each time to allow a greater coolant flow through the radiator. In the meantime, the radiator fan speed was increased to promote

external convective heat transfer. The opposite is true when the heat load was removed at time $t = 21min$.

Table 5.1: Summary of experiments with desired temperature, $T_{ed} = 80°C$ (NAMIMO: Nonlinear adaptive multiple input and multiple output, NAB: Nonlinear adaptive backstepping, SF: State flow)

Test No.	Controller Design	Heat input rate, q_{in} (kW); Coolant Mass Flow Rate, $\dot{m}_{cool}$ (kg/s)				Ram Air	
		Time (min)					
		[0,1)	[1,11)	[11,21)	[21,31]	[0,1)	[1,31]
1	NAMIMO	20; 1	55; 1	90; 1	20; 1	OFF	OFF
2							ON
3	NAB						OFF
4							ON
5	SF						OFF
6							ON
7	NAMIMO	20; 0.6	55; 0.8	90; 1	20; 0.6		OFF

Table 5.2: List of system model and controller parameters

Symbol	Value	Units	Symbol	Value	Units	Symbol	Value	Units
C_e	17.14	$kJ/°C$	K_1	0.5	-	$\hat{q}_{inl}$	35	kW
Cp_a	1	$kJ/kg°C$	K_2	0.5	-	T_{ed}	80	$°C$
Cp_c	4.18	$kJ/kg°C$	$\dot{m}_{cmax}$	1	kg/s	T_H	82	$°C$
C_r	8.36	$kJ/°C$	N_{fmax}	5000	RPM	T_L	78	$°C$
H_{max}	0.95	-	N_{fmin}	0	RPM	T_M	80	$°C$
H_{nom}	0.50	-	N_{fnom}	2500	RPM	T_{rdh}	65	$°C$
H_{min}	0.05	-	q_{inu}	100	kW	T_{rdl}	55	$°C$
k_1	0.5	-	q_{ramu}	60	kW	T_{rdm}	60	$°C$
k_2	0.5	-	$\hat{q}_{inh}$	75	kW			

As show in Figure 5.5(a), the desired radiator temperature, T_{rd}, (green dash line) changed automatically subject to the various heat loads. Figure 5.6 displays the estimated heat input, $\hat{q}_{in}$, as well as the desired radiator temperature, T_{rd}, verses time for Test 1.

The selection of the desired radiator temperature per equation (5.34) results in the stepped profile. For example, when the heat load was suddenly increased from $55kW$ to $90kW$ at time $t = 11min$, the estimated heat load, $\hat{q}_{in}$, climbed from $\hat{q}_{in} \approx 55kW$ to $\hat{q}_{in} \approx 90kW$ which exceeded the upper threshold, $\hat{q}_{inh} = 75kW$ at time $t = 12.3\,min$. To cool the engine, the desired radiator temperature shifted from $60°C$ to $55°C$ which produced a sharp increase in the radiator fan speed ($4{,}000RPM$ to $5{,}000RPM$ as shown in Figure 5.5(d)). In contrast, when the heat load was suddenly removed at time $t = 21\,min$, the estimated heat load decreased to $\hat{q}_{in} \approx 20kW$. This corresponded to a value below the lower threshold, $\hat{q}_{inl} = 35kW$. Consequently, the desired radiator temperature increased from $55°C$ to $60°C$, and then $65°C$ as the thermal load was removed.

Table 5.3: Test results to establish overall controller performance (NAMIMO: Nonlinear adaptive multiple input and multiple output, NAB: Nonlinear adaptive backstepping, and SF: State flow)

Test No.	Controller Design	Settling Time (s)			Average Radiator Fan Power Consumption, P_{fan} (kW)			Average Pump Power Consumption, P_{pump} (kW)			Mean Absolute Temperature Error $(°C)$		
		Time Range (min)											
		[1,11)	[11,21)	[21,31]	[1,11)	[11,21)	[21,31]	[1,11)	[11,21)	[21,31]	[1,11)	[11,21)	[21,31]
1	NAMIMO	106.4	129.1	148.0	0.72	3.08	0.31				0.79	0.85	1.14
2		112.5	137.4	163.1	0.65	3.01	0.22				0.66	0.78	1.60
3	NAB	162.1	336.1	>600	0.53	2.52	0.32				0.83	1.15	2.11
4		190.1	339.0	>600	0.49	2.51	0.12	0.07			0.75	1.30	3.40
5	SF	-	-	-	1.26	3.33	0.42				1.12	1.00	1.12
6		-	-	-	1.23	3.32	0.27				1.20	0.99	1.38
7	NAMIMO	110.1	105.1	148.0	0.71	3.10	0.30	0.06	0.07	0.05	0.82	0.79	1.15

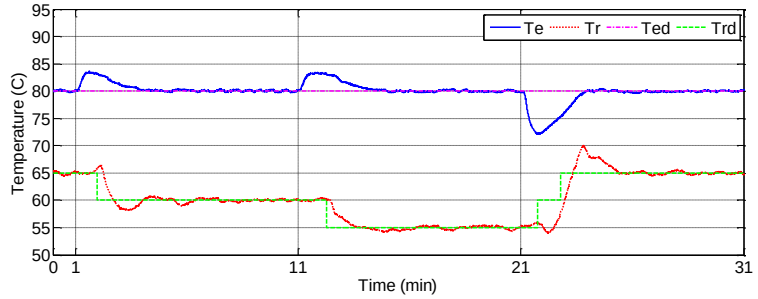

(a)

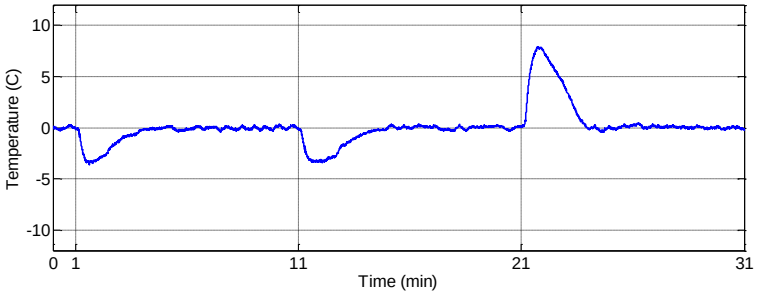

(b)

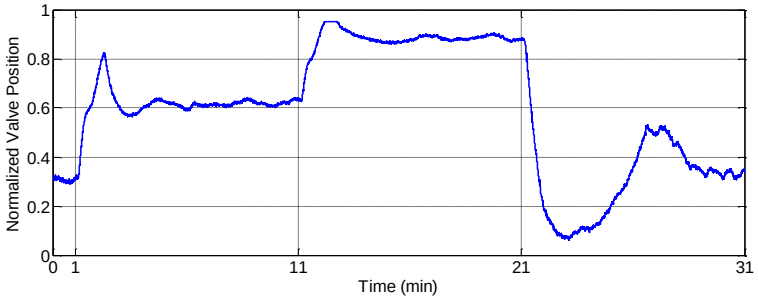

(c)

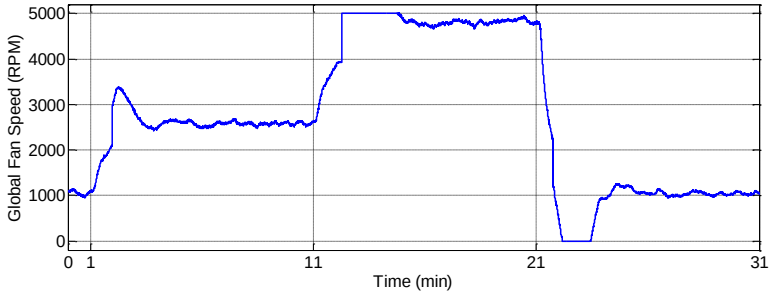

(d)

Figure 5.5: System response of Test 1 - (a) engine, radiator, and desired radiator temperature, (b) engine temperature tracking error, (c) valve position, and (d) global fan speed verses time

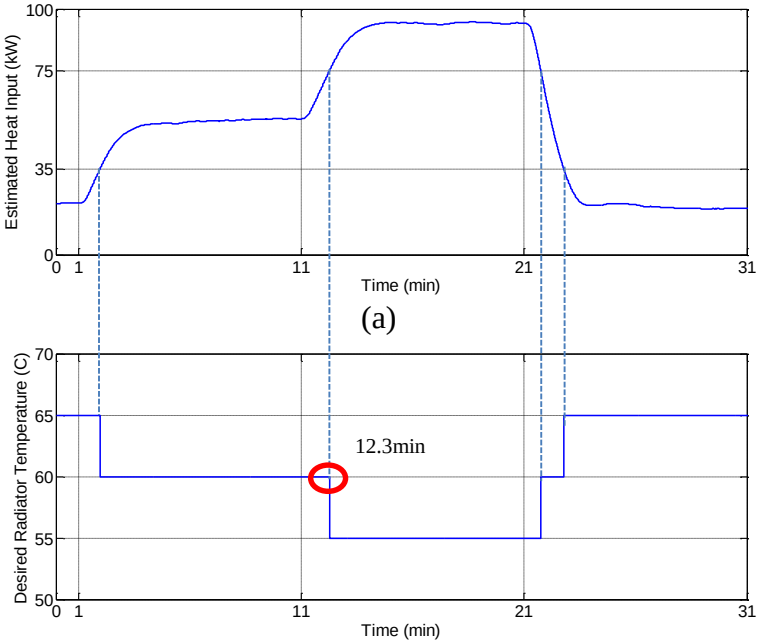

Figure 5.6: (a) Estimated heat input, $\hat{q}_{in}$, and (b) desired radiator temperature, T_{rd}, for Test 1 verses time

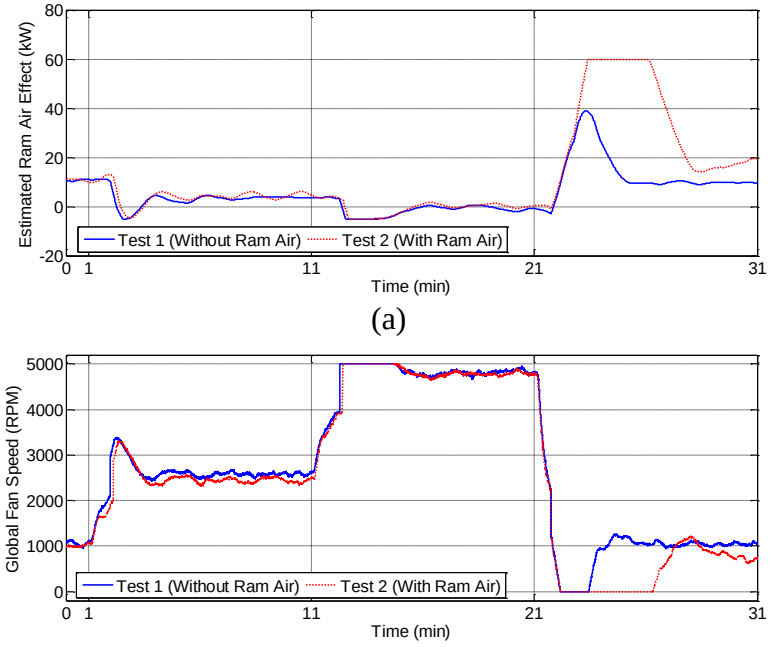

Figure 5.7: Compared results for Tests 1 and 2 - (a) estimated ram air effect, $\hat{q}_{ram}$, and (b) global fan speed, N_f, verses time

The estimated ram air effect, as well as the global fan speeds, for Tests 1 and 2 is presented in Figure 5.7. An interesting observation can be made from these graphs and the average radiator fan power consumption listed in Table 5.3. When the heat load was high ($q_{in} = 90kW$) at time $t \in [11,21)\ min$, the ram air effect was not significant in this study. The difference between the average radiator fan power consumption of Tests 1 ($3.08kW$) and 2 ($3.01kW$) was only 2.3%. On the other hand, when the heat load was small ($q_{in} = 20kW$) at time $t \in [21,31]\ min$, a greater difference in the radiator fans speed can be noticed. The ram air effect removed most of the heat under this scenario and reduced the radiator power consumption up to 40.9%. The similar phenomenon can be observed in Tests 3-6 per Table 5.3. This phenomenon may be attributed to the experimental test configuration; the axial fan was located in front of CAN bus controlled radiator fan array and heat exchangers. As a result, the air mass flow rate across the radiator generated by the axial fan may be small when compared to the radiator fans if they are operated on high speed. In the vehicle, the ram air effect given in equation (5.8) may be greater when the chassis and/or wind speeds are high. As discussed in Case 2, Section 5.2, this phenomenon corresponds to highway operation and a pump–valve combination control strategy may be implemented with the radiator fans shut off.

5.5.2 Comparison of Controllers for Overall Performance

The system performance of Tests 1, 3, and 5 are summarized in Figure 5.8 to compare the three proposed control strategies. Figure 5.8(a) displays the engine tracking error, e, verses time which indicates that the NAMIMO controller offered a much faster response than the NAB control law (e.g., 34% faster when comparing Tests 1 and 3 for

$t \in [11,21)\ min$ according to Table 5.3). Why? The NAMIMO controller operated the valve position which changed the proportion of the cold and hot coolant that flowed into the engine. On the other hand, the NAB controller adjusted the radiator fans speed which only changed the heat transfer among the different interfaces (e.g., air, metal, and coolant). Further, the NAB control law showed its weakness at low heat load conditions, $t \in [21,31]\ min$. Lastly, the SF controller was unable to maintain the engine temperature in a steady state manner. However, it successfully regulated the engine temperature in an $|e| < 5°C$ range.

From a power consumption perspective, Figure 5.8(c) and Table 5.3 indicate that the NAB control consumes the least radiator fan power followed by the NAMIMO and SF controllers.

5.5.3 Pump-Valve Combination

An independent test, Test 7, was performed to study the combination of the system input '1', $u_1 = \dot{m}_{cool}H$. In this instance, the heat load, q_{in}, and the ram air effect, q_{ram}, corresponded to the setting of Test 1. However, the pump speed was manually adjusted over several time ranges. The results in Figure 5.9 may be compared with Test 1. From Figures 5.9(a) and 5.9(c), the coolant flow rate, $\dot{m}_{cool}$, does not impact the error tracking performance, e, nor the radiator fan operation, u_2. The two system inputs, u_1 and u_2, were prescribed independently of each other per equations (5.20) and (5.21). Figure 5.9(b) illustrates that the coolant flow rate had a significant impact on the valve position. The valve positions coincide when the coolant flow rates were the same, $\dot{m}_{cool} = \dot{m}_{cmax} = 1kg/s$, for Tests 1 and 7 at time $t \in [11,21)\ min$. During another

time range, $t \in [1,11)\ min$, the valve opened more in Test 7 than in Test 1 to obtain the same value of system input '1', $u_1 = \dot{m}_{cool} H$. From a power consumption view, when the coolant flow rate decreased in Test 7, the power consumption of the pump decreased as expected (e.g., a 28.6% power saving at time $t \in [21,31]\ min$).

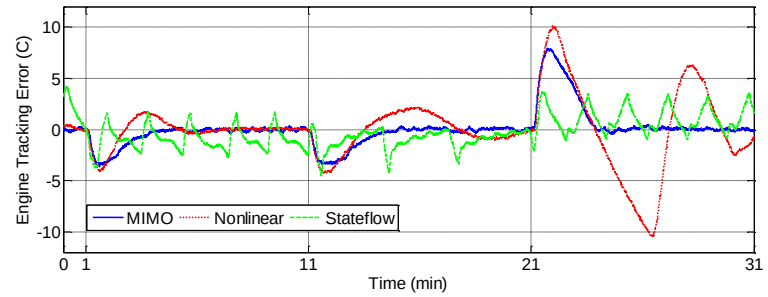

(a)

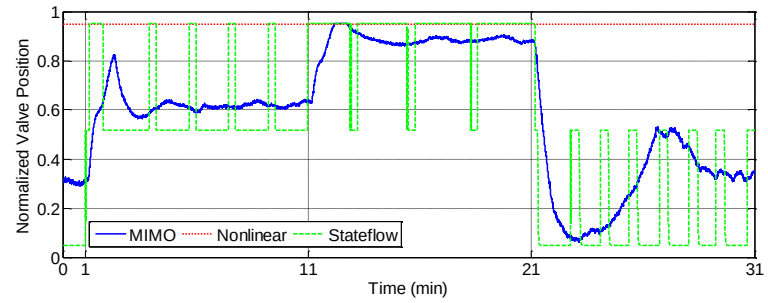

(b)

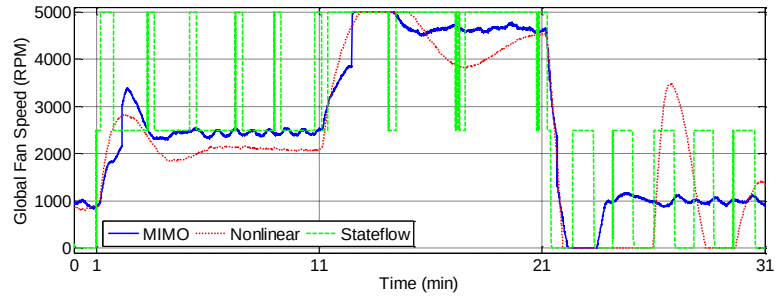

(c)

Figure 5.8: Compared results for Tests 1, 3, and 5 - (a) engine temperature tracking error, (b) valve position, and (c) global fan speed verses time

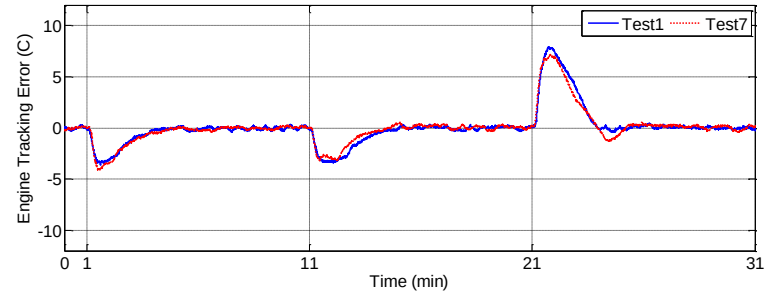

(a)

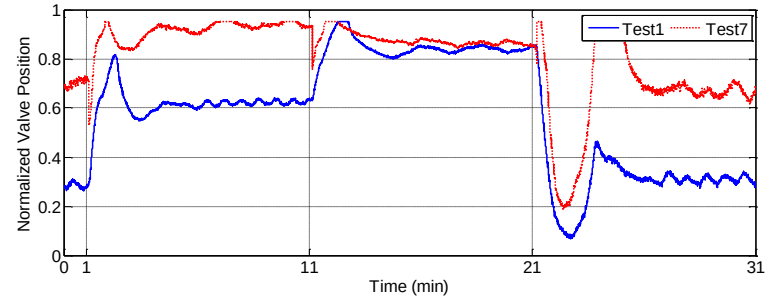

(b)

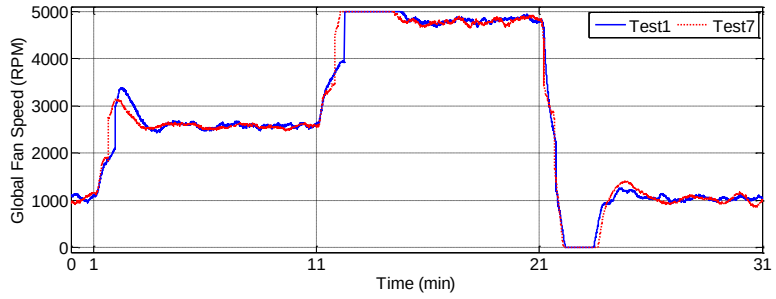

(c)

Figure 5.9: Compared results for Tests 1 and 7 - (a) engine temperature tracking error, (b) valve position, and (c) global fan speed verses time

5.6 Summary

Advanced automotive cooling systems can regulate the internal combustion engine temperature within a specified temperature range while minimizing subsystem power consumption. In this chapter, the cooling system dynamics and control laws were derived and applied to a 6.8L engine. The proposed NAMIMO control law operated the valve position and radiator fan speed. For comparison purposes, a NAB control strategy

and a SF control law were introduced. The test results showed that the NAMIMO controller can successfully regulate the engine temperature to the desired value and compensate for unknown heat loads and ram air effects. Although the NAB controller consumed the least electric actuator power, the performance was characterized by a slow response and weakness at low heat input conditions. The SF controller, although it demonstrated greater temperature oscillation and consumed much more actuator power, was easy to realize and maintained the coolant temperature in an acceptable range. The test results also revealed that as the ram air effect decreased, the commanded radiator fan speed increased as expected. Finally, an independent test demonstrated that the operation of the pump-valve combination has great potential to further minimize the actuator power.

CHAPTER VI

INTERACTIVE THREE DIMENSIONAL VISUALIZATION BASED ENGINEERING TECHNOLOGY EDUCATION – MODELING AND ANIMATION

Advanced three-dimensional visualization and virtual reality technology can play an important role in improving the engineering technology education process. These advanced methods offer technical colleges an opportunity to transition student learning from primarily the classroom and laboratory to an approach that includes online educational materials. E-courses allow more curriculum materials to be available for students desiring additional background materials given a perceived subject weakness based on the content delivery method. In this chapter, an advanced education method for engineering technology students using the three-dimensional visualization of engineering concepts and object animation based on virtual reality technology has been presented for workforce development. The modeling tool set and selected automotive and aerospace system components were discussed to highlight the development process. A case study was introduced to illustrate the overall conceptualization and creation methodology, followed by the educational materials offered online to the technical college students for interactive learning. The preparation of students for emerging technical careers requires the successful integration of learning materials and channels delivery.

6.1 Introduction

The background of technical college students may vary from teenagers recently graduated from high school, to adults seeking new job skills and professional credentials.

The advent of online educational methods have complemented, or replaced, traditional classroom learning to accommodate individual schedule needs and personal learning preferences. Current methods used in the engineering education process at some South Carolina technical colleges cannot easily contain the complex design details, intricate assembly, and equipment functions which were beneficial for students to understand. The traditional teaching and studying approaches, such as textbooks and two dimensional (2D) drawings or photographs, although acceptable, have limitations which may lengthen a student's learning time (Perdomo *et al.,* 2005). In 2D drawings, only the length and height or a variation with depth was presented which may lead to a lack of details. In addition, if limited to only the 2D drawing and accompany description, students may have difficulty understanding the assembly method since when completed, many of the components were no longer visible. For the study of engineering equipment functionality, traditional methods often cannot provide a full visual representation of the operation with motion. Besides, current teaching methods restrict the time and place of both the instructor and students to the college campus.

To remove the constraints of the typical teaching paradigm and education resources discussed above, advanced three dimensional (3D) visualization and virtual reality (VR) technology was introduced which offer several advantages over traditional methods. Specifically, this advanced education approach tends to be more efficient, facilitates standardization, and supports distance learning. Students can directly manipulate the 3D models to rotate them along different axes or scale them in various directions for better viewing. Realistic texture mapping and rendering technology with different materials can

give a "real feeling" of the models so that they resemble the actual object. The third dimension when viewing an assembly was helpful as it offers a spacial perspective and greater understanding as to the connection between different assembly components. With the help of animation and VR technology, the application process for the given toolset may be expressed step-by-step for the end user. Other benefits provided by virtual reality include rapid feedback, greater opportunity for practice, ability to learn in a familiar work environment, and enhanced development of critical thinking skills.

In many educational fields, interactive 3D visualization and VR technology have been successfully used to enhance the teaching experience. Perdomo *et al.* (2005) addressed the impact of using 3D teaching as a tool for construction education and its advantages. Lee *et al*. (2004) described the creation of a 3D modeling and visualization virtual reality markup language (VRML) tool for the human brain which can be shared on the World Wide Web. Bell *et al*. (2004) presented the work of applying 3D visualization and VR technology in virtual chemical plants, virtual laboratory accidents, and a virtual University of Illinois Chicago campus. Ou *et al.* (2009) established a learning content management system for engineering hydrology courses with the help of the virtual learning environment. Sampaio *et al.* (2010) applied the virtual reality techniques into the civil engineering education which brought new perspectives to the teaching of the civil construction field. Angelov *et al.* (2007) developed learning modules to maintain electrical plants by means of VRML which allows online development and utilization of 3D virtual strategies.

The effective incorporation of technology into meaningful learning experiences

can be cumbersome and sometimes appear to create dissonance. However, when technology is judiciously integrated in an instructional design model, it has the potential to positively impact student learning and meet the educational needs in new ways on local levels. As a component of the overall learning design, technology was represented in the Center for Aviation and Automotive Technical Education using Virtual E-School (CA^2VES) instructional design model primarily in the form of interactive 3D visualizations. The development of an instructional design model assimilating local industry need, multiple technology systems scattered across various community colleges and high schools, and input from a broad spectrum of stakeholders presented Clemson University's Center for Workforce Development (CUCWD) with a unique challenge. Extrapolation of the various objectives of each resulted in identification of a primary characteristic which became the central focus of the CA^2VES instructional design model which represents influence from various leading models (Morrison *et al.*, 2007 and Herrington *et al.*, 2000).

The focal point, around which all elements of the instructional design model revolve, was improving student learning and performance for identified module objectives. Each time a module was used, student learning has been assessed in several ways. First, an informal learning analysis may be administered by an instructor where he/she will ask (via a live or online discussion) "orienting questions" designed to gather feedback on present student knowledge in key objective areas as well as to initiate conversations to scaffold student learning. Next, informal assessment was provided by activities interspersed throughout the module which offered students and instructors with learning checks as new information was presented. Finally, formal assessment may be performed in two

manners: (1) successful completion of activities in the 3D virtual reality environment (for example entering accurate measurement readings for the precision tools modeled), and (2) instructor selected activities taken from an Assessment Guide which coordinated with module learning activities – assessments were designed to test multiple levels of cognition through providing traditional test questions (e.g., multiple choice and true/false format), design of physical lab activities, use of discussion prompts to extend module learning, and implementation of critical thinking activities (including paraphrasing, summaries, sequencing, Venn diagrams). The combination of these informal and formal assessments provides a greater understanding of student learning levels before, during, and after completion of e-materials. The remainder of the model interacts in a relational-radial matrix fashion with each component having an equal impact on the overall goal. There are four components in the CA^{2}VES model, shown in Figure 6.1, which include learning design, theories, educational philosophy, technology, and visualization.

A pilot study was also designed to aid in better quantifying the impact of the learning design and virtual reality modules on student learning. The initial study will contain two groups. The control group which will be taught using materials and face-to-face methods currently utilized in the technical college. In contrast, the experimental group (from the same college) will be taught by the same instructor but instead will use the CA^{2}VES online learning tools and virtual reality simulations. Learning for both groups will be assessed through standardized pretests, short learning quizzes, and a final formal assessment incorporating questions with varying levels of difficulty. The pilot study results will be analyzed to determine the CA^{2}VES online learning tool impacts as related to

student learning and performance.

This chapter presents advanced education methods for technical college engineering by using 3D visualization and VR technology as developed in a collaborative fashion by CUCWD and CA^{2}VES researchers. The chapter has been organized as follows. Section 6.2 presents the construction of an instructional design model integrating 3-D visualization. The computer model tools, followed by the virtual reality and online learning strategies, are introduced in Section 6.3. Section 6.4 contains a case study. Finally, Section 6.5 presents the summary.

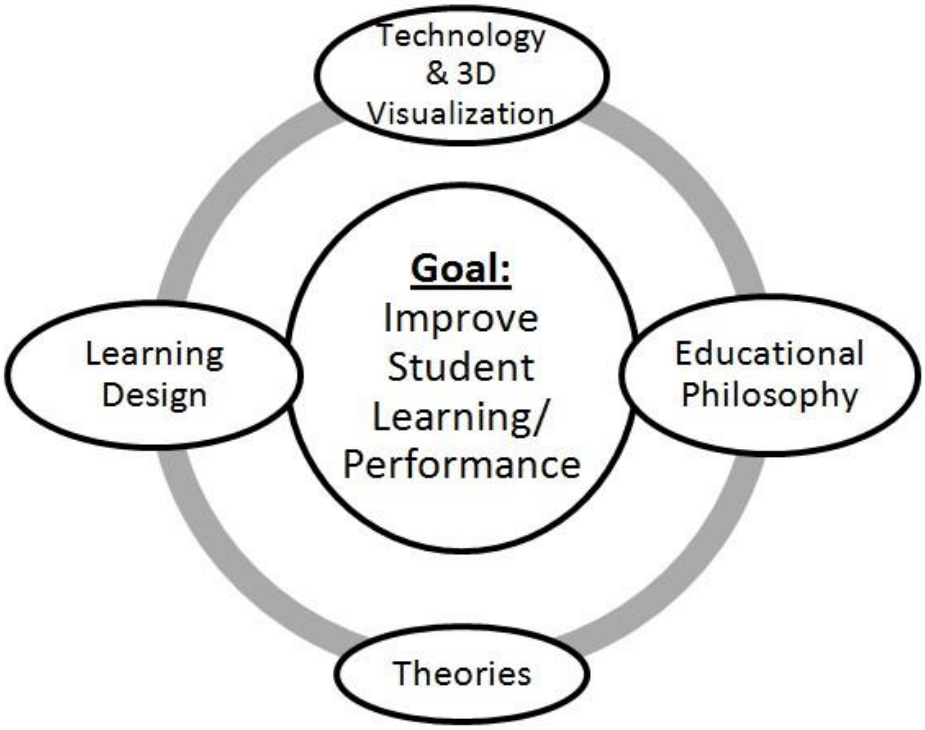

Figure 6.1: Four components of the Center for Aviation and Automotive Technical Education using Virtual E-School (CA2VES) model

6.2 Computer Modeling Tools

For an interactive 3D visualization and VR system, computer modeling establishes the foundation. The virtual world was constructed by various modules created by multi- disciplinary groups of engineers and educators. For instance, the students should be able to understand machines, processers, and/or devices through representative 3D computer based physical models. These computer models may contain geometric, scene, and/or assembly relationships. After representing the physical entities on the computer, the modules, parts, and/or assemblies were converted into a specified format and saved as a digital resource to share with the development team. In this project, all the modules were converted into a ".dae" (digital assent exchange) format since it offers a convenient method for interactions by the virtual reality team members. This format was defined by COLLADA (Collaborative Design Activity) as an open standard XML (Extensive Makeup Language) schema for exchanging digital assents among various graphics software applications. The converted models may be imported into VR tools for further development.

6.2.1 Software and Hardware Tools

Early in the development process, several types of computer aided design (CAD) software packages were evaluated to create the engineering systems and technical tools. Some of the software utilities included CATIA, ProE, SolidWorks, and 3DMAX. SolidWorks was selected as the CAD modeling software toolset for several reasons. First, this software package was recognized as a standard CAD tool around world. Second, it has been widely used in diverse engineering fields and was familiar to the project partners

and the team members. Third, the individual creating the drawing could use a parametric feature-based approach to create models and assemblies. Finally, using the add-in, the CAD modules file can be easily exported and converted into the ".dae" format with all details then imported into VR tools. For hardware needs, the development team selected standard PC workstations which feature multiple high speed CPUs and a high performance graphics card to meet the demands of the large scale modeling challenges.

6.2.2 Data Library Modules

In this project, a number of different modules were developed to meet the engineering education requirement. At the highest level, the module library currently contains measurement tools, electronic components, automotive subsystems, aviation subsystems, and safety as show in Figure 6.2. The introduction of these modules has been described below to offer insight into the current features.

a) Measurement Tools: The measurement tools that have been virtually modeled include a caliper, micrometer, combination square, oscilloscope, and multimeter. All of these items have been described as 3D CAD modules based on real tools with full details and functionality. These modules may be operated by the students in the virtual environments to help them learn the basic knowledge of metrology and develop specific skills. To work with these measurement instruments, the geometric dimensions of standard parts, such as gears, bearings, and valves were also modeled.

b) Electronic Components: The electronic components module contains basic electronic devices such as resistors, capacitors, breadboards, batteries, and lamps.

These electronic components have been created according to the developed requirements and allow students to assemble them to into different electronic circuits. These components may have individual properties and values that can be adjusted.

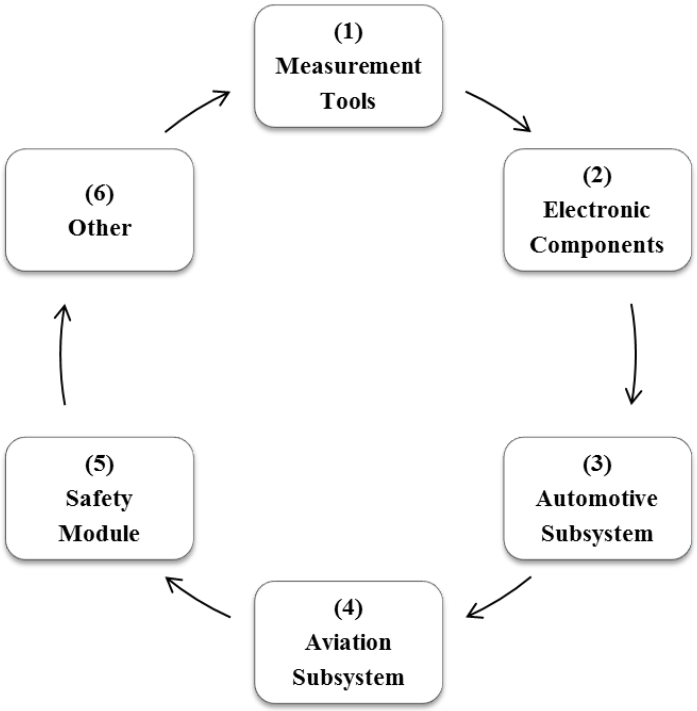

Figure 6.2: CAD module library with content ranging from measurement tools to safety

c) Automotive Subsystems: The automotive elements include the engine block, vehicle frame, drive line, disk brakes, transmission, drum brakes, suspension, and steering. These systems were modeled as individual assemblies with full details including the assembly relationship of the parts and the governing physical laws which describe their dynamic motion. The parts should be developed so that they may be controlled and operated by the students separately. From the assembly re-

lations, the students can also get full information of how the parts connect and integrate into a vehicle.

d) Aviation Subsystems: The aviation subsystems include a gas turbine, aerospace vehicle frame, and flight surfaces. The gas turbine was modeled as an assembly, including the blades, combustor, compressor, fuel tubes, and shaft. The internal combustion propulsion engine, in addition to the other system components, provided an overview of the basic turbine operation and aircraft maintenance concepts for students.

e) Safety Modules: An assortment of machines and robots were available within the safety module to allow students to virtually interact with these system elements. All of these machines should be operated with full functionality and realism. Particularly, in this part, the safe operation was the main priority so that participants can understand the health/safety aspects. As a result, the correct operation method must be considered when modeling the members.

f) Other: As the project evolved, a variety of additional modules were added to the library to support the learning process. A representative sampling of the module elements have been compiled in Figure 6.3.

6.2.3 Reference Materials

The reference materials, including documents, photographs, drawings, have been collected from various sources to support the creation of the e-learning materials. Some of these sources include Clemson University's Department of Mechanical Engineering, the college machine shop, on-campus laboratories, government agencies, and extensive

industrial and academic interactions. The CAD modeling team regularly identified materials and then evaluated the resources to create the 3D CAD modules.

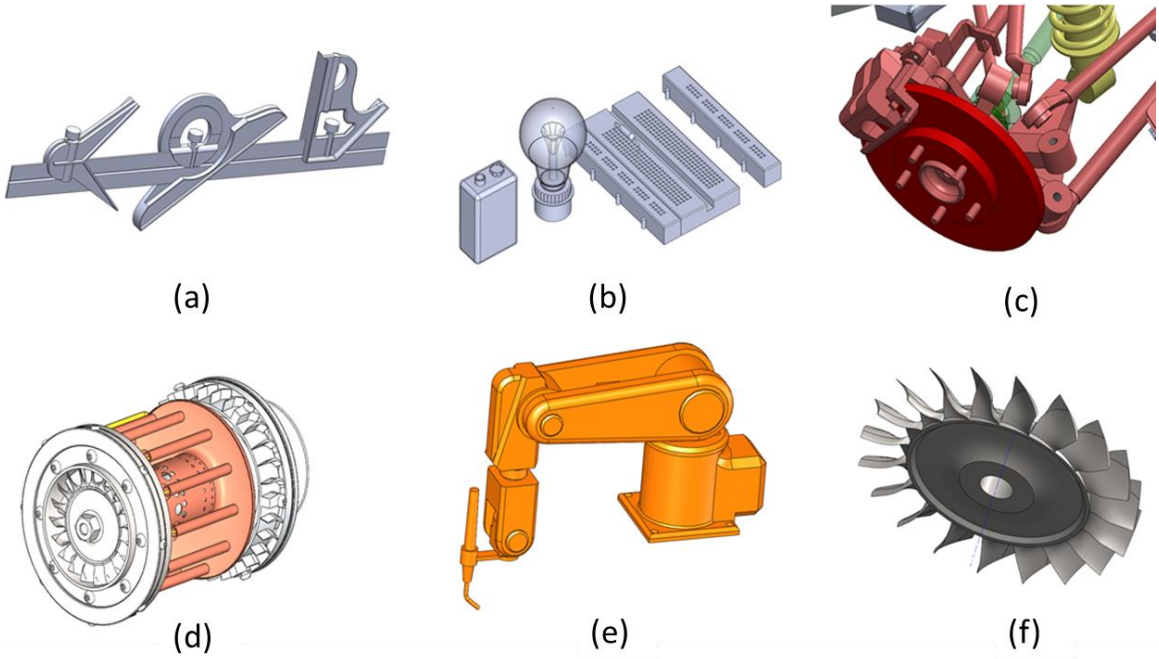

Figure 6.3: CAD module examples - (a) combination square, (b) electrical components, (c) automobile subsystem, (d) gas turbine combustor, (e) 6 degree-of-freedom robot arm, and (f) gas turbine fan assembly

6.2.4 CAD Modules Creation Process

The CAD modeling research team (i.e., Department of Mechanical Engineering at Clemson University) received the 3D module requests from CUCWD. The customer requested various 3D module types based on the education needs; they also provided detailed instructions. The team members collected the materials from available resources. After evaluation, the CAD models were developed and preliminarily reviewed before conversion into a "dae" format as a digital source to submit to the VR team. The team provided feedback so that the CAD modules were modified until they satisfy the re-

quirements; Figure 6.4 displays a flow chart for the task.

When developing the CAD modules, the designers should create the features based on the following the working process.

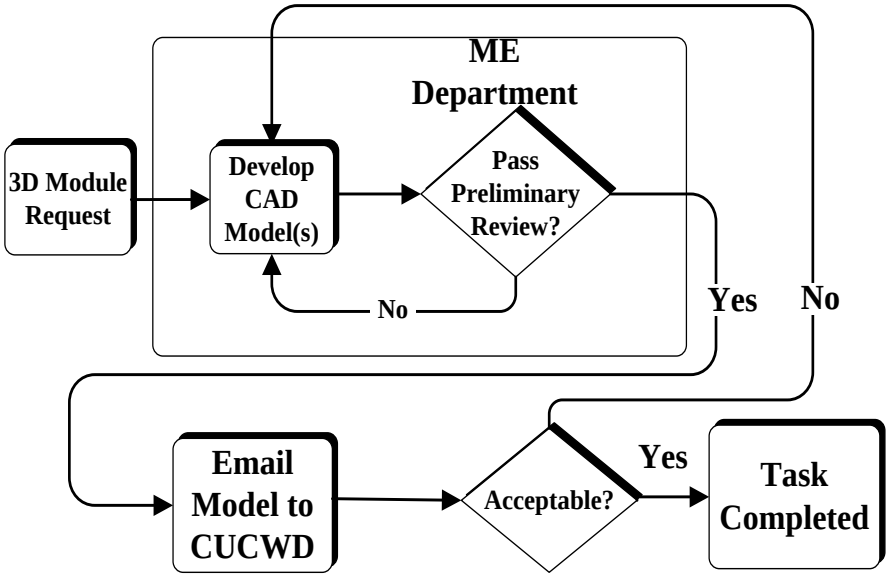

Figure 6.4: Flow chart for CAD module creation process

Draw Sketches: Sketches are the starting point for creating 3D solid part features in SolidWorks. A sketch tends to be a 2D profile, or cross section, which is made up of such basic geometry such as a line, rectangle, circle, arc, etc. With provided menus and speed tool buttons, the designer can easily create sketches, specify dimensions, and add geometric relationships among the components.

Generate 3D Solid Features: After the sketches are finished, the designers may extrude, rotate, loft or sweep sketches to create the desired 3D part features. They may then specify the necessary dimensions to define the 3D part features.

Assemble Body: Once the individual 3D solid part has been created, the designer

should assemble these parts together into the complete body. Using the geometric constraints (e.g., coincident, distance, parallel, and/or concentric), the position of each part and the relationship between them may be identified.

Save Part Feature: The created 3D CAD module must be saved by the designer to a feature database and then converted into a specified digital resource.

6.3 Virtual Reality and Online Learning

The virtual reality technology and accompanying online learning concept was heavily utilized in this educating program. The CAD modules were imported in the virtual reality system and then VR tools applied to develop an immersion study system. The advent of online learning, or e-course, has helped to create a new method of flexible distance education.

6.3.1 Virtual Reality (VR)

The virtual reality component, contained within learning modules, provides students with an opportunity to engage in high-impact, hands-on, authentic learning. This tool contributes new flexibility to educational experiences through immersion in real-world scenarios where students manipulate multiple variables, use tools, and develop skills. Research suggests that implementation of this type of tool with its highly interactive and learner-centric approach has the ability to impact learning and retention. (Hord 2009 and Huk *et al.,* 2003) In this project, two groups worked on the 3D interactive and virtual reality application, the Southeastern Institute of Manufacturing and Technology, Florence, SC, and Clemson University's School of Computer Science. After the CAD modules were converted into the ".dae" format, the digital source was sent to these two

groups to be imported into the VR tools so that the properties and functions were introduced.

6.3.2 Online Learning

The instructional design model driving the online learning design of CA^{2}VES strives to incorporate leading research outlining best practices in the implementation of online learning tools. One element of the CA^{2}VES online learning tool design was a virtual reality component, contained within learning modules, providing students with an opportunity to engage in high-impact, hands-on, authentic learning. This tool contributes new flexibility to the educational experience through immersion in real-world scenarios where students can manipulate multiple variables, use tools, and develop skills. Research suggests that the implementation of this type of tool with its highly interactive and learner-centric approach has the ability to impact learning and retention. (Hodgins, 2000) Other benefits provided by virtual reality include rapid feedback, more opportunity for practice, ability to learn in a familiar work environment, and greater development of critical thinking skills.

6.4 Case Study - Measurement Module

A case study illustrates the application of the e-learning modules to the topic of measurement tools. The team started the overall project with the measurement devices given their widespread usage in automotive and aerospace systems. The metrology CAD modules were created and the interactive features designed in the virtual world. The objective was to help the learner understand the basic functionality and the appropriate operation method of the caliper. The 3D visualization and virtual reality was seamlessly in-

tegrated into the courses and modules incorporating course plans, exercises, quizzes, exams, and laboratory manuals resulting in an integrated assessment approach.

In the virtual environment, each module contains four sections-introduction, guided practice, exercise, and assessment as shown in Figure 6.5. First, the introduction offers basic information about the instrument and how to interact with the simulation. It also includes information on how to interpret the caliper measurement correctly. Second, the guided practice engages the user in a step-by-step process to ensure that they understand each step required in taking a proper measurement. For example, they are presented an abstract solid object and requested to take measurements. Instructions are displayed and after the user completes the instruction, the next step was displayed. Third, the exercise section asks the user to take a measurement of a real world object and convert the measurement between different units. Once the measurement has been taken, the real world object was randomly scaled and the user requested to perform the new measurement. Finally, the assessment section consists of randomly scaled measurement tasks identical to the exercise section where the assessment measurement tasks may be graded and the final score both displayed for the student and sent to an instructor. Users may navigate to each section at any time by clicking on the tabs at the top of the screen. The virtual environment was designed to mimic the physics of the real world and users interact with the simulation by clicking and dragging the instruments into place and recording their measurements. Special interactions such as zooming are represented by icons.

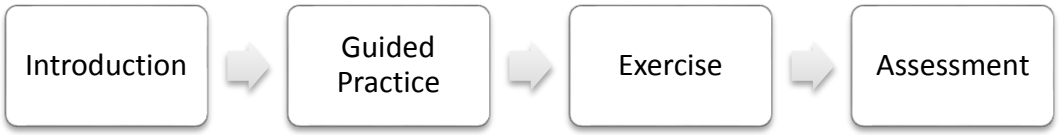

Figure 6.5: General categories of the virtual environment user interface

The Vernier caliper and relevant measured parts were modeled in the CAD software package. The research team measured the caliper dimensions and modeled it as a parts assembly including the main scale part, Vernier part, retainer, and the stop block. Further, a gear with holes and an integrated bearing may also be created in a standard measurement. After modeling both the caliper and the measured parts, these modules were saved and converted, and then submitted to the School of Computer Science with an instruction document. The texture (including the material property and the print markers) were mapped on the CAD modules. After the visualization part was finished, the school of Computer Science added module functions. The overall working process has been shown in Figure 6.6.

6.5 Summary

The rapidly evolving education environment for engineering technology integrates electronic learning with traditional classroom and laboratory experiences. This chapter outlines the recent efforts undertaken in the development and application of advanced interactive 3D visualization based technical engineering education. The division and cooperation between different departments, CUCWD, CA^{2}VES, and other departments have been introduced. A series of learning modules have been created including

measurement, electronic, automotive and aviation subsystems, safety modules, etc. The research team modeled these components using a commercial 3D software package. The standard model development process, from concept to digital file, flowing from modules independent work group through the concept to the application of online learning, was established. Finally, a measurement tool case study was presented to demonstrate the overall concept and methodology.

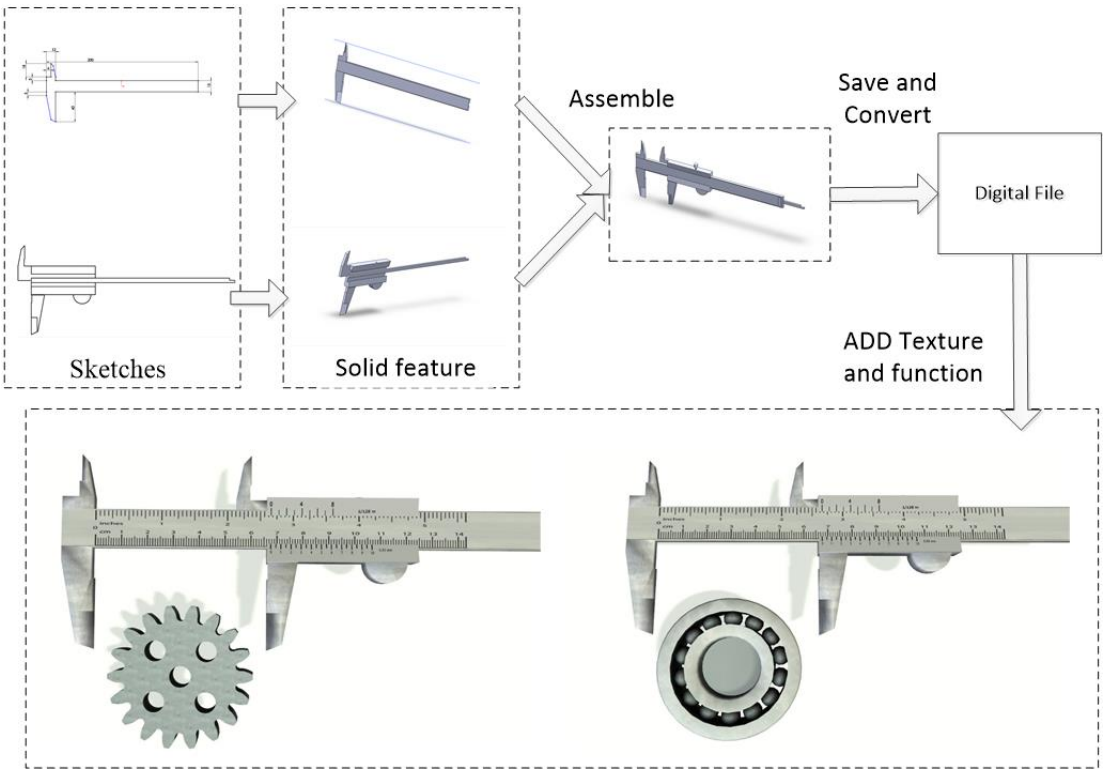

Figure 6.6: Working process (from CAD modules to virtual environment) for the caliper in the measurement tools module in Section 6.2

CHAPTER VII

CONCLUSION

Fuel efficiency is one of the most important factors regarding the performance of ground vehicles. Many innovative technologies have been integrated into modern automobiles to improve the fuel economy. Among these technologies, updating the engine cooling system has the greatest short term potential and has not been widely adopted. This dissertation comprehensively investigates advanced engine cooling systems from a dynamic analysis perspective and the program to control strategies design. The contribution of this research can be reviewed within the content of control and testing:

First, an optimizing control strategy has been presented to regulate the radiator fan matrix to minimize the electric power consumption. A mathematical model for the radiator fan(s) dynamics was developed which established a mixed integer nonlinear programming problem. Several experimental tests have been implemented to evaluate the mathematical model and demonstrated the proposed control law. Both the numerical simulation and the laboratory test results indicated similar control strategies. This operation principle can reduce the fan matrix power consumption by up to 67% for the specified thermal load.

Second, a series of experimental laboratory tests were conducted to exam the contributions of the cooling actuators: smart valve, variable speed pump and the radiator fans. From the tests result, the smart valve and variable speed pump impact the system temperature by adjusting the heat transfer rate between the engine and the radiator. On

the other hand, the radiator fan(s) operation affects the engine's temperature by changing the heat rejection rate of the radiator. The smart valve's operation changes the engine's temperature magnitude the greatest amount (4.0%) followed by the radiator fan(s) (1.6%) and the coolant pump (0.5%). The radiator fan(s) consumes the most engine power in comparison to the two other actuators.

Third, to track a desired engine temperature, a Lyapunov based nonlinear control strategy for the radiator fan matrix was presented. A reduced order mathematical model has been formulated for analyzing the closed-loop feedback system. This study is focused on the high load condition in which the valve position and pump speed are set as their maximum capacities. The numerical and experimental tests demonstrated that the advanced control strategy can regulate the engine temperature tracking error within 0.12°C and compensate for the unknown heat load. The nonlinear controller provided the best performance in terms of power consumption and temperature tracking when compared to a classical PI with lookup table based controller and a bang bang controller.

Fourth, a nonlinear adaptive multi-input and multi-output (NAMIMO) controller to simultaneously operate the valve and radiator fans has been presented to adapt the cooling system working under complex environment conditions: wide heat load range and various ram air effects. A series of test results demonstrated that the proposed NAMIMO controller can regulate the engine temperature to a desired value under various heat loads and ram air effects. The results also showed that the NAMIMO controller had the fasted response when compare with the previously proposed controllers. Further, the simple state flow controller was characterized by greater oscillations and electrical power

consumption but acceptable error tracking performance ($|e| < 5°C$).

This dissertation also introduced an advanced education method for engineering technology students using the three dimensional visualization and virtual reality technology. To highlight the development process, the computer aided design software was selected and discussed. A case study was presented to illustrate the overall conceptualization and creation methodology, followed by the educational materials offered online to the technical college students for interactive learning. The preparation of students for emerging technical careers requires the successful integration of learning materials.

APPENDICES

A. SUPPLEMENTARY MATERIAL FOR CHAPTER II – SELECTION OF THE PARAMETERS

In this Appendix, the methodologies to select the heat transfer efficiency, ε_a, and efficiency, η, constants will be presented. Table A.1 summarizes the experimental measured data including the fan speed, N_f, air flow rate, $\dot{m}_{air}$, and the calculated heat rejected, q_{out}, based on the relationship

$$q_{out} = \dot{m}_{cool} Cp_{cool} (T_{RI} - T_{RO}) \tag{A.1}$$

where T_{RI} and T_{RO} are the radiator coolant inlet and outlet temperatures (refer to Figure 2.3) which can be measured by thermocouple sensors. The variable $\dot{m}_c$ is the coolant mass flow rate listed in Table 2.1. The heat transfer efficiency, ε_a, is calculated based on equation (2.3) with $\varepsilon_a = \frac{q_{out}}{\dot{m}_{air} Cp_a (T_{aout} - T_\infty)}$ where the air specific heat, Cp_a, and $\Delta T = T_{aout} - T_\infty$ are summarized in Table A.1. The curve of the heat transfer efficiency, ε_a, verses the different mass air flow rates, $\dot{m}_{air}$, based on tests result is represented in Figure A.1. Using the Matlab curve fitting tool, a quadratic equation $\varepsilon_a = a\dot{m}_{air}{}^2 + b\dot{m}_{air} + c$ was fitted.

The efficiency, η, is calculated based on equation (2.10) with $\eta = \frac{2\pi k}{60 P_e} N_f{}^3$ where the factor k is listed in Table 2.1. Through experimental testing, the fan speed, *N*, and the fan power, P_e, were recorded and summarized in Table A.2. The fan power consumption, P_e, was calculated as the average value for Test VI in Chapter II as listed in Table 2.2. Figure A.2 shows the trend curve of the fan speed verses efficiency. A second order curve fitting was selected with $\eta = dN_f{}^2 + eN_f + f$ to determine the relationship between the fan speed, *N*, and efficiency, η.

Table A.1: Heat transfer efficiency, ε_a, verses mass air flow rate, $\dot{m}_{air}$, at different heat rejection and fan combinations

Fan Speed, N_f, (RPM)	Number of Fans, n	Heat Rejected, q_{out}, (kW)	Mass Flow Rate, $\dot{m}_{air}$, (kg/s)	Heat transfer effectiveness, ε_a
1,000	1	9	0.46	0.978
2,000		16	0.92	0.87
3,000		19	1.38	0.688
4,000		25	1.84	0.679
5,000		29	2.3	0.63
1,000	2	16	0.92	0.87
2,000		28	1.84	0.761
3,000		38	2.76	0.688
4,000		48	3.68	0.652
5,000		54	4.6	0.587
1,000	3	20	1.38	0.725
2,000		38	2.76	0.688
3,000		50	4.14	0.604
4,000		61	5.52	0.553
5,000		72	6.9	0.522
1,000	4	27	1.84	0.734
2,000		44	3.68	0.598
3,000		60	5.52	0.543
4,000		76	7.36	0.516
5,000		83	9.2	0.451
1,000	5	33	2.3	0.717
2,000		56	4.6	0.609
3,000		75	6.9	0.543
4,000		85	9.2	0.462
5,000		97	11.5	0.422
1,000	6	37	2.76	0.67
2,000		62	5.52	0.562
3,000		81	8.28	0.489
4,000		94	11.04	0.426
5,000		108	13.8	0.391

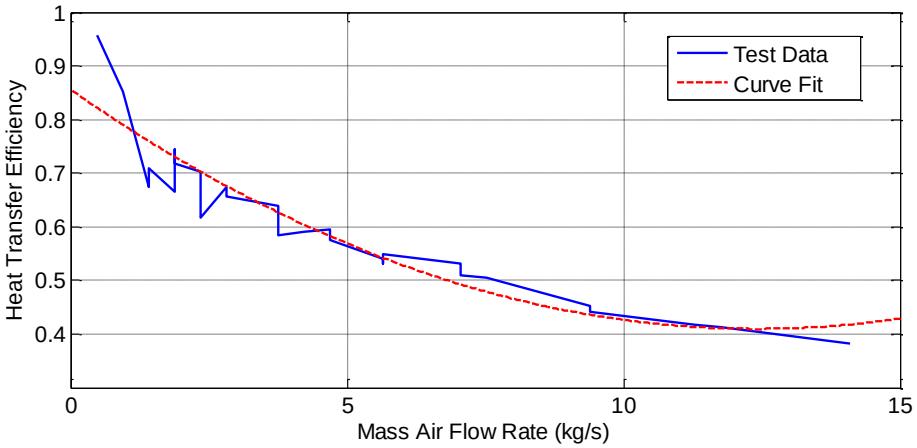

Figure A.1: Heat transfer efficiency, ε_a, verses mass air flow rate, $\dot{m}_{air}$

Table A.2: Efficiency, η, verses different fan speed, N_f

Fan Speed, N_f (RPM)	1,000	2,000	3,000	4,000	5,000
Fan Power, P_e (kW)	0.05	0.08	0.16	0.31	0.56
Efficiency, η	0.1	0.47	0.72	0.85	0.9

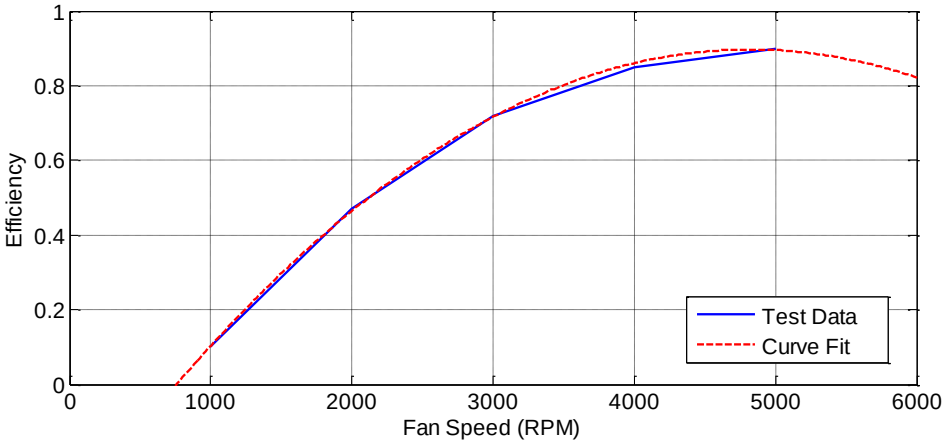

Figure A.2: Efficiency, η, verses different fan speed, N_f, combinations

B. SUPPLEMENTARY MATERIAL FOR CHAPTER II – MATHEMATICAL MODEL VALIDATION

A series of experimental tests were performed on the cooling system to validate the mathematical models proposed in Sections 2.2 and 2.3. The specific test results considered include (a) radiator air mass flow rate, $\dot{m}_{air}$, (b) heat rejected from the radiator, q_{out}, and (c) fan matrix power consumption, P_e, for different fan speeds, N_f, and number of fans, n. To demonstrate the versatility of the dynamic models, two fans (no. 1 and no. 2) were selected for operation. The test profile and the corresponding results are listed in Table B.1. As demonstrated through laboratory testing, the mathematical model adequately estimates the system behavior.

Table B.1: Mathematical model validation test profile with fans no. 1 and no. 2 operated

	Air Mass Flow Rate, $\dot{m}_{air}$, (kg/s)		Heat Rejected, q_{out}, (kW)		Power Consumption, P_e, (kW)	
Fan Speed (RPM)	Model Result	Test Result	Model Result	Test Result	Model Result	Test Result
1,000	0.92	0.81	15.0	17.3	0.08	0.10
2,000	1.84	1.61	27.8	25.0	0.14	0.19
3,000	2.76	2.69	38.6	37.0	0.31	0.33
4,000	3.68	3.66	47.8	41.8	0.62	0.60
5,000	4.60	4.59	55.6	54.8	1.16	1.05
Absolute Average Error %	6.2%		8.9%		11.9%	

B.1 Radiator Air Mass Flow Rate Model Validation

The relationship between the fan configuration (e.g., fan speed, N_f, and number of fans, n) and the air mass flow rate through the radiator, $\dot{m}_{air}$, can be expressed as

$$\dot{m}_{air} = \frac{4\pi^2 \rho_{air} r_m^3 \Phi_m N_f n}{60} \left(\frac{1-v^2}{1+v^2}\right) \sqrt{\frac{k_f}{k_r}} \tag{B.1}$$

when there is this no ram air effect, $\dot{m}_{ram} = 0$, from equations (2.7) and (2.15). Alternatively, the radiator air mass flow rate, $\dot{m}_{air}$, can be experimentally determined by measuring the air speed exiting the radiator, v_{air}^*, and introducing some system parameters into the corresponding basic engineering calculations. Thirty points were marked on the radiator as shown in Figure B.1 to establish a grid and data collected for different fan rotational speeds, N_f. The average air flow speed, $\overline{v}_{air}^*$, was calculated based on the collected wind speed data to obtain the total air mass flow rate, $\dot{m}_{air}^*$, through the radiator area.

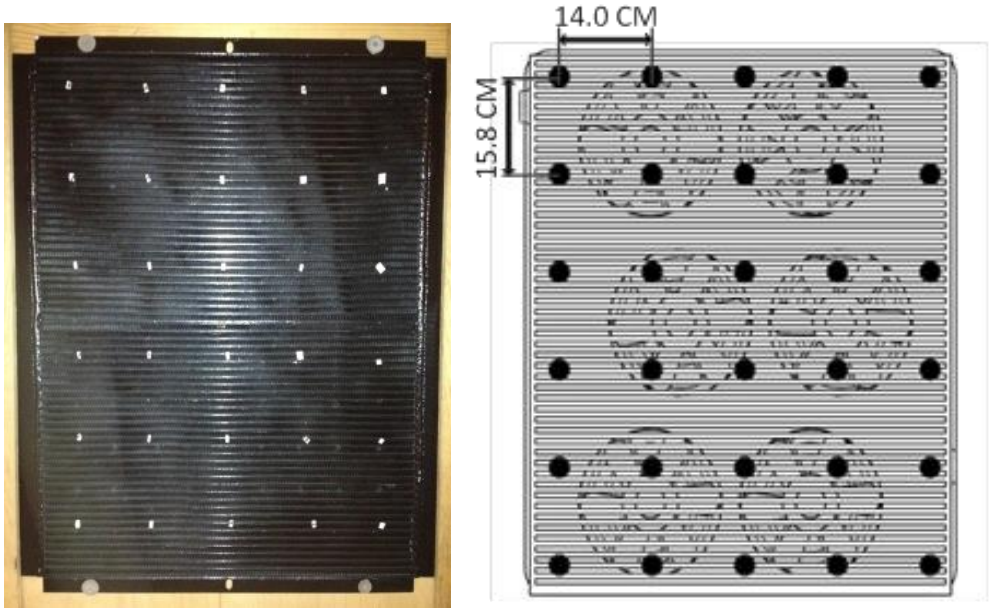

Figure B.1: Selected points on the radiator frontal area used

For example, the air flow speed, $v_{air_i}^*$ ($i = 1,2,\ldots,30$), at each point with a fan speed of $N_f = 2{,}000 RPM$ has been listed in Table B.2. In these tests, the average air speed cross the radiator is $\overline{v}_{air}^* = 1.33\, m/s$, and the testing mass flow rate, $\dot{m}_{air}^*$, can be

calculated using equation (2.4) as $\dot{m}^*_{air} = \overline{v}^*_{air} A_r \rho_{air} = 1.61 kg/s$.

Table B.2: Air speed recordings for fans no. 1 and no. 2 operating at $2{,}000 RPM$

Air Speed, $v^*_{air_i}$, (m/s)						
Vertical and Horizontal Points	1	2	3	4	5	Ave.
1	3.18	2.72	1.81	3.18	2.72	2.72
2	0.57	2.84	2.61	1.36	2.04	1.88
3	1.70	1.25	1.25	1.82	1.02	1.41
4	0.57	0.57	0.57	0.45	0.68	0.57
5	0.79	0.68	0.57	0.57	1.02	0.73
6	0.79	0.91	0.45	0.45	0.91	0.70
Ave.	1.27	1.49	1.21	1.30	1.40	1.33

The three dimensional surfaces corresponding to the measured air mass flow rate profile, $\dot{m}^*_{air}$, for increasing fan speed are displayed in Figure B.2. The calculated air mass flow rate using the mathematical model and the test data are summarized in Figure B.3 and Table B.1. The average absolute error between the mathematical model and the experimental results is 6.2%.

B.2 Heat Rejected from Radiator Model Validation

The radiator heat rejection, q_{out}, will be validated as described by equation (2.19). As stated in equation (A.1), the coolant's thermal response can be used as an alternative representation of the heat rejection from the radiator, q_{out}, provided that the system has reached equilibrium. Each test was operated for a $500s$ time period and the temperatures at steady state are selected to calculate the heat output. Figure B.4 presents the coolant temperature at the radiator inlet, T_{RI}, and outlet, T_{RO}, when the twin radiator fans are operated at $2{,}000 RPM$ and $5{,}000 RPM$, respectively. For example, when the

fans spin at $2{,}000RPM$, the temperature at the radiator inlet is $T_{RI} = 79.9°C$ while at the outlet $T_{Ro} = 74.7°C$. According to equation (A.1), the heat rejection from the radiator is $q_{out} = 25.0kW$. In comparison, the numerical result from the mathematical model of equation (2.19) is calculated as $q_{out} = 27.8kW$. The test results for all cases are listed in Table B.3. The summarized experimental and numerical results are presented in Figure B.5 and Table B.1; the average absolute error is 8.9%.

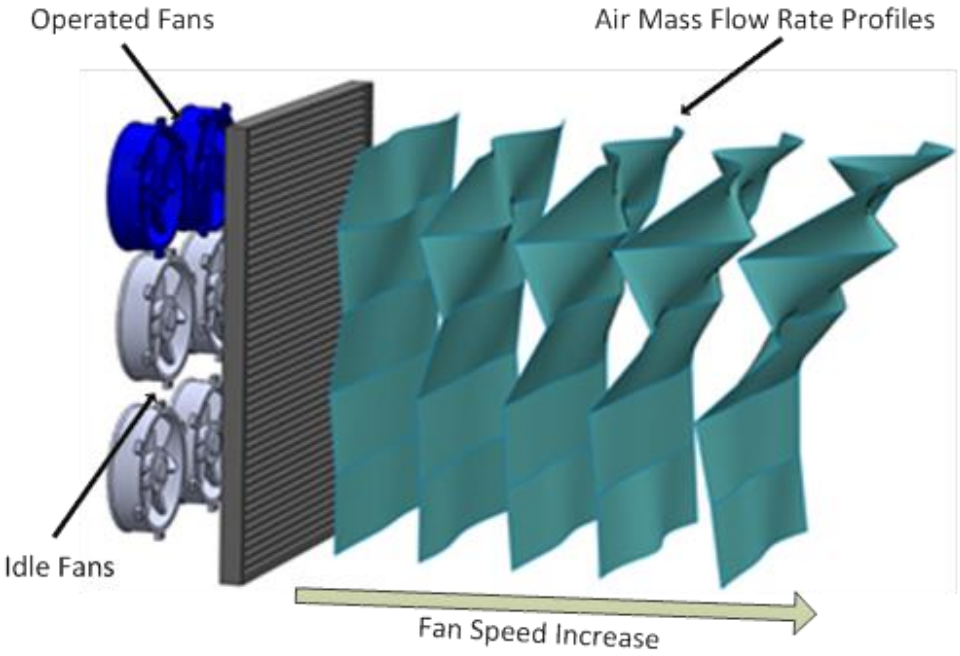

Figure B.2: Air mass flow rate profiles, $\dot{m}^*_{air}$, for increasing fan speeds, $1{,}000RPM < N_f < 2{,}000RPM$, with no. 1 and no. 2 fans operating

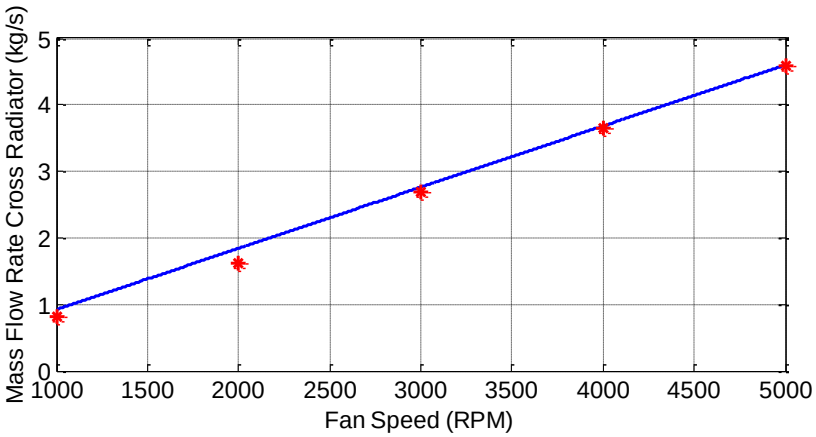

Figure B.3: Air mass flow rate, $\dot{m}_{air}$, verses fan speed, N_f, with no. 1 and no. 2 fans operational for both the mathematical model (blue line) and the experimental test (red scatters)

Table B.3: Coolant temperature and heat rejected calculation results for fans no. 1 and no. 2 operating at various speed

Fan Speed, N_f, (RPM)	1,000	2,000	3,000	4,000	5,000
Radiator Inlet, T_{RI}, $(°C)$	80.1	79.9	80.4	81.0	80.2
Radiator Outlet, T_{Ro}, $(°C)$	76.5	74.7	72.7	72.3	68.8
Heat Rejected, q_{out}, (kW)	17.3	25.0	37.0	41.8	54.8

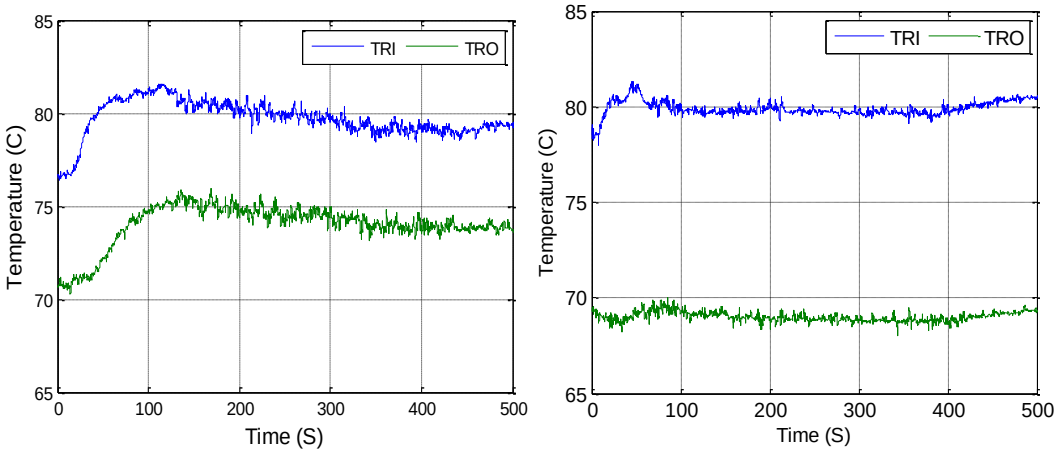

(a) (b)

Figure B.4: Temperature of radiator inlet, T_{RI}, and outlet, T_{RO}, when the fan speed is (a) $2{,}000RPM$, and (b) $5{,}000RPM$

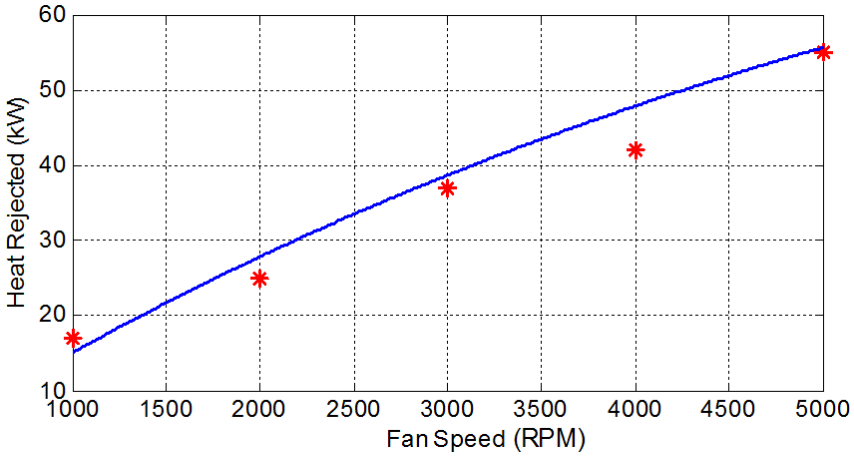

Figure B.5: Heat rejected from radiator, q_{out}, verses fan speed, N_f, with no. 1 and no. 2 fans operational for both the mathematical model (blue line) and the experimental test (red scatters)

B.3 Radiator Fan Power Consumption Model Validation

To investigate the accuracy of equation (2.13), the operating current of the radiator fans has been measured during the test matrix. The supply voltage is fixed at $V_s = 30V$. The recorded current, i, and the calculated power consumption, $P_e = iV_s$, are listed in Table B.4. The summarized results are listed in Table B.1 and Figure B.6 to compare with the mathematical model. The average absolute error is 11.9%.

Table B.4: Current and power for no. 1 and no. 2 fans operation at $V_s = 30V$

Fan Speed, N_f, (RPM)	1,000	2,000	3,000	4,000	5,000
Test Current, i, (A)	3.3	6.4	10.9	19.8	35.0
Test Fan Power, $P_e = iV_s$, (kW)	0.10	0.19	0.33	0.60	1.05

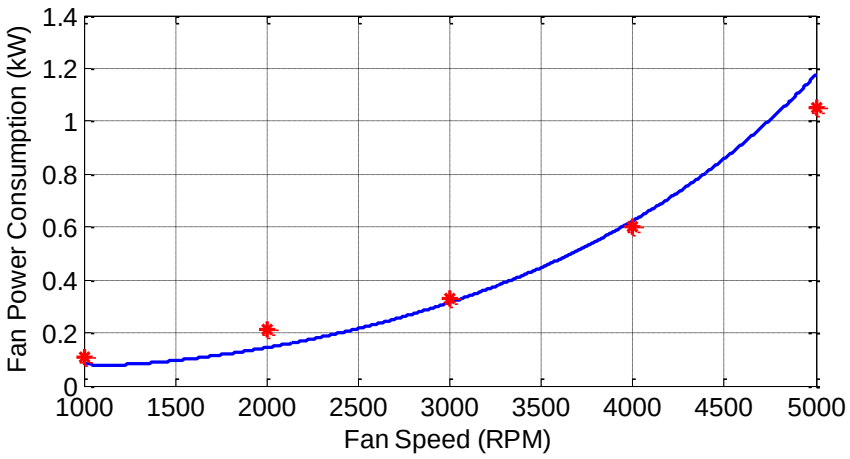

Figure B.6: Fan power consumption, P_e, verses fan speed, N_f, with no. 1 and no. 2 fans operational for both the mathematical model (blue line) and the experimental test (red scatters)

C. SUPPLEMENTARY MATERIAL FOR CHAPTER IV - DESIGN OF BANG BANG AND PROPORTIONAL INTEGRAL (PI) WITH LOOKUP TABLE BASED CONTROLLERS

In this Appendix, the design of the bang bang and proportional integral (PI) with lookup table based controllers will be briefly introduced.

C.1 Bang Bang Controller Design

The bang bang control strategy, also known as an ON/OFF controller, is a real time feedback control law widely used in traditional system applications. This controller design was introduced in Tests 3 and 7 in Chapter IV. A general flow chart and signal diagram for this controller has been sketched in Figure C.1.

To better describe this controller, we conveniently define the feedback error, e^*, as

$$e^* = -e = T_{ed} - T_e \tag{C.1}$$

In this expression, the engine temperature, T_e, is hotter than the desired temperature, T_{ed}, when $e^* > 0$ and vice versa. The "Fan ON/Fan OFF" states of the cooling system operation are defined as

$$\text{Fan On:} \quad N = 5{,}000RPM,\ n = 6$$

$$\text{Fan OFF:} \quad N = 0RPM, n = 6 \tag{C.2}$$

The parameters e_{high} and e_{low} are the selected upper and lower error bands, respectively. When this controller is engaged, the fan matrix operation switches from "OFF" to "ON" when the error, e^*, is beyond the upper error bands or $e^* > e_{high}$. The fan matrix will stay "ON" until the error, e^*, reaches the lower error band or $e^* < -e_{low}$.

C.2 Proportional Integral (PI) with Lookup Table Based Controller Design

Tests 4 and 8 used a classical proportional integral (PI) controller in which the error, e^*, is defined in equation (C.1). The mathematical formulation for this well-known controller can be stated as

$$u(N,n) = K_p e^* + K_I \int e^* \, dt + u(N,n)_0 \tag{C.3}$$

where $u(N,n)$ is the calculated control authority. The terms K_p and K_I are the selected positive proportional and integral controller gains. The variable $u(N,n)_0$ is the initial fan matrix operation value which can be obtained from a calibration basis. Specifically, an engineer can calibrate the fan operation based on the engine load, environmental temperature, and ram air effects. This test data can be stored in a three-dimensional table for lookup purpose. In this limited study, the test environment temperature and engine load fell into entry V for no ram air per Table C.1. From the baseline experimental testing and calibration, the initial fan matrix operation is selected as

$$u(N,n)_0 : N = 3{,}000 RPM, n = 6 \tag{C.4}$$

The controller gains, K_p and K_I, were adjusted through experimental testing to obtain the smallest steady state error.

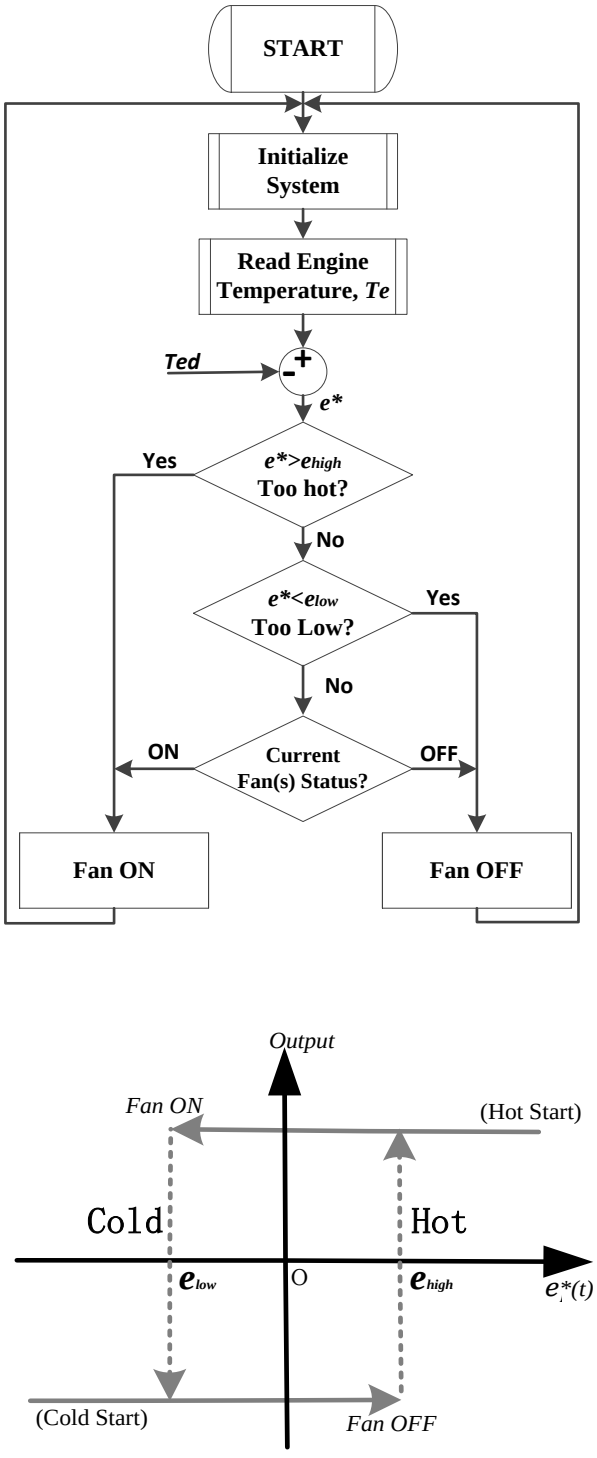

Figure C.1: Flow chart and signal switching of bang bang fan controller

Table C.1: Table for PI with lookup table based controller

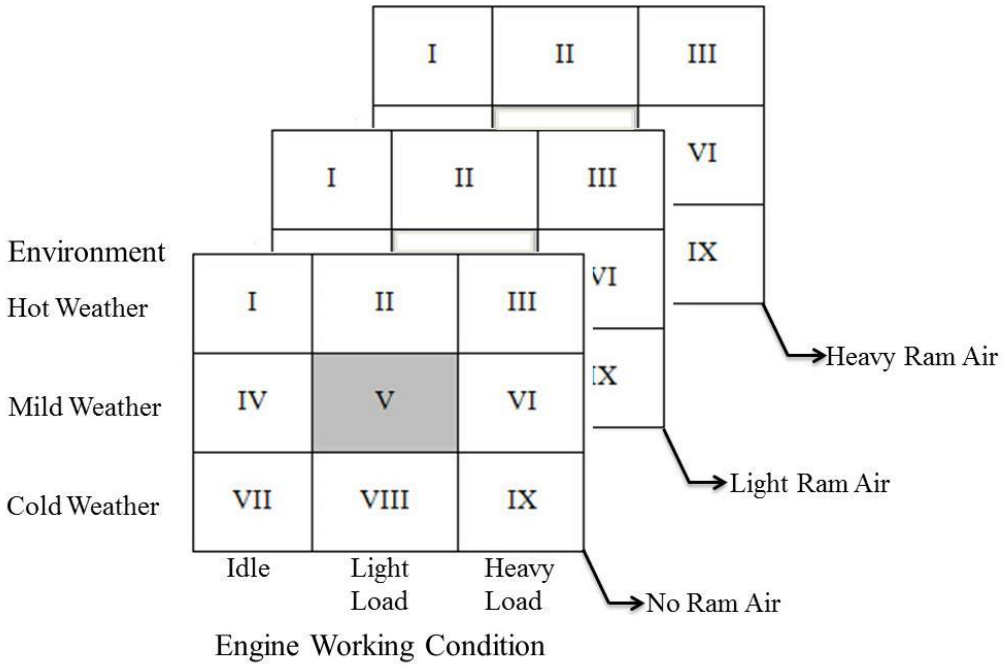

D. SUPPLEMENTARY MATERIAL FOR CHAPTER V - STATE FLOW CONTROLLER DESIGN

If the system is constrained by the available engine control unit's (ECU) speed/memory, a logic based control law may be introduced to adjust the valve's position and radiator fan speed. State flow (SF) control, used to control automotive subsystems, considers the logical expressions of state machines. A SF controller switches between different outputs according to the system states and pre-programmed control law.

The control states are defined as $S = \{Idle, Nominal, High\ load\}$. The logic flow diagram is shown in Figure D.1. The variables T_H, T_L, and T_M are the selected thresholds that have been chosen according to baseline calibrations and listed in Table 5.2. The operations of the actuators in each state will be briefly described.

Idle State: When the engine temperature, T_e, is below the lower threshold, T_L, which denotes a warm up/cold start condition, the system inputs 1 and 2 are operated at their lower limits to keep the engine temperature increasing toward the desired working range. In mathematical form, $[u_1, u_2] = [u_{1min}, u_{2min}]$. Once the engine temperature reaches the middle threshold, T_M, the system will shift to the nominal state.

Nominal State: In the nominal state, the valve-pump combination, and the radiator fans are operated at their normal condition, $[u_1, u_2] = [u_{1nom}, u_{2nom}]$. Considering the thermal inertia, this system condition may be switched to from either the idle state when the engine is too hot, $T_e > T_M$, or from the high load state when the engine is too hot, $T_e < T_M$.

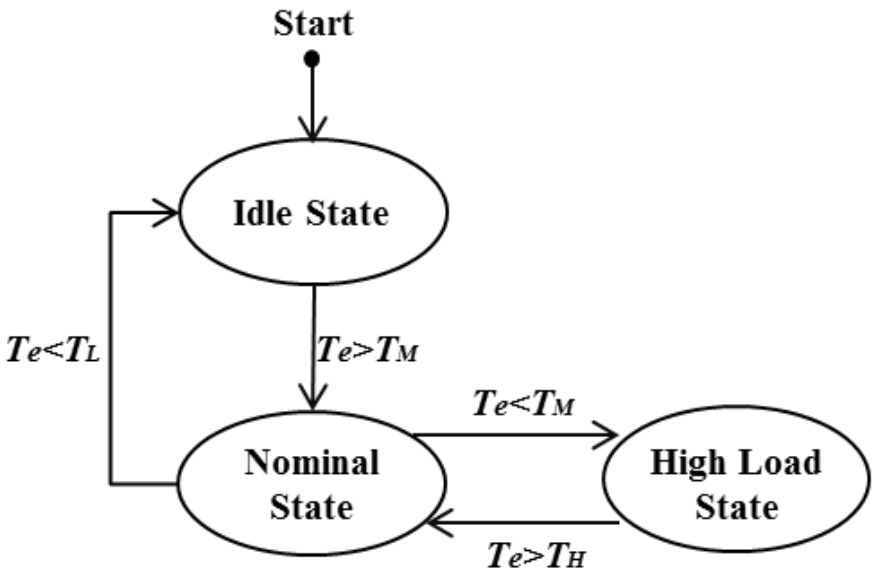

Figure D.1: State flow control structure

High Load State: If the engine temperature exceeds the prescribed higher threshold, T_H, then the controller transitions to the high load state. The system inputs are all operated at their maximum capacity to reject heat from the engine. The cooling control behavior will be realized as $[u_1, u_2] = [u_{1max}, u_{2max}]$.

As mentioned in Section 5.5, the coolant mass flow rate is a constant, $\dot{m}_{cool} = \dot{m}_{cmax}$. The state of system input '1' was represented by the valve position, $u_{1min,nom,max}$, as reflected by $H_{min,nom,max}$. The system input '2' state, $u_{2min,nom,max}$, corresponding to the air mass flow rate, is reflected by the radiator fan motor speed, $N_{fmin,nom,max}$. The parameter values for $H_{min,nom,max}$ and $N_{fmin,nom,max}$ can be found in Table 5.2.

REFERENCES

Allen, D., and Lasecki, M., "Thermal Management Evolution and Controlled Coolant Flow," proceedings of the *Vehicle Thermal Management Systems Conference & Exposition*, Paper: 2001-01-1732, Nashville, TN, May 2001.

Angelov, A., and Styczynski, A., "Computer-Aided 3D Virtual Training in Power System Education," proceedings of the *Power Engineering Society General Meeting*, pp. 1-4, Tampa, FL, June 2007.

Ap, N., "A Simple Engine Cooling System Simulation Model," proceedings of the *SAE World Congress*, Paper: 1999-01-0237, Detroit, MI, March 1999.

Aschemann, H., Prabel, R., Grob, C., and Schindele, D., "Flatness-Based Control for an Internal Combustion Engine Cooling System," proceedings of the *IEEE International Conference on Mechatronics*, pp. 140-145, Istanbul, Turkey, April 2011.

Badekar, R., Mahajan, J., Kakaye, S., Khire, P., and Gopalkrishna, K., "Development of Control System for Electrical Radiator Fan Using Dual Sensor & Microprocessor Based Electronic Unit," proceedings of the *SAE World Congress*, Paper: 2006-01-1035, Detroit, MI, April 2006.

Bell, J., and Fogler, H., "The Application of Virtual Reality to (Chemical Engineering) Education," *IEEE Virtual Reality Conference*, pp. 217-218, Chicago, IL, March 2004.

Biggs, M. C., "Constrained Minimization Using Recursive Quadratic Programming," proceedings in *Towards Global Optimization*, pp. 341-349, Amsterdam, North-Holland, 1975.

BP, "BP Statistical Review of World Energy," 63rd edition, June 2014.

Brace, C., Hawley, G., Akehurst, S., Piddock, M., and Pegg, I., "Cooling System Improvements - Assessing the Effects on Emissions and Fuel Economy," *Journal of Automobile Engineering*, vol. 222, pp. 579-591, 2008.

Butt, S.S., Prabel, R., and Aschemann, H., "Multi-Variable Flatness-Based Control for an Engine Cooling System," proceedings of the *IEEE conference on Control Applications*, pp. 1551-1556, Juan Les Antibes, France, October 2014.

Butt, S.S., Prabel, R., Grimmecke, R., and Aschemann, H., "Nonlinear Model-Predictive Control for an Engine Cooling System with Smart Valve and Pump," proceedings of the *Methods and Models in Automation and Robotics*, pp. 520-525, Miedzyzdroje, Poland, September 2014.

Byrd, R. H., Hribar, M. E., and Nocedal, J., "An Interior Point Algorithm for Large-Scale Nonlinear Programming," *SIAM Journal on Optimization*, vol. 9, no. 4, pp. 877-900, 1999.

Chanfreau, M., Gessier, B., Farkh, A., and Geels, P., "The Need for an Electrical Water Valve in a Thermal Management Intelligent System (THEMIS)," proceedings of the *SAE World Congress*, Paper: 2003-01-0274, Detroit, MI, March 2003.

Chastain, J., Wagner, J., and Eberth, J., "Advanced Engine Cooling Components, Testing and Observations," proceedings of the *6th IFAC Symposium Advances in Automotive Control*, pp.294-299, Munich, Germany, July 2010.

Choi, K., Kim, H., Cho, W., and Lee, K., "Investigation of Emission Reduction Effect by Controlling Cooling System in a Diesel Engine," proceedings of the *Powertrain & Fluid Systems Conference and Exhibition*, Paper: 2007-01-4064, Chicago, IL, October 2007.

Colwell, J., and Biswas, K., "Steady-State and Transient Motor Vehicle Exhaust System Temperatures," *SAE International Journal of Passenger Cars-Mechanical Systems*, vol. 2, no. 1, pp. 206-218, January 2009.

Dequeiroz, M., Dawson, D., Nagarkatti, S., and Zhang, F., "Lyapunov-Based Control of Mechanical Systems," Springer: New York, NY, July 2000.

Dube, P., Natarajan, S., Mulemane, A., and Damodaran, V., "A Numerical Approach to Develop the Front End Cooling Package in a Vehicle Using Predicted Engine Fan Performance Data and Vehicle System Resistances," proceedings of the *SAE World Congress*, Paper: 2007-01-0542, Detroit, MI, April, 2007.

Environmental Protection Agency and Department of Transportation National Highway Traffic Safety Administration, "2017 and Later Model Year Light-Duty Vehicle Greenhouse Gas Emissions and Corporate Average Fuel Economy Standards; Final Rule," Federal Register, vol. 77, no. 199, 2012.

Environmental Protection Agency and Department of Transportation National Highway Traffic Safety Administration, "Light-Duty Vehicle Greenhouse Gas Emission Standards and Corporate Average Fuel Economy Standards; Final Rule," Federal Register, vol. 76, no.88, 2010.

Environmental Protection Agency, "Light-Duty Automotive Technology, Carbon Dioxide Emissions, and Fuel Economy Trends: 1975 Through 2014," 2014.

Fukano, T., and Jang, C., "Tip Clearance Noise of Axial Flow Fans Operating at Design and Off-Design Condition," *Journal of Sound and Vibration*, vol. 275, issue 3-5, pp. 1027-1050, 2004.

Geels, P., Gessier, B., Chanfreau, M., and Tarquis, M., "Advance Control Strategy for Modern Engine Cooling Thermal Systems, and Effect on CO2 and Pollutant Reduction," proceedings of the *6th Vehicle Thermal Management Systems Conference*, pp. 631-641, Brighton, U.K., May 2003.

Han-Sang, K., and Kyoungdoug, M., "Experimental Investigation of Dynamic Responses of a Transparent PEM Fuel Cell to Step Changes in Cell Current Density with Operating Temperature," *Journal of Mechanical Science and Technology*, vol. 22, no.11, pp. 2274-2285, November 2008.

Herrington, J., and Oliver, R., "An Instructional Design Framework for Authentic Learning Environments," *Educational Technology Research and Development*, vol. 48, no. 3, pp. 23-48, 2000.

Heywood, J., "Internal Combustion Engine Fundamentals," McGraw-Hill, New York, NY, April 1988.

Hodgins, H., "Into the Future: A Vision Paper," produced for the *Commission on Technology and Adult Learning*, 2000.

Hord, S., "Professional Learning Communities: Educators Work Together Toward a Shared Purpose-Improved Student Learning," *Journal of Staff Development*, vol. 30, no. 1, pp. 40-43, 2009.

Huk, T., and Flotto, C., "Computer Animations in Education: The Impact of Graphical Quality (3D/2D) and Signals," proceedings of *World Conference on E-Learning in Corporate, Government, Healthcare, and Higher Education*, pp. 1036-1037, Phoenix, AZ, October 2003.

International Council on Clean Transportation (ICCT), "Factsheet-EU28 Light Duty Vehicle Efficiency Standards," 2014. http://www.theicct.org/sites/default/files/info-tools/pvstds/EU_PVstds-facts_dec2014.pdf

International Council on Clean Transportation (ICCT), "Factsheet- China Light Duty Vehicle Efficiency Standards," 2014. http://www.theicct.org/sites/default/files/info-tools/pvstds/China_PVstds-facts_dec2014.pdf

International Organization of Motor Vehicle Manufacturers (OICA), "World Motor Vehicle Production by Country and Type," 2014.

Jorgensen, R., "Fan Engineering," 8th edition, published By Buffalo Forge Company, Buffalo, NY, September, 1982.

Kanefsky, P., Nelson, V., and Ranger, M., "A Systems Engineering Approach to Engine Cooling Design," proceedings of the *SAE International Truck and Bus Meeting*, Paper: 1999-01-3780, Detroit, MI, November 1999.

Khaled, M., Mangi, F., Hage, H., Harambat, F., and Peerhossaini, H., "Fan Air Flow Analysis and Heat Transfer Enhancement of Vehicle Underhood Cooling System-Towards a New Control Approach for Fuel Consumption Reduction," *Journal of Applied Energy*, vol. 91, no.1, pp. 439-450, 2012.

Khodabakhshian, M., Feng, L., and Wikander, J., "Predictive Control of the Engine Cooling System for Fuel Efficiency Improvement," proceedings of the *Automation Science and Engineering Conference*, pp. 61-66, Taipei, August 2014.

Kim, H., Shon, J., and Lee, K., "A Study of Fuel Economy and Exhaust Emission According to Engine Coolant and Oil Temperature," *Journal of Thermal Science and Technology*, vol. 8, no. 1, pp. 255-268, 2013.

Lee, S., Yoo, S., Kim, Y., Jung, H., Kim, S., Yun, M., Lee, J., and Kim, H., "Modeling and Localization of Web-based Fusion Image using VRML in Clinical Stroke Case," proceedings of *2004 Medical Imaging 2004: Visualization, Image-Guided Procedures, and Display*, vol.5367, pp.758-765, San Diego, CA, Feb. 2004.

Lelkes, A., and Bufe, M., "BLDC Motor for Fan Application with Automatically Optimized Commutation Angle," proceedings of the *35th Annual IEEE Power Electronics Specialists Conference*, vol. 3, pp. 2277-2281, Villingen, Germany, June 2004.

Melzer, F., Hesse, U., Rocklage, G., and Schmitt, M., "Thermomanagement," proceedings of the *SAE World Congress*, Paper: 1999-01-0238, Detroit, MI, March, 1999.

Mitchell, T., Salah, M., Wagner, J., and Dawson, D., "Automotive Thermal Valve Configurations: Enhanced Warm-Up Performance," *ASME Journal of Dynamic Systems, Measurement and Control*, vol. 131, no. 4, pp. 239-244, July 2009.

Morrison, G., Ross, S., and Kemp, J., "Effective Instruction," New York, NY: John Wiley & Sons, 2007.

Moyle, D., Lasecki, M., and Cornish, B., "Thermal Kits for Truck Fleets," proceedings of the *SAE* Commercial *Vehicle Engineering Congress*, Paper: 2006-1-3542, Chicago, IL, October 2006.

Ou, J., Dong, Y., and Yang, B., "Virtual Reality Technology in Engineering Hydrology Education," proceedings of the *1st International Symposium on Computer Network and Multimedia Technology*, Wuhan, China, January 2009.

Page, R., Hnatczuk, W., and Kozierowski, J., "Thermal Management for the 21st Century- Improved Thermal Control and fuel Economy in an Army Medium Tactical Vehicle," proceedings of the *Vehicle Thermal Management Systems Conference & Exposition*, Paper: 2005-01-2068, Toronto, Canada, May 2005.

Perdomo, L., Shiratuddin, F., Thabet, W., and Ananth, A., "Interactive 3D Visualization As a Tool For Construction Education," proceeding of the *6th International Conference on Information Technology Based Higher Education and Training*, Santo Domingo, DR, July 2005.

Regin, F., "A Numerical Analysis on Air-cooling Performance of Passenger Cars," proceedings of the *SAE World Congress*, Paper: 2010-01-0554, Detroit, MI, April, 2010.

Salah, M., Frick, P., Wagner, J., Dawson,D., "Hydraulic Actuated Automotive Cooling Systems - Nonlinear Control and Test," *Control Engineering Practice*, vol. 17, pp. 609-621, May 2009.

Salah, M., Mitchell, T., Wagner, J., and D. Dawson, "A Smart Multiple Loop Automotive Cooling System Model, Control, and Experimental Study," *IEEE/ASME Transactions on Mechatronics*, vol. 15, no. 1, pp. 117-124, 2010.

Salah, M., Mitchell, T., Wagner, J., and Dawson, D., "An Advanced Engine Thermal Management System: Nonlinear Control and Test," *IEEE/ASME Transactions on Mechatronics*, vol. 10, no. 2, pp. 210-220, April 2005.

Sampaio, Z., Ferreira, M., Rosario, P., and Martins, P., "3D and VR Models in Civil Engineering Education: Construction, Rehabilitation and Maintenance," *Automation* in Construction, vol. 19, no. 7, pp. 819-828, November 2010.

Sermeno, S., Bideaux, E., Morgan, T., and Nguyen, D., "Heavy Duty Vehicle Cooling System Auxiliary Load Management Control: Evaluating the Maximum Gain of Implementing an Advanced Control Strategy," proceedings of the *SAE Commercial Vehicle Engine Congress*, Paper: 2014-01-2341, Rosemont, IL, October 2014.

Setlur, P., Wagner, J., Dawson, D., and Marotta, E., "An Advanced Engine Thermal Management System: Nonlinear Control and Test," *IEEE/ASME Transactions on Mechatronics*, vol. 10, no.2, pp.210-220, 2005.

Shome, B., and Joshi, R., "CFD Based Air-to-Boil Temperature Prediction for Sport Utility Vehicle Radiator," proceedings of the *SAE Powertrain & Fluid Systems Conference and Exhibition*, Paper: 2006-01-3266, Toronto, Canada, October 2006.

Shutty, J., and Pinto, R., "Advanced Thermal Management Strategies," proceedings of the *SAE Commercial Vehicle Engineering Congress*, Paper: 2013-36-0542, Rosemont, IL, October 2013.

Shutty, J., Wenzel, W., Becker, M., Bohan, S., and Kowalske, G., "Advanced Thermal Management of a Light Duty Diesel Vehicle," proceedings of the *SAE World Congress*, SAE Technical Paper 2013-01-0546, Detroit, MI, April 2013.

Smith, S., "The Scientist and Engineer's Guide to Digital Signal Processing," 2nd edition, California Technical Publishing: San Diego, CA, 1999.

Taylor, C., and Toong, T., "Heat Transfer in Internal-Combustion Engine," proceedings of the *ASME-AiChE Heat Transfer Conference*, Paper: 295, University Park, PA, August 1957.

Wagner, J., Ghone, M., and Dawson, D., "Cooling Flow Control Strategy for Automotive Thermal Management Systems," proceedings of the *SAE World Congress*, Paper: 2002-01-0713, Detroit, MI, March 2002.

Wagner, J., Paradis, I., Marotta, E., and Dawson, D., "Enhanced Automotive Engine Cooling System - a Mechatronics Approach," *International Journal of Vehicle Design*, vol. 28, no. 1-2-3, pp. 214-240, 2002.

Wambsganss, M., "Thermal Management Concepts for Higher - Efficiency Heavy Vehicles," proceedings of *SAE World Congress*, Paper: 1999-01-2240, Detroit, MI, 1999.

Wang, T., and Wagner, J., "A Smart Engine Cooling System - Experimental Study of Temperature Transient Responses," proceedings of the *SAE World Congress*, Paper: 2015-01-1604, Detroit, MI, April 2015.

Wang, T., and Wagner, J., "Advanced Automotive Thermal Management – Nonlinear Radiator Fan Matrix Control," *Control Engineering Practice*, vol. 41, pp. 113-123, August 2015.

Wang, T., Jagarwal, A., Wagner, J., and Fadel, G., "Optimization of an Automotive Radiator Fan Array Operation to Reduce Power Consumption," *IEEE/ASME Transactions on Mechatronics*, vol. 20, pp. 2359-2369, December 2014.